Operator based robust nonlinear control design for an L-shaped arm driven by linear motor

Yanfeng Wu

Department of Electronic and Information Engineering

The Graduate School of Engineering

(Doctoral Course)

TOKYO UNIVERSITY
OF AGRICULTURE AND TECHNOLOGY

December, 2017

ACKNOWLEDGEMENTS

The guidance and support of the following people are invaluable. I would like to express my sincere appreciation to everyone who helped me scientifically and emotionally throughout my Ph.D study.

Firstly, I would like to express my sincere gratitude to my supervisor Prof. Mingcong Deng, for his continuous support for my Ph.D study and the related research, for his patience, encouragement, and immense knowledge. His insightful guidance has helped me in all the time of research and writing of this dissertation. Without his guidance, it would be impossible to complete this dissertation.

Besides my supervisor, I would like to express my gratitude to this dissertation committee: Prof. Yasuhiro Takaki, Prof. Ken Nagasaka, Prof. Toshihisa Tanaka and Prof. Kenta Umebayashi, their insightful comments, valuable suggestions incent me to widen my research from various perspectives.

My sincere thanks also go to my fellow lab mates for the stimulating discussions, for the time we were working together and for all the fun we have had in the last three years. Special thanks go to Assistant Professor Yuichi Noge, Technical Staff Masanori Suda, Dr. Fazhan Tao, Ms. Mengyang Li, Mr. Xudong Gao and Mr. Guang Jin for their kind advices and supports.

I would like to deeply thank my family: my parents, brother and sisters, for supporting me spiritually throughout this study and my life; my mother-in-law, who have took care of my wife and my son during these years, such

that I can concentrate on my research. Especially, I would like to express deep gratitude to my beloved wife Yan Li and son Yizhuo Wu for their love, patience, encouragement and supports during my Ph.D study. I would dedicate this Ph.D dissertation to them; without their encouragement and support, it would be impossible to complete this dissertation.

ABSTRACT

In this dissertation, the operator-based robust nonlinear vibration control is proposed for an L-shaped arm driven by a linear pulse motor. The aim of this study is to allow the motor move fast and reduce the arm vibration by controlling the motion of the motor and the behaviour of the piezoelectric actuator simultaneously.

Much manipulating devices in the industrial system are constructed with flexible arms and driven by motors. When the system works, the vibration of the arm will degrade the system performance. To control the vibrations, there are mainly two active ways. One way is controlling the motor motion such that the vibrations are reduced. Another way uses smart materials as actuator on the flexible arms to suppress the vibrations. In this dissertation, the L-shaped arm pasted with a piezoelectric actuator is driven by a linear pulse motor. It is difficult to control the linear motor and the piezoelectric actuator at same time to meet all the requirements, while the system has uncertainties and hysteresis nonlinearities. The operator-based nonlinear control approach is effective and easy implemented for these nonlinear systems. Therefore, two robust nonlinear controls based on the nonlinear operator control theory are designed to control the motor motion and the behavior of the piezoelectric actuator simultaneously, such that the motor moves fast while the arm vibration is reduced as much as possible.

First, for the L-shaped arm without load, its forced vibration caused by the linear motor is modelled by assuming the arm as two interacted can-

tilever Euler-Bernoulli beams. The first three modes of the arm vibration are considered in the control design, other higher modes are considered as uncertainties which are compensated in the control design. Prandtl-Ishlinskii model is utilized to model the behaviour of the piezoelectric actuator. The model is divided into two parts, one part is linear to be combined into the operator among the control design; the residual part including the hysteresis is to be compensated in the tracking controller such that the stability of the system is guaranteed. Based on the operator-based nonlinear control approach, two controllers are designed to control the system in parallel. One controller controls the motor motion in optimal trajectory while reducing the arm vibration. Another one controls the behaviour of the piezoelectric actuator such that the arm vibration is further reduced. The hysteresis nonlinearity of the actuator is compensated in a tracking controller. Simulations are conducted in Matlab comparing with the Proportional-Integral (PI) control to confirm the effectiveness of the proposed control design. The results illustrate that the operator-based control systems designed in this dissertation is effective to reduce the arm vibration while control the motor motion in less time and can guarantee robust stability of the system.

Second, for the arm with unknown load, its forced vibration is modelled as a whole two dimensional Euler-Bernoulli beam. The relationship between the arm vibration, motor motion and the load mass is obtained. By integrating an on-line discrete wavelet transform (DWT) with the operator-based robust control approach, the proposed control for the system is designed. The wavelet transform is utilized to process the real-time arm vibration. By

decomposition, processing and reconstruction, the undesired disturbances in the arm vibration signal are removed before it is served for the operator-based controller. The operator-based right coprime factorization method is utilized to guarantee the robust stability of the motor-arm system. The piezoelectric actuator is controlled to further reduce the arm vibration. With a modified compensator, the hysteresis of the piezoelectric actuator is compensated in the control design by using a Prandtl-Ishlinskii hysteresis model. The load is estimated by DWT and fast Fourier transform (FFT) method based on the relationship between vibration model of the L-shaped arm and the mass of load, such that the main parameters of the system dynamic is determined. The DWT is used to decompose the arm vibration signal and extract the first mode of the arm vibration, FFT is then used to transform the arm vibration signal from time domain into frequency domain. Simulation results comparing with previous control are demonstrated to validate performance of the proposed control design. The results show that the on-line DWT is effective to remove the influence of some uncertainties and improve the performance of the operator-based control; the load estimation method is workable.

In addition, the main parameters of the L-shaped arm vibration experimental system are identified; the proposed two control designs are programmed into C++ code to test their performances in experiments. For the arm without load, experiments are conducted comparing with the conditional PI control and minimum time control, the results indicate that the proposed control design is effective. For the L-shaped arm with load, experiments are performed comparing with the previous operator- based control.

The results show that the arm vibration is reduced more effectively when the on-line DWT is involved, the performance of the operator-based control is improved and the load mass is estimated.

To sum up, this dissertation proposes two kinds of robust nonlinear system control design for an L-shaped arm driven by a linear pulse motor in two different situations. The operator-based nonlinear optimal vibration control focuses on the finite time motor motion control and arm vibration control for the arm without load, where the nonlinearity of piezoelectric actuator is compensated in the controller. Beside these control tasks, another control design also addresses the situation when the arm is loaded with an unknown mass; the on-line DWT is involved to remove the influence of some unwanted disturbances and estimate the load mass. Both control designs are validated by simulations and experiments, the results show that the proposed control designs meet all the requirements.

Contents

List of Figures

List of Tables

Chapter 1

Introduction

1.1 Background

For the flexible beams or arms, when they are driven or manipulated with speed change, their vibrations are inevitable. In much industrial plants, warehouses ports and transfer robotic systems, the carrying system used for handling objects are designed into different structures to meet different requirements and various occasions. The vibration will influence the manipulation and degrade the system performance [1, 2]. Some manipulating devices are designed into two-dimensional or more complicated structures, which aggravates the vibration complexity. To reduce the arm vibration is always a challenging issue in engineering. The countermeasure to reduce arm vibration mainly falls into two categories: passive vibration control and active vibration control. The passive vibration control relies on the optimal structural design and material selection considering the damping features; the well-known measures are using various vibration dampers and absorbers in the system structure. The active vibration control relies on some sen-

sors to feed back the real time vibration states and reducing the unwanted vibration by the anti-force generated by powered actuators [3–6].

The traditional actuating components usually use pneumatic devices, linear motors, electromagnetic devices etc. in vibration control. Thanks to the reciprocal physical characteristic of smart materials including magnetostrictive materials, shape memory alloys and piezoelectric materials etc., they are much commonly used in modern engineering to suppress the structural vibrations. Among them, piezoelectric material is one kind of such materials that produces strain and stress when voltages are applied, and vice versa. Therefore, it has been utilized as sensors and actuators and being studied by much researchers [7–9].

A flexible arm is usually modelled as an infinite dimensional plant, if it is under forced vibration with uncertainties, the dynamics will be a nonlinear plant. It's difficult to design a stable and robust controller for the nonlinear arm-motor model combined with the nonlinear piezoelectric actuator using common approaches. An operator theory has been studied by much researches [10–15], which can guarantee the bounded-input, bounded-output (BIBO) stability of a nonlinear feedback control system based on robust right coprime factorization. To ensure the robust stability of linear systems, a small gain theorem based simple adaptive control scheme was proposed in [16]. A robust control approach using passivity-based robust right coprime factorization was proposed in [17]. Deng *et al.* [18] have developed the conditions for the output tracking problem with disturbance, then with continuous extensions, operator-based nonlinear control approach

has become more comprehensive and effective. It has been used in many practical applications [19–24].

The wavelet transform can convert the signal into time-scale domain, has attracted increasing attentions for its ability to extract signal features [25–30]. Wavelet transform has been extended to civil engineering, machining condition monitoring and detection [31–33]. However, most approaches are off-line precess or need the whole length of signals, which limits its on-line applications for real-time control. Some researchers propose on-line or real-time segmented wavelet transform applying for wheel system, rotor and other rotational machines [34–38].

1.2 Current development of arm vibration control

For the arm driven by a motor, there are mainly two active ways to reduce the arm vibration during operation. One way is controlling the motor motion, another way is using smart materials as actuator. In the motor motion control, the system is considered as an underactuated plant, by searching for optimal trajectories of the motor, the arm results in small vibration. Researchers have proposed different approaches for this kind of trajectory planning problem, especially for the overhead crane systems [2, 39–52]. Sun et al. propose a amplitude-saturated output feedback control approach for underactuated crane systems exhibiting double-pendulum effects [75]. For one kind of underactuated systems with rotational-translational actuator, Sun et al. propose a nonlinear continuous control to globally stabilize both

the rotation and translation of the rotational-translational actuator systems influenced by nonvanishing matched disturbances [76]. In this study, the whole system is a Multi-Input Multi-Output (MIMO) plant. For the MIMO nonlinear plants, some operator-based approaches are proposed for tackling the coupling problem in [53–56]. However, these plants have the same number of inputs as outputs, not suitable for the plants with unequal inputs and outputs.

Another way to reduce the arm vibration is using smart materials as actuators. Different approaches have been proposed by researchers in this field. Among them, using piezoelectric material as actuator has been proved to be an effective method for the small size flexible arm [7, 8]. Recently, different control methods have been investigated for the active vibration control with piezoelectric material, such as Proportional-Integral-Differential (PID) control, sliding mode control, optimal control [57–59]. Khorshidi *et al* [60] studied the active vibration control of plates coupled with piezoelectric layers by using Linear-Quadratic Regulator (LQR) and Fuzzy Logic Controller (FLC). With these methods, by controlling the input voltages, the piezoelectric material acts as a actuator generating opposite moment to suppress the arm vibration. However, the piezoelectric actuator has a nonlinear property called hysteresis, the output error will lower the performance of the piezoelectric actuator. To represent the hysteresis behavior and control the piezoelectric actuator accurately, some models have been proposed, including Duhem model, Dahl model, Bouc-Wen model, Preisach model and Prandtl-Ishlinskii model [9, 61–73, 81]. The Prandtl-Ishlinskii model is commonly

utilized to describe hysteresis nonlinearity using stop hysteresis operators or play hysteresis operators because of its simplicity, accuracy and ease of implementation. However, these operators are symmetric, which will still result in compensation error. Al Janaideh *et al* [82] proposed an analytic inverse of a generalized Prandtl-Ishlinskii model, it can be conveniently implemented as a real-time feed-forward compensator to compensate for hysteresis nonlinearities. A non-symmetric Prandtl-Ishlinskii hysteresis model with unknown slopes was given to describe the hysteresis in [73], the nonlinear compensator based on this model can compensate the hysteresis more effectively.

An operator-based nonlinear control method has been given to control the vibration of a flexible arm using the piezoelectric actuator [86]. However that paper only studied the free vibration of a simple uniform clamped-free beam and without considering the hysteresis of actuator. For controlling the free vibration of an aircraft-tail-like plate using the piezoelectric actuator, an operator-based nonlinear system control technique has been given by Katsurayama et al. [74], the lower order modes of vibration are considered. However, that study only considered the free vibration the plate without driving source control.

The L-shaped arm considered in this dissertation is forced vibration and vibrating in two dimensions which is more complicated and difficult to be controlled. Moreover, the linear motor control system has two outputs and only one control input, namely, it is an underactuated nonlinear MIMO plant. To deal with this kind of problem, many control strategies have been proposed, especially for the overhead crane systems, such as the adaptive control,

sliding-mode control, fuzzy control and optimal control. Wen *et al*. [52] used data-based support vector machine (SVM) to estimate the swing angle, found an optimal trajectory to reduce the payload swing using operator-based control. However the control object in that paper is a payload driven by a linear motor with cable, the swaying of the payload is much more slowly and quite different from the arm vibration. As the L-shaped arm has a more complicated vibration dynamics, it is difficult for the SVM to learn. Therefore the control method in that paper is not suitable for this L-shaped arm vibration.

1.3 Motivations of the dissertation

Scaled down from a real industrial transported system, a flexible L-shaped arm driven by a linear pulse motor is studied in this dissertation. When the system is working, vibration of the arm is inevitable. It is necessary to seek appropriate methods to control the motor motion while reduce the arm vibration at the same time.

Motivated by the optimal motor motion control for the underactuated system, this dissertation intend to set up an optimal control method for the linear motor. The motor is controlled with optimal trajectory resulting in less time consumption and less arm vibration. It means that the arm vibration status will be measured by sensors and feed back into the motor motion control. The main difficulty is to meet two output requirements with one control input while keep the system stable and robust.

Motivated by the superior advantages of the piezoelectric material, this dissertation intend to use piezoelectric material as sensors and actuator, to

measure and suppress the arm vibration. Prandtl-Ishlinskii model is used to model the hysteresis of the piezoelectric actuator and modify it according to the control design method, its nonlinearity will be considered to be compensated to improve the control performance.

Motivated by the superior advantages of the operator-based nonlinear control method, this dissertation intend to use the method to factorize the system model and design optimal controllers to control the linear motor motion and reduce the L-shaped arm vibration at the same time. The system has two control inputs including driving force of linear pulse motor and voltage for the piezoelectric actuator, three outputs including the moving distance of linear motor and the vibrations of two parts of arm. In the above mentioned papers, the arm was simple cantilever type without load. In practice, the arm manipulates different loads, which will determine the parameters in the controller relating to the plant dynamics. It is inconvenient to measure the load mass in advance. Therefore, an automatic load mass estimation combined with the controller is necessary. In addition, the operator-based control uses the outputs of system directly as feedback signals for the controller, the system performance is influenced by the quality of the signal. The disturbances and uncertainties will lower the control performance. For this end, the output signal should be processed by appropriate measures, wavelet transform can undertake such tasks. An on-line DWT is to be proposed to use in the operator-based nonlinear control, working together for the nonlinear L-shaped arm vibration system. Operator-based right coprime factorization method is used to guarantee the stability and robustness of the

system. The on-line DWT is constructed to estimate the unknown load, remove the influence of some uncertainties and improve the performance of the operator-based control.

In summary, this dissertation intend to use operator-based nonlinear control approach and on-line DWT in control design for actively control the L-shaped arm vibration system, and validate the control design in simulation and experiment. The aim of this research is to allow the motor move fast and reduce the arm vibration as much as possible while keep the system stable and robust.

1.4 Contributions of the dissertation

For the L-shaped arm experiment system control design, the difficulty is controlling the linear motor and the piezoelectric actuator at same time to meet all the requirements, while the system has uncertainties and hysteresis nonlinearities. We design two controllers based on the nonlinear operator control theory to accomplish it. One controller allows the fast movement to destination while reducing the vibration of the arm, the other one controls the piezoelectric actuator to further reduce the vibration. The main contributions of this study are summarized as follows.

(1) The vibration of the Motor-Arm system with and without load is modelled.

For the L-shaped arm without load, its vibration with linear motor is modelled by assuming the arm as two interacted cantilever Euler-Bernoulli beam. For the arm with unknown load, the arm is modelled as a two dimen-

sional Euler beam by mechanical analysis based on Euler-Bernoulli theory, and the relationship between the load and the vibration mode is given. By introducing a evaluation index, the dominant modes of the arm vibration are considered in the control design, other higher modes are considered as uncertainties compensated in the control design.

(2) The load estimation method is given by using DWT and FFT.

Based on the vibration model of the L-shaped arm with load, the relationship between the load mass and the natural frequency of the arm vibration is obtained. When the arm vibration is measured in time domain signal, after decomposing by the DWT, the first mode vibration is isolated and transformed into frequency domain by FFT. The load is estimated using the obtained relationship, such that the main parameters of the system dynamic is determined.

(3) Two operator-based nonlinear controllers for motor motion and arm vibration are designed employing a short-symmetrical on-line DWT.

One operator-based robust nonlinear control is proposed for the linear pulse motor to be fast while reducing the arm vibration. Another operator-based robust nonlinear control with hysteresis compensation is proposed for the piezoelectric actuator to further reduce the arm vibration. When the L-shaped arm has unknown load, a short-symmetrical on-line DWT is used in the control design so as to reduce the impact of disturbances and uncertainties and to estimate the unknown load mass.

1.5 Organization of the dissertation

Beginning with theoretical preliminaries and problem statement, this dissertation is organized as follows.

In **Chapter 2**, some fundamental definitions and the theoretical basis are provided for the system modelling and control design in this dissertation. Euler-Bernoulli beam theory is utilized to model the flexible arm vibration; Prandtl-Ishlinskii model is used to model the hysteresis of the piezoelectric actuator. Some fundamental definitions of operator theory are introduced, the operator-based nonlinear control approach and the discrete wavelet transform are given. Based on the background and these theories, the problem to be studied in this dissertation is stated.

In **Chapter 3**, the forced vibration of the L-shaped arm driven by a linear pulse motor is modelled by considering it as two connected Euler-Bernoulli beams. Based on the operator-based nonlinear control approach, two controllers are designed to control the system in parallel. One controller aims to control the motor motion in optimal trajectory while reducing the arm vibration. Another one aims to control the behaviour of the piezoelectric actuator to further reduce the arm vibration. The hysteresis nonlinearity of the actuator is compensated in a tracking controller. Simulation is conducted to confirm the effectiveness of the proposed control design.

In **Chapter 4**, the L-shaped arm is modelled as a two dimensional Euler-Bernoulli beam and an unknown load is considered in the model. An on-line DWT is constructed to remove the influence of some uncertainties and im-

prove the performance of the operator-based control. Involving the on-line DWT, two operator-based controllers are proposed. One is to control the motor motion resulting in less arm vibration. Another one is to further reduce the arm vibration by using a piezoelectric actuator. Simulations comparing with previous control are demonstrated to validate performance of the proposed control design. The load estimation method using FFT and DWT is given based on the system model.

In **Chapter 5**, the structure of the L-shaped arm vibration experimental system is introduced, the main parameters of the devices are identified. Using the operator-based nonlinear optimal control proposed in Chapter 3, experiments are conducted comparing with the conditional PI control to test the experimental performance of the control design. Using the operator-based nonlinear control with on-line DWT proposed in Chapter 4, comparative experiments are conducted for the L-shaped arm with unknown load to validate the load estimation method and test the performances of the control designs correspondingly.

In **Chapter 6**, the main work of this dissertation is summarized, the results are discussed and the problem stated in Chapter 2 is concluded. Based on the performance of the proposed control design, the main contributions of this dissertation are conformed and reiterated in detail. The limitations and future works of this dissertation are provided for the probable researches in this field.

Chapter 2

Preliminaries and problem statement

2.1 Introduction

This chapter provides the mathematical and theoretical basis for the system modelling and control design in the following chapters of this dissertation. It also specify the aims and objectives of this research.

In **Section 2.2**, the dynamics of flexible arm vibration is introduced, and its modelling method based on Euler-Bernoulli beam theory is provided.

In **Section 2.3**, the dynamics of the piezoelectric actuator is introduced, the hysteresis of the piezoelectric actuator is modelled using a Prandtl-Ishlinskii hysteresis model.

In **Section 2.4**, the fundamental definitions of operator theory are introduced, the operator-based nonlinear control approach is outlined.

In **Section 2.5**, the theoretical basis of wavelet transform is given, some related definitions of DWT is introduced.

In **Section 2.6**, the problem to be studied in this dissertation is stated.

Primarily, the framework of modelling the L-shaped arm vibration and hysteresis of the piezoelectric actuator, operator-based control design utilizing DWT is outlined.

2.2 Flexible arm vibration model

If a thin uniform arm has external distributed transverse force $q(x,t)$ on it, shown as in Fig. 2.1(a), take any element of the beam with length dx as object, its free-body diagram is shown in Fig. 2.1(b), where $V(x,t)$ is the shear force, $M(x,t)$ is the bending moment, ρ is the mass density.

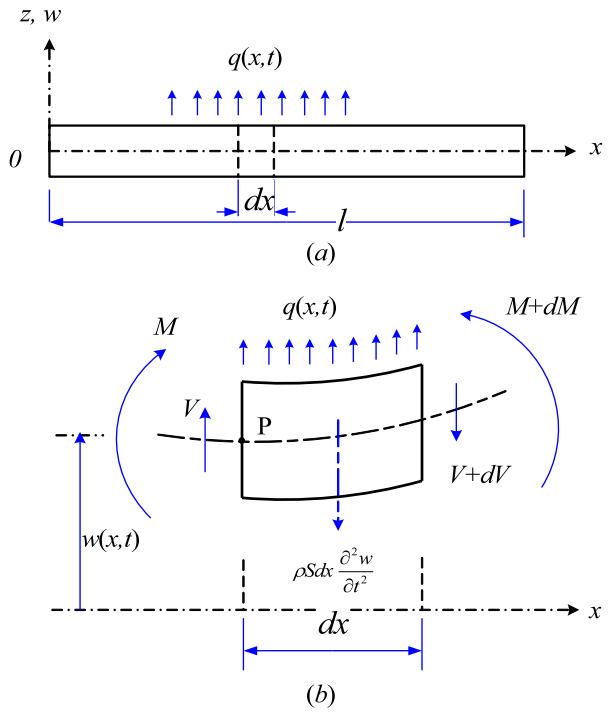

Figure 2.1: Transverse vibration of a uniform thin arm

Neglecting the torsional vibration, based on the Euler-Bernoulli theory

[77], force and moment equilibrium, the forced transverse vibration of the uniform arm is obtained as:

$$E_a I \frac{\partial^4 w}{\partial x^4} + c_s I \frac{\partial^5 y(x,t)}{\partial x^4 \partial t} + \rho S \frac{\partial^2 w}{\partial t^2} = q(x,t) \tag{2.1}$$

where $q(x,t)$ is the external distributed forces on the arm, including the linear motor driving force and the piezoelectric actuator moment. w, standing for $w(x,t)$, is the transverse displacement along the neutral axis of the arm. E_a, I, ρ, S, c_s are the Young's modulus, moment of inertia, density, cross-sectional area and strain-rate damping coefficient of the arm, respectively.

The equation (2.1) can be solved using the boundary conditions and the arm's initial conditions.

2.3 Model of piezoelectric actuator

For the piezoelectric actuator pasted on an arm, when voltages are applied, the actuator will generate moments and deform the arm in a certain way. By controlling input voltage, the actuator is utilized to reduce the arm vibration. However, the relationship between the output moment and the control input is a nonlinear process, because the piezoelectric actuator has a hysteresis nonlinear property. To represent the hysteresis behavior and control the piezoelectric actuator accurately, some models have been proposed, including Duhem model, Dahl model, Bouc-Wen model, Preisach model and Prandtl-Ishlinskii model. The Prandtl-Ishlinskii model is commonly utilized to describe hysteresis nonlinearity using stop hysteresis operators or play hysteresis operators because of its simplicity, accuracy and ease of imple-

mentation. To consider this effect in the system model, in this dissertation, the Prandtl-Ishlinskii hysteresis model based on the play hysteresis operator is utilized, represented as follows.

$$M_p(t) = D_{PI}(u)(t) + \Delta_{PI}(u)(t) \tag{2.2}$$

The output of piezoelectric actuator is represented as two terms. The first term D_{PI} is an invertible operator for certain parameters, the residual term Δ_{PI} is the nonlinear part of the model, which will change with the input $u(t)$ and be influenced by the design parameters, it needs to be compensated by the controller. The details of D_{PI} and Δ_{PI} are shown as follows.

$$D_{PI}(u(t)) = Ku(t) = u(t)\int_0^H p(h)dh, \tag{2.3}$$

$$\Delta_{PI}(u(t)) = -\int_0^{h_x} S_n h p(h)dh + \int_{h_x}^H p(h)[F_h(u(t_i)) - u(t)]dh, \tag{2.4}$$

$$S_n = \text{sign}(u(t) - F_h(u(t_i)))$$

$$F_h(u(t)) = \begin{cases} u(t)+h & u(t) \le F_h(u(t_i)) - h \\ F_h(u(t_i)) & -h < u(t) - F_h(u(t_i)) < h \\ u(t)-h & u(t) \ge F_h(u(t_i)) + h \end{cases}$$

$$t_i < t \le t_{i+1},\ 0 \le i \le N-1 \tag{2.5}$$

$$0 = t_0 < t_1 < \cdots < t_N = t_E,\ [0, t_E].$$

where, $u(t)$ and h are the input voltage and the threshold of play hysteresis operator, respectively. The initial condition is given by $F_h(u)(0) = \max(u(0) - h, \min(u(0) + h, (u_1)^*)$. h_x is the upper limit of h that satisfies $h \le |u(t) - F_h(u(t_i))|$. $p(h)$ is the density function satisfying $p(h) \ge 0$ with $\int_0^\infty hp(h)dh < \infty$ to be determined through experiments.

2.4 Operator-based nonlinear control approach

2.4.1 Definitions of spaces

In this dissertation, the operator theory is based on several spaces in mathematics, which are defined as follows.

Normed linear space:

Denote a space X of time functions, it is said to be a vector space if it is closed under addition and scalar multiplication. It is said to be *normed* if each element x in X is endowed with norm $\|\cdot\|_X$, satisfying the follow conditions:

1) $\|x\| > 0$, if $x \neq 0$.

2) $\|ax\| = |a|\|x\|$.

3) $\|x_1 + x_2\| \leq \|x_1\| + \|x_2\|$.

Banach space:

A Banach space is a vector space X over the real or complex numbers with a norm $\|\cdot\|$ such that every Cauchy sequence (with respect to the metric $d(x, y) = \|x - y\|$) in X has a limit in X. Many spaces of sequences or functions are infinite dimensional Banach spaces.

Extended linear space:

Let Z be the family of real-valued measurable functions defined on $[0, \infty)$, which is a linear space. For each constant $T \in [0, \infty)$, let P_T be the Pro-

jection operator mapping from Z to another linear space, Z_T, of measurable functions such that

$$f_T(t) := P_T(f)(t) = \begin{cases} f(t), & t \leq T \\ 0, & t > T \end{cases} \tag{2.6}$$

where, $f_T(t) \in Z_T$ is called the truncation of $f(t)$ with respect to T. Then, for any given Banach space X of measurable functions, if

$$X^e = \{f \in Z : \ \|f_T\|_X < \infty, \text{for all } T < \infty\}, \tag{2.7}$$

the space X^e is called the extended linear space associated with the Banach space X.

This dissertation uses the extended linear space because the control signals are finite time-duration in experiments.

2.4.2 Definitions of operators

Let U and Y be linear spaces over the field of real numbers, and let U_s and Y_s be normed linear subspaces, called the stable subspaces of U and Y, respectively.

Operator:

An operator $Q : \mathbf{U} \to \mathbf{Y}$ is a mapping defined from input space $\mathbf{U}$ to the output space $\mathbf{Y}$. The operator Q can be expressed as $y(t) = Q(u)(t)$ where $u(t)$ is the element of $\mathbf{U}$ and $y(t)$ is the element of $\mathbf{Y}$.

Invertible:

An operator Q is said to be invertible if there exists an operator P such that

$$Q \circ P = P \circ Q = I. \tag{2.8}$$

P is called the inverse of Q and is denoted by Q^{-1}, where, I is identity operator, and $Q \circ P$ (or simply $Q(P(\cdot))$ or QP) is an operation satisfying

$$\mathcal{D}(Q \circ P) = P^{-1}(\mathcal{R}(P) \cap \mathcal{D}(Q)). \tag{2.9}$$

Unimodular operator:

Let $\mathcal{S}(U, Y)$ be the set of stable operators mapping from U to Y. Then, $\mathcal{S}(U, Y)$ contains a subset defined by

$$\mathcal{U}(U, Y) = \{M : M \in \mathcal{S}(U, Y),\ M \text{ is invertible with } M^{-1} \in \mathcal{S}(Y, U)\}. \tag{2.10}$$

Elements of $\mathcal{U}(U, Y)$ are called unimodular operators.

Lipschitz operator:

For any subset $D \subseteq U$, let $\mathcal{F}(D, Y)$ be the family of nonlinear operators Q such that $\mathcal{D}(Q) = D$ and $\mathcal{R}(Q) \subseteq Y$. Introduce a (semi)-norm into (a subset of) $\mathcal{F}(D, Y)$ by

$$\|Q\| \ := \ \sup_{\substack{x, \tilde{x} \in D \\ x \neq \tilde{x}}} \frac{\big\|Q(x) - Q(\tilde{x})\big\|_Y}{\|x - \tilde{x}\|_U}$$

if it is finite. In general, it is a semi-norm in the sense that $\|Q\| = 0$ does not necessarily imply $Q = 0$. In fact, it can be easily seen that $\|Q\| = 0$ if Q is a constant operator (need not to be zero) that maps all elements from D to the same element in Y.

Let $Lip(D, Y)$ be the subset of $\mathcal{F}(D, Y)$ with its all elements Q satisfying $\|Q\| < \infty$. Each $Q \in Lip(D, Y)$ is called a Lipschitz operator mapping from D to Y, and the number $\|Q\|$ is called the Lipschitz semi-norm of the

operator Q on D. A Lipschitz operator is bounded and continuous on its own domain.

Generalized Lipschitz operator:

Let U^e and Y^e be extended linear spaces associating respectively with two given Banach spaces U and Y of measurable functions defined on the time domain $[0, \infty)$, and let D be a subset of U^e. A nonlinear operator $Q : D \to Y^e$ is called a generalized Lipschitz operator on D if there exists a constant L such that

$$\big\|[Q(x)]_T - [Q(\tilde{x})]_T\big\|_Y \leq L\|x_T - \tilde{x}_T\|_U \tag{2.11}$$

for all $x, \tilde{x} \in D$ and for all $T \in [0, \infty)$. Note that the least such constant L is given by the norm of Q with

$$\begin{aligned} \|Q\|_{Lip} &:= \|Q(x_0)\|_Y + \|Q\| \\ &= \|Q(x_0)\|_Y \\ &+ \sup_{T\in[0,\infty)} \sup_{\substack{x,\tilde{x}\in D \\ x_T \neq \tilde{x}_T}} \frac{\big\|[Q(x)]_T - [Q(\tilde{x})]_T\big\|_Y}{\|x_T - \tilde{x}_T\|_U} \end{aligned} \tag{2.12}$$

for any fixed $x_0 \in D$.

Based on (2.12), it follows immediately that for any $T \in [0, \infty)$

$$\begin{aligned} \big\|[Q(x)]_T - [Q(\tilde{x})]_T\big\|_Y &\leq \|Q\|\|x_T - \tilde{x}_T\|_U \\ &\leq \|Q\|_{Lip}\|x_T - \tilde{x}_T\|_U. \end{aligned} \tag{2.13}$$

Lemma 2.1 *Let U^e and Y^e be extended linear spaces associating respectively with two given Banach spaces U and Y, respectively, and let D be a subset*

of U^e. The following family of Lipschitz operators is a Banach space:

$$Lip(D, Y^e) = \left\{ Q : D \to Y^e \middle| \|Q\|_{Lip} < \infty \text{ on } D \right\}. \tag{2.14}$$

Bounded input bounded output (BIBO) stability:

Let Q be a nonlinear operator with its domain $\mathcal{D}(Q) \subseteq U^e$ and range $\mathcal{R}(Q) \subseteq Y^e$. If $Q(U) \subseteq Y$, Q is said to be input output stable. If Q maps all input functions from U_s into the output space Y_s, that is $Q(U_s) \subseteq Y_s$, then operator Q is said to be bounded input bounded output (BIBO) stable or simply, stable. Otherwise, if Q maps some inputs from U_s to the set $Y^e \backslash Y_s$ (if not empty), then Q is said to be unstable. For any stable operators defined following in this dissertation stands for BIBO stable.

2.4.3 Right coprime factorization

Represent a nonlinear time varying system with uncertainties as operator $P + \Delta P : U \to Y$. Where P is the nominal plant, ΔP stands for the uncertainties, U and Y denote the input and output space of the plant.

Right factorization:

By introducing an intermediate variable $\omega \in W$, W is called a quasi-state space of P, the input and output of the operator P are expressed as $y = N(\omega)$ and $u = D(\omega)$. If D is invertible, $\omega(t) = D^{-1}(u)(t)$, then $P(u)(t) = N(\omega)(t) = ND^{-1}(u)(t)$; if further N and D are two stable operators, the operator P is said to have a right factorization, as shown in Fig. 2.2.

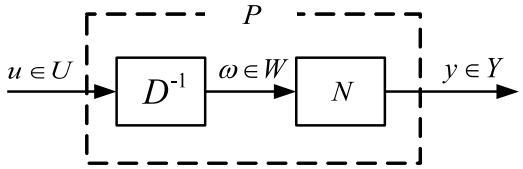

Figure 2.2: Right factorization of a nonlinear plant

Right coprime factorization:

After right factorization of a plant P into $(N,\ D)$, if two operators A and B satisfy the following Bezout identity, the factorization is said to be right coprime factorization.

$$AN + BD = M \tag{2.15}$$

Where B is invertible and $M \in \mathcal{U}(W, U)$ is a unimodular operator. The block diagram of the right coprime factorization of a nonlinear system P is shown in Fig. 2.3. Fig. 2.3 is therefore to be said as a operator-based

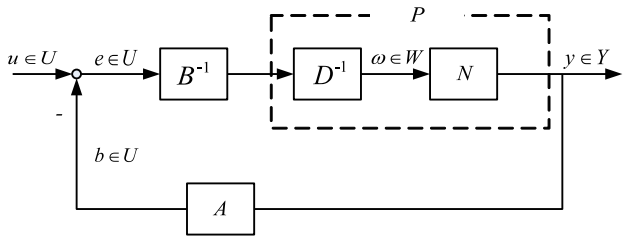

Figure 2.3: Right coprime factorization of a nonlinear plant

feedback control for the nonlinear plant P, and the operators A and B serve as controllers.

It is worth to mention that the initial state should also be considered, namely, $AN(w_0, t_0) + BD(w_0, t_0) = M(w_0, t_0)$ should be satisfied. In this

dissertation, $t_0 = 0$ and $w_0 = w_0(t_0)$ are selected.

Well-posedness:

The feedback control system shown in Fig. 2.3 is said to be well-posed, if for every input signal $r \in U$, all signals in the system (i.e., e, u, w, b and y) are uniquely determined.

Overall stable:

The feedback control system shown in Fig. 2.3 is said to be overall stable, if $r \in U_s$, implies that $u \in U_s$, $y \in V_s$, $w \in W_s$, $e \in U_s$ and $b \in U_s$.

Lemma 2.2 *Assume that the system shown in Fig. 2.3 is well-posed. If the system has a right factorization $P = ND^{-1}$, then the system is overall stable if and only if the operator M in (2.15) is a unimodular operator.*

Robustness:

For a nonlinear plat $\tilde{P}$, it is represented as a nominal plant P and bounded uncertainty ΔP, and $\tilde{P} = P + \Delta P$. The right factorization of the nominal plan P and the overall plant $\tilde{P}$ are

$$P = ND^{-1} \tag{2.16}$$

and

$$P + \Delta P = (N + \Delta N)D^{-1} \tag{2.17}$$

where N, ΔN, and D are stable operators, D is invertible, ΔN is unknown but the upper and lower bounds are known. According to **Lemma 2.2**, if

the following Bezout identity is satisfied,

$$A(N + \Delta N) + BD = \tilde{M} \tag{2.18}$$

and $\tilde{M}$ is a unimodular operator, the the nonlinear feedback control system is said to be BIBO stable.

With the determined operators A and B, if they further satisfy the following condition,

$$\|[A(N + \Delta N) - AN]M^{-1}\|_{Lip} < 1 \tag{2.19}$$

then the robustness of the uncertain system is guaranteed, where $\|\cdot\|_{Lip}$ is a Lipschitz operator norm. The robust feedback control system is shown in Fig. 2.4.

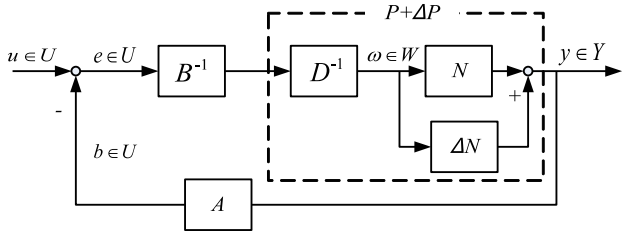

Figure 2.4: Nonlinear feedback control system with uncertainties

Lemma 2.3 *Let U_s^e be a linear subspace of the extended linear space U^e associated with a given Banach space U_B, and let $(A(N-\Delta N)+AN)M^{-1} \in Lip(U_s^e)$. With the Bezout identity of the nominal plant and the overall plant $AN + BD = M \in \mathcal{U}(W, U)$, $A(N + \Delta N) + BD = \tilde{M}$, respectively. If*

$$\|(A(N + \Delta N) - AN)M^{-1}\| < 1 \tag{2.20}$$

then the system shown in Fig. 2.4 is said to be robust stable.

For more details about the operator theory, please refer to [15, 18, 21, 24].

2.5 Fundamental theories on discrete wavelet transform

2.5.1 Wavelet transform

Wavelet transform is performed by using wavelet functions for time domain signal, the wavelet function is usually expressed in the following form.

$$\Psi_{a,b} = \frac{1}{\sqrt{b}}\Psi(\frac{t-a}{b}) \tag{2.21}$$

Where a is the shifting parameter and b is the scaling parameter.

For a time domain signal $x(t)$, the one-dimensional continuous wavelet transform (CWT) is a convolution of $x(t)$ and the complex conjugate of a wavelet function, which can be expressed as follows.

$$cwt(a,b) = \frac{1}{\sqrt{b}}\int x(t)\Psi^*(\frac{t-a}{b}) \tag{2.22}$$

where $\Psi^*(\cdot)$ is the complex conjugate of a wavelet function $\Psi(\cdot)$.

2.5.2 Discrete wavelet transform

CWT need a large amount of computation and resources, which is not suit for the control in practice. It is needed to transit from CWT to discrete wavelet transform (DWT). By insinuate the parameters a and b with a dyadic scales, the DWT is changed in the follow form.

$$\psi_{m,k}(t) = 2^{-m/2}\psi(2^{-m}t - k) \tag{2.23}$$

where m is the scale parameter and k is the shift parameter, both which are integers. The filter bank includes a cascading low-pass filter g and a high-

pass filter h. A sampled signal x is decomposed by passing the filters. At one certain decompose level, the outputs giving the detail coefficients (from the high-pass filter) and approximation coefficients (from the low-pass) as follows.

$$\begin{aligned} y_{low}[n] &= \sum_n x[k]g[2n-k] \\ y_{high}[n] &= \sum_n x[k]h[2n-k] \end{aligned} \tag{2.24}$$

The number of decomposition levels are decided by the frequency band of every level and the frequency frequency of desired signal. The frequency band for the approximation AC_j and the detail DC_j at level j are given by

$$\begin{aligned} 0 \leq f_{AC_j} &\leq \frac{f_s}{2^{j+1}} \\ \frac{f_s}{2^{j+1}} \leq f_{DC_j} &\leq \frac{f_s}{2^j} \end{aligned} \tag{2.25}$$

where j is the wavelet decomposition level, f_s is the signal sampling frequency. If the reconstruction level is determined by (2.25), by selecting the gains K_{a1}, K_{dj} $(j = 1, 2, \cdots, L)$, the processed signal is reconstructed, as shown in Fig. 2.5.

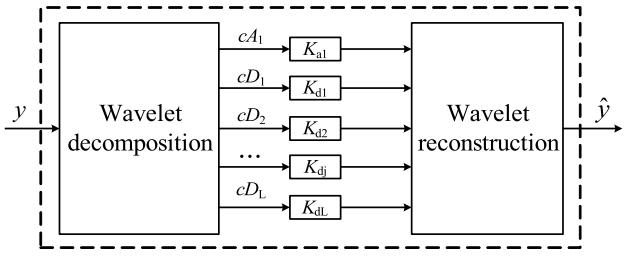

Figure 2.5: DWT processing scheme

2.6 Problem statement

In this dissertation, the L-shaped arm pasted with a piezoelectric actuator is driven by a linear pulse motor. The motor is required to move to destination with less time consuming, while the arm vibration is required to be reduced as much as possible. The difficulty is controlling the linear motor and the piezoelectric actuator at same time to meet all the requirements, while the system has uncertainties and hysteresis nonlinearities. Moreover, if the arm has different loads, the mass of load will impact the system dynamics, therefore, the load mass is required to be determined before control.

Firstly, the L-shaped arm is driven by a linear pulse motor, motivated by the optimal motor motion control for the underactuated system, this dissertation intend to find control method for the linear motor. The motor is controlled with optimal trajectory resulting in less time consumption and less arm vibration. It means that the arm vibration status will be measured by sensors and feed back to the motor motion control. The flexible arm is usually modelled as an infinite dimensional plant, however it cannot be fully considered in the control design in practice; the common method is to select the first several dominant modes, other higher modes are considered as uncertainties. When the arm is driven by a motor, the vibration and disturbances of the motor will influence the arm vibration, the whole plant is nonlinear for the control system. It's difficult to design a stable and robust controller for the nonlinear forced arm vibration. The vibration of L-shaped arm existing in two dimensions is more complicated and difficult to be controlled. There-

fore, one of the objectives is how to design an optimal controller to control this underactuated system such that the motor move fast in a optimal trajectory, the arm results in less vibration, while keep the system stable and robust.

Secondly, motivated by the superior advantages of the piezoelectric material, this dissertation intend to use piezoelectric material as sensors and actuator, to measure and suppress the arm vibration. Prandtl-Ishlinskii model is used to model the hysteresis of the piezoelectric actuator and modify it according to the control design method. The main difficulty is how to use the model and design controller to compensate the hysteresis of the piezoelectric actuator.

Thirdly, motivated by the superior advantages of the operator-based nonlinear control method, this dissertation intend to utilize the method to factorize the system model and design optimal controllers to control the linear motor motion and reduce the L-shaped arm vibration at the same time. The system has two control inputs including driving force of linear pulse motor and voltage for the piezoelectric actuator, three outputs including the moving distance of linear motor and the vibrations of two parts of arm. The main difficulty is how to design the two controllers working together to meet the system requirements.

Moreover, when the arm has different loads on it, it is difficult to measure the load mass in advance. Therefore, an automatic load mass estimation combined with the controller is necessary. The disturbances and uncertainties will lower the control performance. For this end, the output signal should

be processed by appropriate measures, wavelet transform can undertake such tasks. An on-line DWT is to be proposed to use in the operator-based nonlinear control, working together for the nonlinear L-shaped arm vibration system. Operator-based right coprime factorization method is used to guarantee the robust stability of the system. The on-line DWT is constructed to estimate the unknown load, remove some uncertainties and improve the performance of the operator-based control.

In summary, this dissertation intend to use operator-based nonlinear control approach and on-line DWT in the control design for actively control the L-shaped arm vibration system, and validate the control design in simulation and experiment. The aim of this research is to allow the motor move fast and reduce the arm vibration as much as possible while keeping the system to be robust stable.

2.7 Conclusion

In this chapter, the dynamics of the flexible arm and the piezoelectric actuator, the theoretical foundation of operator-based control and discrete wavelet transform are introduced. In addition, the problem to be tackled in this dissertation is stated, which provides framework of this study.

Chapter 3

Operator-based control design for the L-shaped arm without load

3.1 Introduction

To address the problems mentioned in Chapter 2, in this chapter, the dynamics on L-shaped arm vibration involving linear motor and piezoelectric actuator is modelled, controls for the motor motion and arm vibration are designed.

In **Section 3.2**, the vibration of the L-shaped arm is modelled by considering it as two connected Euler-Bernoulli beams, the relationship between the arm vibration and linear motor, piezoelectric actuator is given.

In **Section 3.3**, based on the operator-based nonlinear control approach, two controllers are designed to control the system in parallel. One controller is designed to allow the motor move fast to destination while reducing the arm vibration. Another one is designed to control the input of the piezoelectric

actuator to further reduce the arm vibration. The hysteresis nonlinearity of the actuator is modelled using a Prandtl-Ishlinskii hysteresis model, and the nonlinear part is compensated in the tracking controller.

In **Section 3.4**, simulation is conducted using the experimental data and comparing with the PI control, the results are shown to confirm the effectiveness of the proposed control design.

In **Section 3.5**, the conclusion of this chapter is given.

3.2 Model of the L-shaped arm vibration

In this dissertation, the L-shaped arm driven by a linear pulse motor which running along the horizontal motor guide is studied, the schematic diagram of the system is shown in Fig. 3.1. When the motor starts running, the arm will unavoidably vibrate.

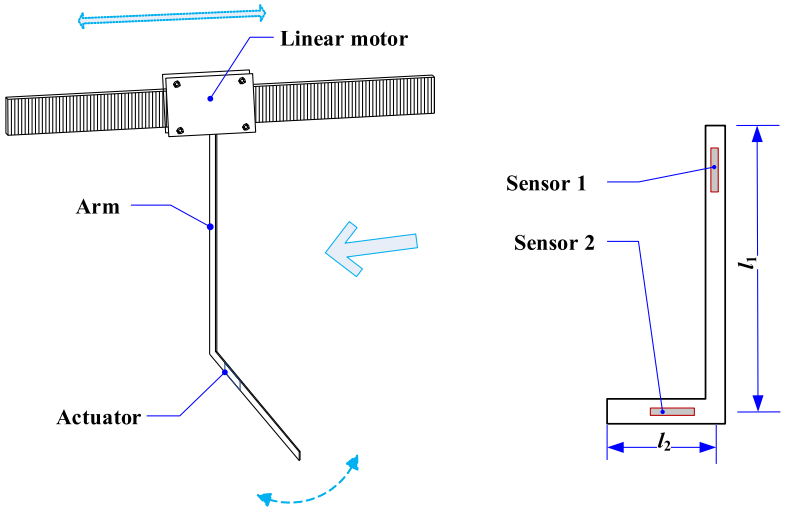

Figure 3.1: Schematic diagram of L-shaped arm system

For easy modelling, the arm is considered as two parts, Arm 1 for vertical

part and Arm 2 for horizontal part. The arm is connected with the motor, when the motor moves, the acceleration or deceleration will cause vibration of the arm. In addition, the transient vibration of motor and the uneven friction between the motor and guide will cause the arm additional vibration. In this chapter, the influences beside the acceleration of the motor will be considered as uncertainties or disturbances of the plant. The transverse vibration of Arm 1 is subjected to the excitation of linear pulse motor, and the Arm 2 subjected to the excitation from Arm 1, both are seen as clamped-free Euler-Bernoulli beams [77]. When modelling the vibration of Arm 1, the Arm 2 is considered as a tip mass at the free end. The excitation on Arm 2 depends on the relative transverse vibrations of Arm 1. Neglecting the external damping factor, only considering the strain-rate damping, the vibration of the arm is represented as

$$\rho S \frac{\partial^2 y_i(x,t)}{\partial t^2} + E_a I \frac{\partial^4 y_i(x,t)}{\partial x^4} + c_s I \frac{\partial^5 y_i(x,t)}{\partial x^4 \partial t} = q_i(x,t) \tag{3.1}$$

where $y_i(x,t)$ is the transverse displacement relative to the clamped end of the arm along neutral axis, $q_i(x,t)$ is external distributed force on the arm, $i(i=1,2)$ is the order number representing for Arm 1 and Arm 2. ρ, S, E_a, I and c_s are density, cross-sectional area, Young's modulus, moment of inertia and strain-rate damping coefficient of the arm, respectively. The external force on Arm 1 is represented as

$$q_1(x,t) = -\left[\rho S + m_2 \delta(x - L_1)\right] \frac{F_{01}(t)}{m_1 + m_2} \tag{3.2}$$

where $\delta(\cdot)$ is the Dirac delta function, $F_{01}(t)$ is the force from the linear motor to drive arm, m_1, m_2 are the masses of Arm 1 and Arm 2, respectively.

Remark 3.1: *In Equation (3.2), the linear motor driving force F_{01} is an equivalent term, because the linear motor used in the experimental system is controlled using the speed mode. The certain level friction between slider and stator does not influence the motor motion, unless it exceeds the output range of the motor.*

The external forces on Arm 2 include the force from Arm 1 and the moment from the piezoelectric actuator, it is represented as

$$q_2(x,t) = -\frac{F_{12}(t)}{L_2} + M_p \frac{\partial^2}{\partial x^2}[H(x - x_{p2}) - H(x - x_{p1})] \tag{3.3}$$

where $F_{12}(t)$ is the equivalent force from Arm 1 driving Arm 2, M_p is the moment generated by the piezoelectric actuator. $H(\cdot)$ is a Heaviside function, x_{p1}, x_{p2} are positions of the piezoelectric actuator on Arm 2.

Considering the boundary conditions of the arm, based on the expansion theorem, the solutions of Equation (3.1) are obtained as

$$y_1(x,t) = \sum_{m=1}^{\infty} J_1^m(x) \int_0^t \left[e^{-\alpha_1^m(t-\tau)} \sin \omega_{1d}^m (t-\tau) f_1^m u_1(\tau)\right] d\tau, \tag{3.4}$$

$$y_2(x,t) = \sum_{m=1}^{\infty} J_2^m(x) \int_0^t \left[e^{-\alpha_2^m(t-\tau)} \sin \omega_{2d}^m (t-\tau)(f_2^m F_{12}(\tau) + f_3^m \tilde{u}_2(\tau))\right] d\tau. \tag{3.5}$$

where $m (m = 1, 2, 3, \cdots)$ is the vibration mode order, $u_1(t) = F_{01}(t)$ is the control input for the linear motor, $\tilde{u}_2(t) = M_p(u_2)(t)$ is the moment from the

piezoelectric actuator. f_i^m are coefficients relative to the external forces.

$$
\begin{aligned}
f_1^m &= -\frac{1}{m_1+m_2}\left[\rho S\int_0^{l_1}\Phi_1^m(x)dx + m_2\Phi_1^m(l_1)\right] \\
f_2^m &= -\frac{1}{L_2}\int_0^{L_2}\Phi_2^m(x)dx \\
f_3^m &= \frac{\partial\Phi_2^m(x_{p2})}{\partial x} - \frac{\partial\Phi_2^m(x_{p1})}{\partial x} \\
F_{12} &= m_2\frac{\partial y_1^2(l_1,t)}{\partial t^2}
\end{aligned}
$$

Other parameters in Equations (3.4) and (3.5) are expressed as follows.

$$
\begin{aligned}
J_i^m(x) &= \frac{\Phi_i^m(x)}{\omega_{id}^m}, & \omega_i^m &= (\frac{\lambda_i^m}{L_i})^2\sqrt{\frac{E_aI}{\rho S}}, \\
\zeta_i^m &= \frac{c_s\omega_i^m}{2E}, & \omega_{id}^m &= \omega_i^m\sqrt{1-\zeta_i^{m2}}, \\
\alpha_i^m &= \zeta_i^m\omega_i^m, & c_s &= c_mE_a.
\end{aligned}
$$

where $\Phi_i^m(x)$ is the mass normalized eigenfunction of the clamped-free arm for the m-th mode [77]. ω_i^m is the undamped natural frequency of the m-th mode, ω_{id}^m is the damped natural frequency, σ_i^m is the damping ratio. The dimensionless frequency parameter of the m-th mode λ_i^m could be obtained from the corresponding characteristic equations. The details about the vibration model arm with load are shown in Appendix A.

Remark 3.2: *In the experimental system, the Arm 2 is not lumped mass and the fixed mechanism of the arm will cause the model error. The vibration mode of the arm can be measured by sensors; the results could be used to estimate the equivalent parameters of the arm so as to correct the error.*

3.3 Proposed robust nonlinear control design

3.3.1 Control scheme for the Arm-Motor system

In the whole plant of the L-shaped arm system, there are three outputs and two inputs. By controlling the linear pulse motor and the piezoelectric actuator, Arm 1 and Arm 2 track the reference trajectories. In addition, the piezoelectric actuator and the arm vibration coupling with unknown disturbances from the motor are both nonlinear systems. To guarantee the robust stability of the system, in this dissertation, we design two controllers based on operator theory, the control scheme is shown in Fig. 3.2.

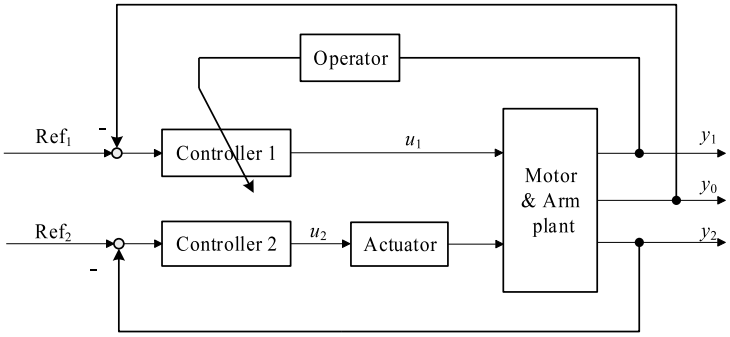

Figure 3.2: Proposed control scheme

Because the output of piezoelectric actuator is smaller enough comparing with the motor force, the piezoelectric actuator's impact on linear motor is neglected. The Controller 1 is designed to control the linear motor motion, the feedback operator is designed to keep the system stable and asymptotically convergent, such that the linear motor be faster and result in smaller arm vibration. The Controller 2 is designed to control the behaviour of the piezoelectric actuator to further reduce the vibration of the arm. The plant

outputs y_1 and y_2 are measured by the two piezoelectric sensors.

In detail, the relationship between the two control loops is shown as in Fig. 3.3. For the linear motor control, the inner loop is designed using operator theory to keep the plant stable and asymptotically convergence. The outer control loop is designed using Proportional-Integral (PI) controller combined with the feedback signals generated by the inner control loop, so as to control the linear motor motion with less time consuming and resulting in smaller arm vibration.

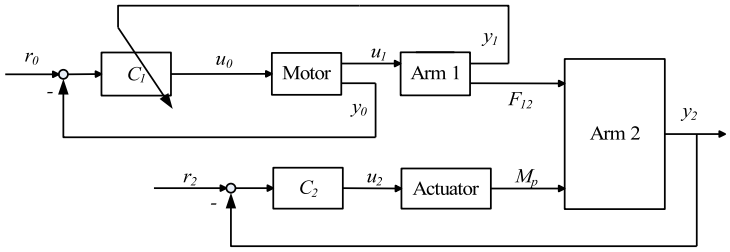

Figure 3.3: Proposed control loop structure

To reduce the measurement noise, filters are designed before the signals feedback. The appropriate filter type and structure depends on the noise feature. In this dissertation, we use an IIR low-pass filter and a notch filter [92–98], which will be discussed later. For simplicity, the filters are not shown in the following control designs, the feedback signals default to filtered signals from the sensors. The flowchart of the proposed control is shown in Fig. 3.4.

3.3.2 Operator-base system representation

Assuming that the uncertainties of the two plants are additive uncertainties, represented as ΔP_i. Using operator theory mentioned above, the two plants

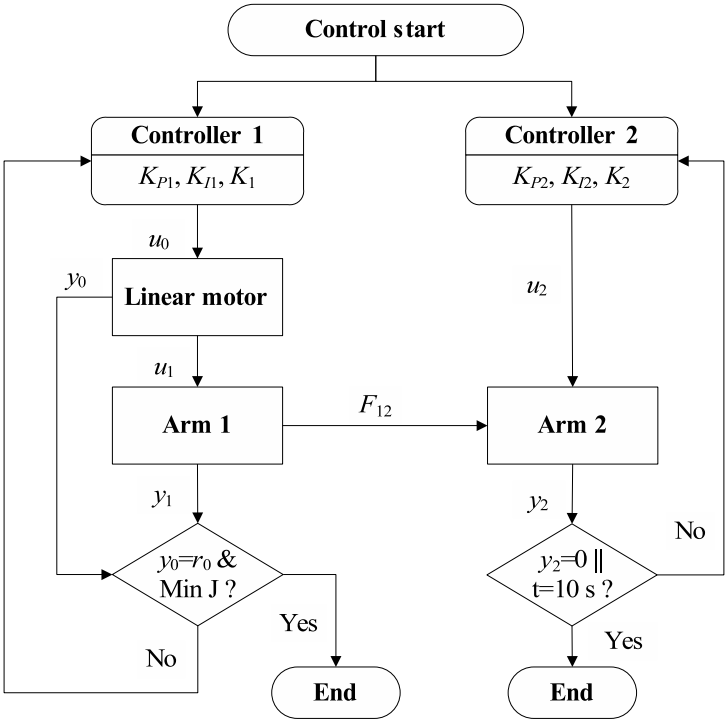

Figure 3.4: The proposed control flowchart

of the control object including linear pulse motor and piezoelectric actuator are expressed as follows.

$$\begin{aligned}[P_1 + \Delta P_1]\,(u_1)(t) =& (1+\Delta_1)\sum_{n=1}^{3} J_1^n f_1^n \int_0^t \big[e^{-\alpha_n(t-\tau)} \\ & \cdot \sin\omega_{dn}(t-\tau)u_1(\tau)\big]d\tau, \qquad (3.6)\\ [P_2 + \Delta P_2]\,(u_2)(t) =& (1+\Delta_2)\sum_{n=1}^{3} J_2^n \int_0^t \big[e^{-\alpha_n(t-\tau)} \\ & \cdot \sin\omega_{dn}(t-\tau)u_2^*(\tau)\big]d\tau. \qquad (3.7)\end{aligned}$$

where P_1, P_2 represent for the plants of Arm 1 and Arm 2 vibration, respectively. $u_2^*(t) = f_2^n F_{12}(t) + f_3^n \tilde{u}_2(t)$ is the input for plant 2. Δ_i are uncertainties of the plants including modelling errors, transient vibration of motor, and

other influencing factors. The first three modes of arm vibration are considered in the plant; the other modes are regarded as uncertainty included in ΔP_i.

According to robust right coprime factorization, plant $P_i + \Delta P_i$ is factorized as follows.

$$D_1(\delta_1)(t) = e^{-\bar{\alpha}t}\delta_1(t), \tag{3.8}$$

$$[N_1 + \Delta N_1](\delta_1)(t) = (1 + \Delta_1)\sum_{n=1}^{3} f_1^n J_1^n e^{-\alpha_n t} \cdot \int_0^t e^{-\hat{\alpha}_n \tau} \sin \omega_{dn}(t-\tau)\delta_1(\tau)d\tau, \tag{3.9}$$

$$D_2(\delta_2)(t) = e^{-\bar{\alpha}t}\delta_2(t), \tag{3.10}$$

$$[N_2 + \Delta N_2](\delta_2)(t) = (1 + \Delta_2)\sum_{n=1}^{3} J_2^n e^{-\alpha_n t} \cdot \int_0^t e^{-\hat{\alpha}_n \tau} \sin \omega_{dn}(t-\tau)\delta_2(\tau)d\tau. \tag{3.11}$$

where $\bar{\alpha} = \sum_{n=1}^{3} \alpha_n$, $\hat{\alpha}_n = \bar{\alpha} - \alpha_n$. (3.8) and (3.10) can be written as $\delta_1(t) = D_1^{-1}(u_1)(t) = e^{\bar{\alpha}t}u_1(t)$ and $\delta_2(t) = D_2^{-1}(u_2^*)(t) = e^{\bar{\alpha}t}u_2^*(t)$. Then we can obtain that $P_1 = N_1 D_1^{-1}$ and $P_2 = N_2 D_2^{-1}$.

3.3.3 Optimal control for the linear pulse motor

The vibration source of arm includes the linear pulse motor's acceleration and its transient vibration. In this dissertation, we only consider the first factor, the transient vibration of motor is seen as uncertainty. It is an underactuated nonlinear plant with two outputs and only one input. Because linear pulse

motor can be seen as a linear system and its acceleration or deceleration decide the arm vibration, the arm vibration displacement can be reduced by controlling the motor motion. However, reducing the acceleration of linear motor will consume more time to get to the destination, there must be a trade-off between the duration of linear motor and vibrating displacement of arm. Therefore, an optimal trajectory for the linear motor motion that consume short travel time with less arm vibration displacement is needed. A cost function is defined as follows.

$$J = t_f - t_0 + \frac{\sigma}{t_f} \int_{t_0}^{t_f+\Delta t} y_1^2(t)dt \tag{3.12}$$

where J is the cost index, t_0 and t_f are the starting time and final time, respectively. σ is a weighting factor for tuning the weight of arm vibration in the cost index. To reflect the vibration during and after motion, the vibration in a period Δt after the motion stop is considered in the function. The optimal problem is to minimize the cost index J.

To make the motor move for a distance r_0 in finite time, we firstly design a Proportional-Integral (PI) tracking controller C_0, b_1 from the operator A_1 is considered as compensation for motor control to reduce the arm vibration. Then, for the plant of Arm 1, operator-based controllers A_1 and B_1 keep it stable. The control scheme for linear motor control considering arm vibration is shown as in Fig. 3.5, Where y_0, y_1, r_0 and C_0 are the moving distance of linear motor and the relative displacement of Arm 1, tracking references and tracking controller for the linear motor, respectively. M stands for the linear motor, B_0 is an operator to satisfy the stable conditions. As motor M is

a linear system and the output is proportional to its real input, so we can combine it in the right coprime factorization, namely, $B_1(u)(t) = B_0(u)(t)$.

$$C_0(e_0)(t) = K_{I1} \int_0^t e_0(\tau)d\tau + K_{P1}e_0(t) \tag{3.13}$$

where K_{I1} and K_{P1} are design parameters, $e_0(t)$ is the error between the output $y_0(t)$ and the target value $r_0(t)$.

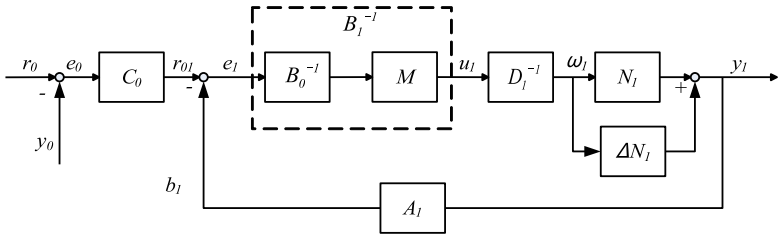

Figure 3.5: Operator-based control system for linear motor

With certain final time t_f and weighting factor σ, the cost index J depends on the gain parameters in operator-based controller and K_{I1} or K_{P1}. Therefore, by selecting a weighting factor σ, the appropriate control parameters can be determined by the minimum cost index J. The linear pulse motor used in this system has speed and acceleration constraints in practical experiments. Under the limits of linear motor, the minimum consuming time t_{fmin} can be determined, starting from t_{fmin}, the different cost index J can be obtained by iterative algorithm.

Using right coprime factorization, the operator-based controllers A_1 and

B_1 for the plant P_1 can be obtained as

$$A_1(y_1)(t) = b_1(t) = \frac{e^{-\alpha_1 t} - K_1}{J_1 \omega_{1d}} \eta_1(t), \tag{3.14}$$

$$\eta_1(t) = \ddot{y}_1 + 2\alpha_1 \dot{y}_1 + (\alpha_1^2 + \omega_{1d}^2) y_1, \tag{3.15}$$

$$B_1(u_1)(t) = K_1 u_1(t). \tag{3.16}$$

where K_1 is a design parameter for tuning the feedback signal from operator A_1. The controllers A_1 and B_1 guarantee the control system to be BIBO stable and robust, the PI tracking controller C_0 with optimization makes the linear motor track the target value r_0. Therefore the motor moves to the desired position with less arm vibration during and after its travel. The operator based optimal control ensures the arm vibration to be stable, and asymptotically converge to zero.

3.3.4 Control system for Arm 2 vibration with piezoelectric actuator

Considering the advantages of piezoelectric materials, in this dissertation, we use piezoelectric sensors and actuator to control the vibration of arm. Because of the hysteresis nonlinear property, the relationship between the moment output M_p of the piezoelectric actuator and the control input is a nonlinear process. In this dissertation, the hysteresis model is represented as follows.

$$M_p(t) = D_{PI}(u)(t) + \Delta_{PI}(u)(t) \tag{3.17}$$

where D_{PI} and Δ_{PI} are represented by the Prandtl-Ishlinskii model using play hysteresis operators, for the details, please refer to [73, 74]. D_{PI} is an

invertible operator, Δ_{PI} is the residual part stands for the nonlinear part of the model, it changes with the input $u(t)$ and is influenced by design parameters, so it needs to be compensated in the control.

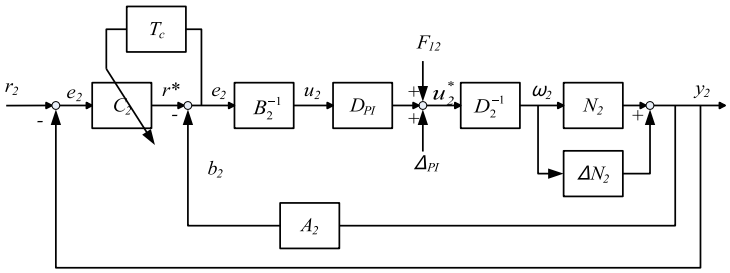

Figure 3.6: Control scheme for Arm 2 vibration

By controlling the motor motion, the first controller can only reduce the vibration of arm at a certain degree but never eliminate it. For Arm 2, we use piezoelectric actuator to suppress the rest vibration. The control input u_2 is the voltage applied to piezoelectric actuator, the output y_2 is the displacement of Arm 2. The control target is to eliminate the vibration of Arm 2, namely, $r_2 = 0$. The control design is shown in Fig. 3.6.

For a certain piezoelectric actuator, D_{PI} is a constant. It is combined into the plant P_2, and denote that $\tilde{D} = D_{PI}^{-1} D$. The residual part Δ_{PI} is a bounded uncertainty, will be compensated by a compensator T_c. Under the new equivalent plant $\tilde{D}$, based on Equation (2.15), the operators A_2 and B_2 are required to satisfy Bezout identity $A_2 N_2 + B_2 \tilde{D}_2 = \tilde{U}$, then A_2 and B_2

are obtained as follows.

$$A_2(y_2)(t) = \frac{e^{-\alpha_2 t} - K_2 K^{-1}}{J_2 \omega_{2d}} \eta_2(t), \tag{3.18}$$

$$\eta_2(t) = \ddot{y}_2 + 2\alpha_2 \dot{y}_2 + (\alpha_2^2 + \omega_{2d}^2) y_2,$$

$$B_2(u_2)(t) = K_2 K(u_2)(t). \tag{3.19}$$

where K_2 is a design parameter. According to the robust right coprime factorization approach, with operators A_2 and B_2, the control system is guaranteed to be BIBO stable. Moreover, if robust condition (2.19) is satisfied, the designed control system is said to be robust.

Remark 3.3: *In Equations (3.14) and (3.18), the output signals y_1 and y_2 are ideal displacement of Arm 1 and Arm 2, respectively. In the experimental system, they may include measuring errors caused by disturbances. Therefore, appropriate filters should be designed, and use the filtered signal in the controllers A_1 and A_2.*

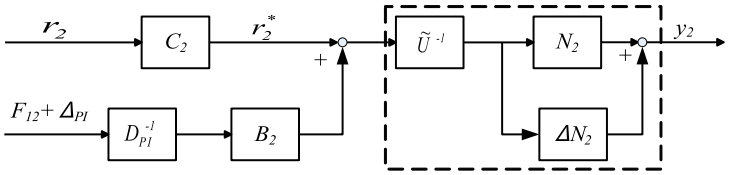

Figure 3.7: Equivalent control system with hysteresis compensator

The compensator T_c is designed to compensate Δ_{PI} and the external force F_{12} on Arm 2. Therefore, an equivalent diagram of control system in Fig. 3.6 is shown as in Fig. 3.7, and the equivalent plant output is expressed as follows.

$$y_2(t) = (N_2 + \Delta N_2)\tilde{U}^{-1}(r^*(t) + B_2 D_{PI}^{-1}(\Delta_{PI} + F_{12})) \tag{3.20}$$

From Fig. 3.7, we can find that the dis-invertible part Δ_{PI} and external force F_{12} can be compensated in the tracking controller C_2, and the control pant is kept BIBO stable and tracks the reference.

Based on the above two operator-based control designs, the robust stability of the whole plant is guaranteed, the three outputs track the reference values. It means that the linear motor runs to destination in finite time, while the vibrations of Arm 1 and Arm 2 are reduced as small as possible.

3.4 Simulation results and discussion

To demonstrate the effectiveness of the proposed design scheme, simulations were conducted by using MATLAB. Parameters of the L-shaped arm and the linear pulse motor are shown in Table 3.1 and Table 3.2, respectively.

Table 3.1: Some parameters of the L-shaped Arm

Parameter	Definition	Value	Units
l_1	Length of OA	0.5	m
l_2	Length of AB	0.3	m
w_a	Width of arm	0.02	m
t_a	Thickness of arm	0.003	m
ρ	Density of arm	8030	kg/m^3
E_a	Young's modulus	197×10^9	N/m^2
c_1	Damping modulus	5×10^{-4}	$-$
x_{p1}	Left end of PZT on AB	0.04	m
x_{p2}	Right end of PZT on AB	0.09	m

In the simulation, the sampling interval was 0.01 s, the output y_0 was controlled to move in one direction for a distance of 0.5 m. The aim of linear

Table 3.2: Parameters of the linear pulse motor

Parameter	Definition	Value	Units
M	Mass of linear motor	1.6	kg
f_s	Friction coefficient of motor	0.48	$N/(m/s)$
r_0	Moving distance	0.5	m
V_{min}	Minimum speed of motor	0.75×10^{-3}	m/s
V_{max}	Maximum speed of motor	0.15	m/s
A_{min}	Minimum accelerate of motor	0.0562	m/s^2
A_{max}	Maximum accelerate of motor	9.09	m/s^2

motor motion control is to reduce the tip displacement of Arm 1 while the motor running as faster as possible with an optimal trajectory.

To be consistent with the experimental conditions, the speed and acceleration of linear motor were limited within a scope. For the piezoelectric actuator control, the voltage was applied when $t > 0$ s, output y_2 was controlled to track zero.

For comparison, firstly we conduct a simulation of the linear motor with minimal time feed-forward control, namely, the motor runs under the maximum speed and acceleration. The vibration of Arm 1 during and after the linear motor motion is shown as the dashed line in Fig. 3.8. As can be seen from the results, the linear motor stops with minimum time consumption at 3.4 s, which leads to biggest arm vibrations, especially at the moment the linear motor starts and stops, which was caused by its biggest accelerations and decelerations, respectively.

Then, by using PI controller without feedback signal from the vibration

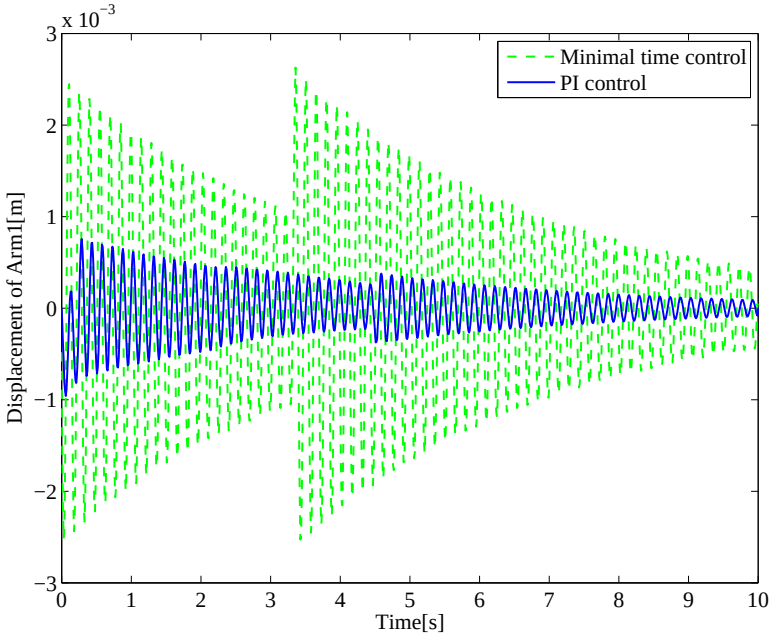

Figure 3.8: Displacement of Arm 1 with and without feedback control

of arm, the motor position and speed is shown in Fig. 3.9. The corresponding vibration of Arm 1 with PI control is compared with the result under minimal time control, as shown in Fig. 3.8, the solid line is displacement under PI control. It illustrates that with PI control, the arm vibration was reduced, but the travel time of the linear motor was longer, arriving at the destination within 4.5 s.

For the optimization problem as shown in Equation (3.12), under a certain weighting factor $\sigma = 1.5 \times 10^7$, and the after stop duration was setted as 0.15 s, with different design parameters, the corresponding cost index J is shown in Fig. 3.10. It illustrates that, by selecting appropriate parameters PI gains K_{P1} or K_{I1} and the operator feedback factor K_1, the cost value can be

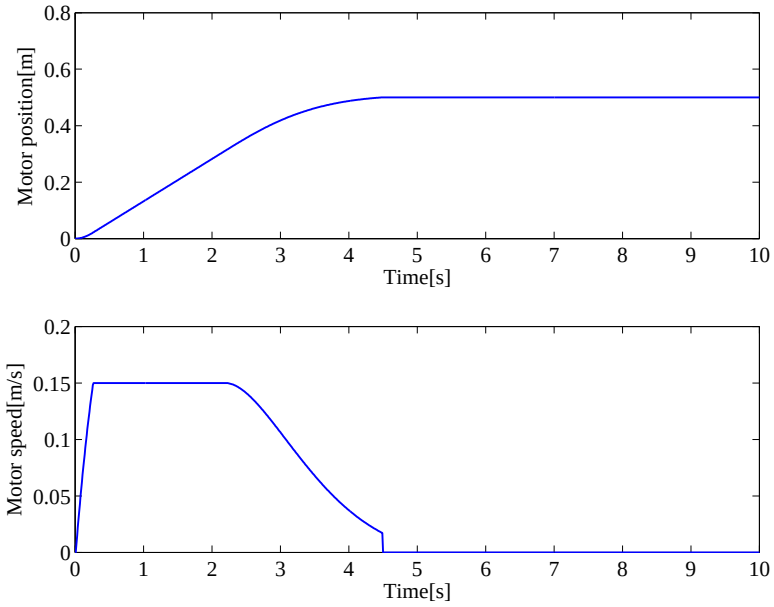

Figure 3.9: Position and speed of motor (with PI control)

minimized, namely, the linear motor motion and arm vibration are balanced.

The corresponding simulation results using the operator-based optimal control for motor motion is shown in Fig. 3.11. The displacement of Arm 1 with the two controllers are shown in Fig. 3.12, the dashed line is displacement with PI control, the solid line is displacement with operator-based optimal control. The results show that the linear motor with operator-based control moves to the desired position within 4.5 s, same as PI control. However, the displacement of Arm 1 was smaller than it under PI control. It illustrates that with the optimal feedback signal of arm vibration, the controller using operator theory can reduce the vibration of arm, especially, the after stop arm vibration was reduced significantly, and the plant was kept to

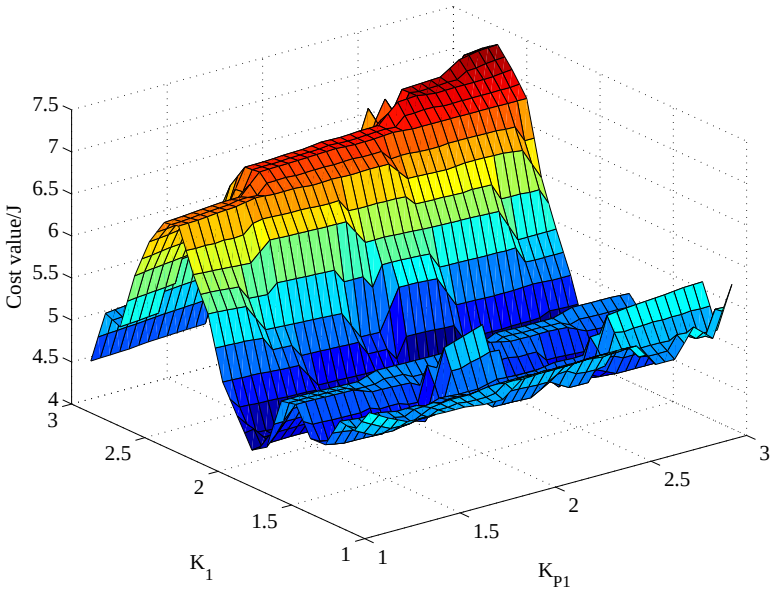

Figure 3.10: Cost indexes under optimal control with different parameters

be stable.

The vibration of Arm 2 without actuator, with actuator no hysteresis compensation and with hysteresis compensation were simulated for comparison. Displacement of Arm 2 without the piezoelectric actuator control and with control but without considering hysteresis are shown in Fig. 3.13, the dashed line is vibration of Arm 2 without control, the solid line is vibration of Arm 2 with actuator control, which indicates that the piezoelectric actuator can reduce the arm vibration with the proposed control. The corresponding control input is shown in Fig. 3.14.

Furthermore, by using the hysteresis compensation tracking controller T_C, the output of Arm 2 is shown in Fig. 3.15 together with the results under control without compensation. The vibration result without compensation

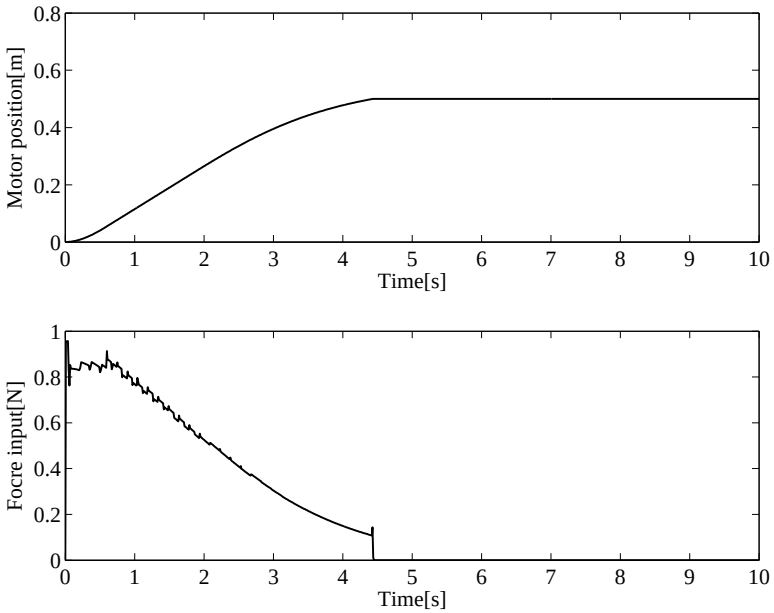

Figure 3.11: Position speed of motor (with optimal control)

shown in dashed line, the solid line the result using the compensator. The corresponding control input is shown in Fig. 3.16. Fig. 3.15 shows that the proposed controller is effective to further reduce the vibration of arm, which means that both the model of hysteresis and the designed hysteresis compensator are effective.

3.5 Conclusion

In this chapter, an L-shaped arm driven by a linear pulse motor was considered to find approaches to control the forced vibration of arm. By considering the L-shaped arm as two connected Euler-Bernoulli beams, the dynamics on arm vibration involving linear motor and piezoelectric actuator was modelled. Two operator-based robust nonlinear control systems were proposed

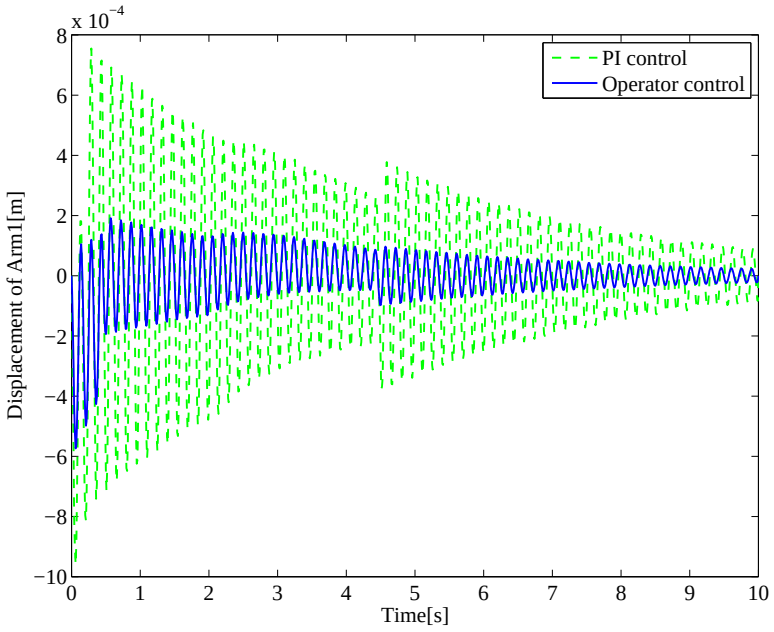

Figure 3.12: Displacement of Arm 1 with PI motor control and proposed motor control

in this chapter, the first one was designed to make the motor not only move to destination in certain time but also reduce the vibration of arm. Another one was designed to control the input of the piezoelectric actuator, the hysteresis nonlinearity of the actuator was modelled using a Prandtl-Ishlinskii hysteresis model, and the nonlinear part was compensated in the tracking controller. Finally, to confirm the effectiveness of the proposed control design, simulations were conducted comparing with the PI control, the results illustrate that the operator-based control systems designed in this dissertation are more effective and can guarantee the system robust stability.

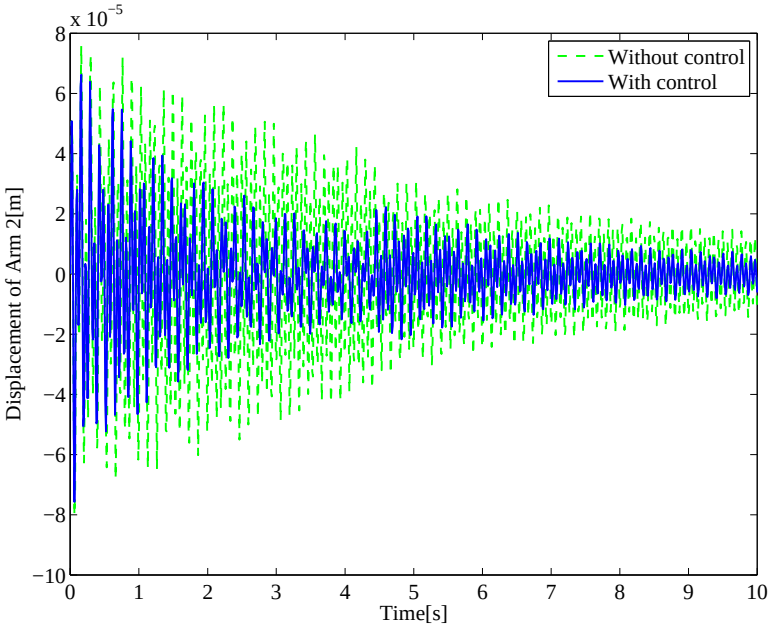

Figure 3.13: Displacement of Arm 2 without and with actuator control (without hysteresis compensation)

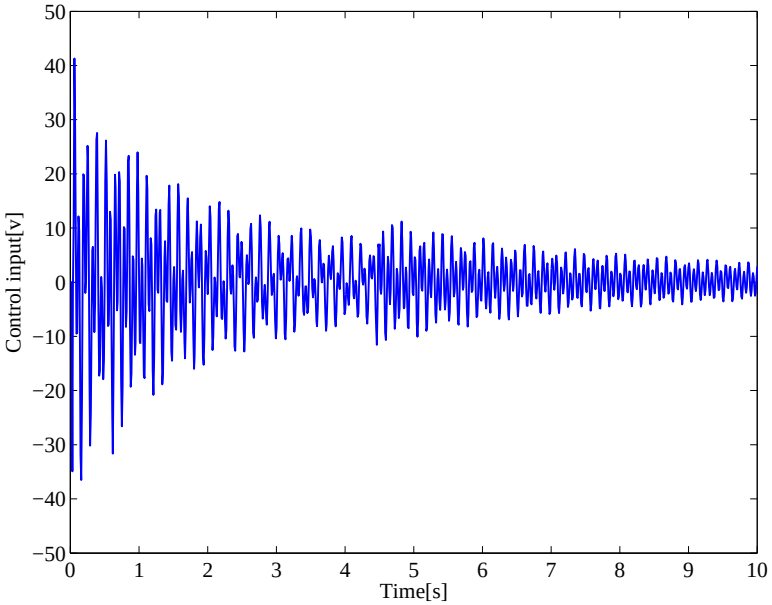

Figure 3.14: Control input for actuator without hysteresis compensation

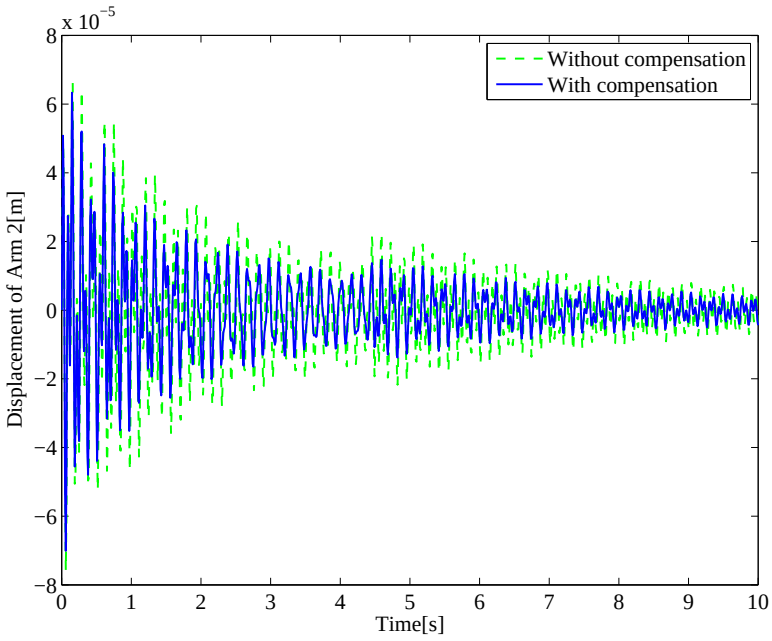

Figure 3.15: Displacement of Arm 2 without and with hysteresis compensation

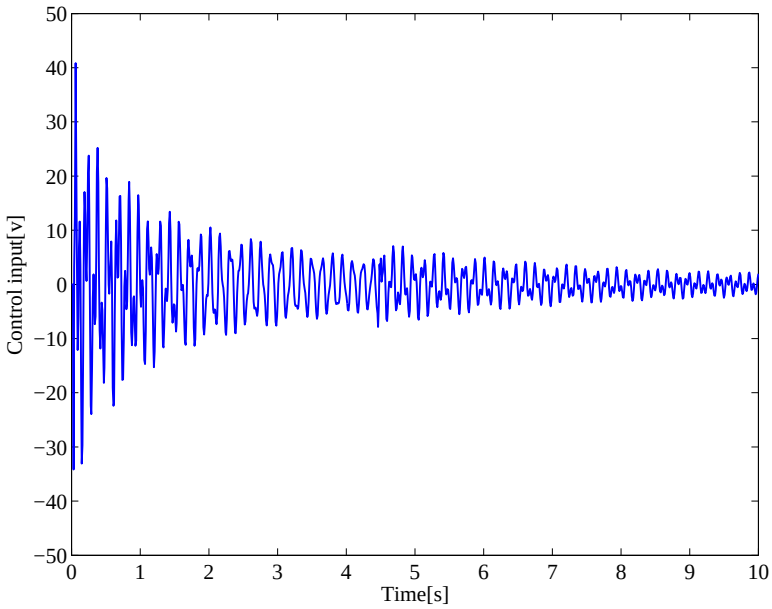

Figure 3.16: Control input for actuator with hysteresis compensation

Chapter 4

Operator-based control design for the L-shaped arm with unknown load

4.1 Introduction

In the above Chapter, the L-shaped arm considered is load-free, and the arm vibration is modelled by assuming the arm as two separated segments. In practice, the arm manipulates different loads, which determines the parameters in the controller relating to the plant dynamics. It is inconvenient to measure the load mass in advance. Therefore, an automatic load mass estimation combined with the controller is necessary. In addition, the operator-based control uses the outputs of system directly as feedback signals for the controller, the system performance is influenced by the quality of the signal. The disturbances and uncertainties will lower the control performance. For this end, the output signal should be processed by appropriate measures, wavelet transform can undertake such tasks.

In **Section 4.2**, different from last Chapter, the L-shaped arm is modelled as a whole, the load is considered in it. The load estimation method is given based on the model.

In **Section 4.3**, base on the DWT theory, a short-symmetrical on-line DWT is constructed to use it in the operator-based control design.

In **Section 4.4**, based on the right coprime factorization method, two operator-based controllers are proposed by using the on-line DWT in it. One controls the motor motion resulting in less arm vibration. Another one further reduces the arm vibration by using a piezoelectric actuator.

In **Section 4.5**, simulations comparing with previous control are demonstrated to validate performance of the proposed control design.

In **Section 4.6**, the main contends of this Chapter is summarized.

4.2 Modelling of the system with load

4.2.1 Model of arm vibration with load

In this chapter, the uniform steel L-shaped arm with load is considered, the Motor-Arm structure is shown in Fig. 4.1. The arm is driven by a linear pulse motor to the destination along the motor guide in y direction.

To analyse the arm vibration dynamics easily and illustrate it clearly, the L-shaped armed is marked with two segments OA and AB, as shown in Fig. 4.2. Two piezoelectric sensors are pasted on one side of the arm to measure the relative vibration displacements of the arm, one at the OA segment, another at AB segment. A piezoelectric actuator is mounted on the

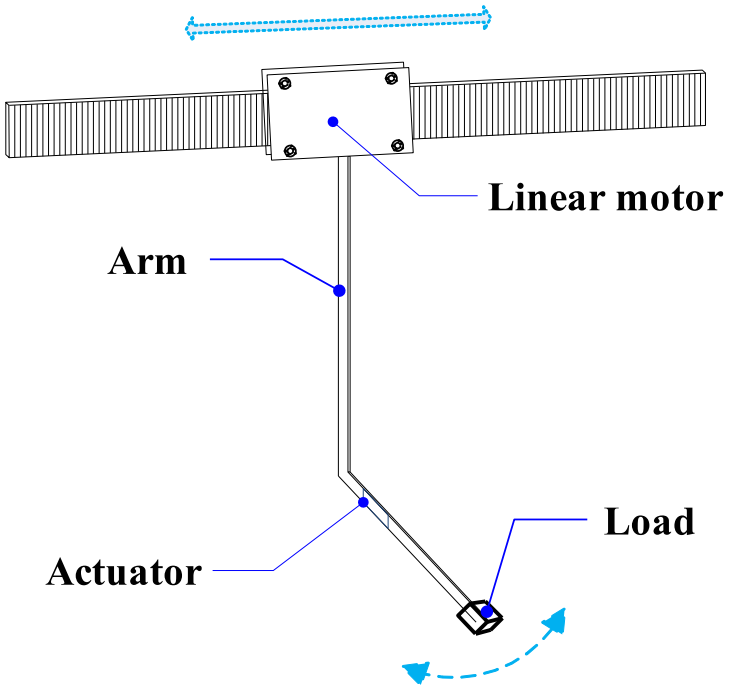

Figure 4.1: System structure

opposite side of AB segment to suppress the arm vibration. The linear motor runs in y direction along the frame, which will result in the arm vibration. Denoting the vibration displacement with time as $w(x,t)$, neglecting the torsional vibration, being seen as an Euler-Bernoulli beam [77], the forced transverse arm vibration is approximated as

$$E_a I \frac{\partial^4 w}{\partial x^4} + c_s I \frac{\partial^5 y(x,t)}{\partial x^4 \partial t} + \rho S \frac{\partial^2 w}{\partial t^2} = q(x,t) \tag{4.1}$$

where $q(x,t)$ is the external distributed forces on the arm, including the linear motor driving force and the piezoelectric actuator moment. w, stands for $w(x,t)$, is the transverse displacement along the neutral axis of the arm. E_a, I, ρ, S are the Young's modulus, moment of inertia, density, and cross-

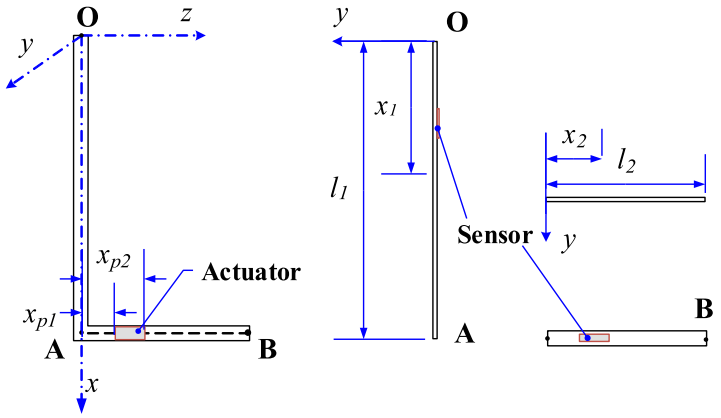

Figure 4.2: The sketch of the L-shaped arm

sectional area of the arm, respectively. The arm vibrations at two segments OA and AB can be determined by variables separation method based on the the boundary conditions and the initial conditions of the system, the details about the vibration model arm with load are shown in Appendix A.

We name the OA segment of the arm as Arm 1 and the AB segment as Arm 2, the relative vibration along Arm 1 as y_1, and vibration along Arm 2 as y_2, they are expressed as follows.

$$y_1(x_1,t) = \sum_{n=1}^{\infty} J_1^n(x_1) \int_0^t \left[e^{-\alpha_n(t-\tau)} \sin\omega_{dn}(t-\tau) f_1^n u_1(\tau)\right] d\tau, \tag{4.2}$$

$$y_2(x_2,t) = \sum_{n=1}^{\infty} J_2^n(x_2) \int_0^t \left[e^{-\alpha_n(t-\tau)} \sin\omega_{dn}(t-\tau)(f_2^n u_2(\tau) + f_3^n)\right] d\tau. \tag{4.3}$$

where, $n(n = 1, 2, 3, \cdots)$ is the vibration mode order, u_1 is the motor force acted on the arm, $u_2 = M_p$ is the moment generated by the piezoelectric actuator. $J_1^n = \Phi_1^n(x_1)/\omega_{dn}$, $J_2^n = \Phi_2^n(x_2)/\omega_{dn}$, $\alpha_n = c_1\omega_n^2$ is the damping factor of the arm vibration. f_i^n is the coefficients relative to the external

forces, shown as follows.

$$f_1^n = -\frac{\rho S}{m_s}\int_0^{l_1} \Phi_1^n(x_1)dx_1,$$
$$f_2^n = \frac{\partial \Phi_2^n(x_{p2})}{\partial x_2} - \frac{\partial \Phi_2^n(x_{p1})}{\partial x_2},$$
$$f_3^n = -\frac{\rho S}{m_s}\int_0^{l_2} \Phi_2^n(x_2)dx_2 - m_t\Phi_2^n(l_2).$$

where $m_s = m_a + m_t$ is the total weight of the arm with load, m_a is the mass of the arm. x_{p1}, x_{p2} are the positions of the both end of the actuator on AB section as shown in the arm sketch Fig. 4.2.

4.2.2 Load estimation method

As shown in the Appendix A, the mass of the load will impact the arm vibration dynamics, especially the important parameters in the vibration model, such as the natural frequency of every mode, the frequency decreases with the increasing of the load mass. According to Eq. (A.24), it obtains that

$$\beta_n = \sqrt[4]{\frac{\rho S(2\pi f_n)^2}{E_a I}} \tag{4.4}$$

From the Eq. (A.21) shown in Appendix A, it yields

$$m_t = \frac{P_I}{P_{II}}\frac{\rho S}{\beta} \tag{4.5}$$

where

$$P_I = \sin\beta l^- \sinh\beta l^+ - \sinh\beta l^- \sin\beta l^+ - 2\cos\beta l_2 \cosh\beta l_2 - 2\cos\beta l_1 \cosh\beta l_1$$
$$- 2\cos\beta l^+ \cosh\beta l^+ - 2$$
$$P_{II} = 2\cos\beta l^+ \sinh\beta l^+ - 2\cosh\beta l^+ \sin\beta l^+ + 2\cos\beta l_2 \sinh\beta l_2 - \cosh\beta l_2 \sin\beta l_2$$
$$+ \cos\beta l^- \sinh\beta l^+ - \cosh\beta l^- \sin\beta l^+ - \sin\beta l^- \cosh\beta l^+ - \sinh\beta l^- \cos\beta l^+$$

According to Eq. (4.5), the relationship between the first mode frequency and load mass is shown in Fig. 4.3.

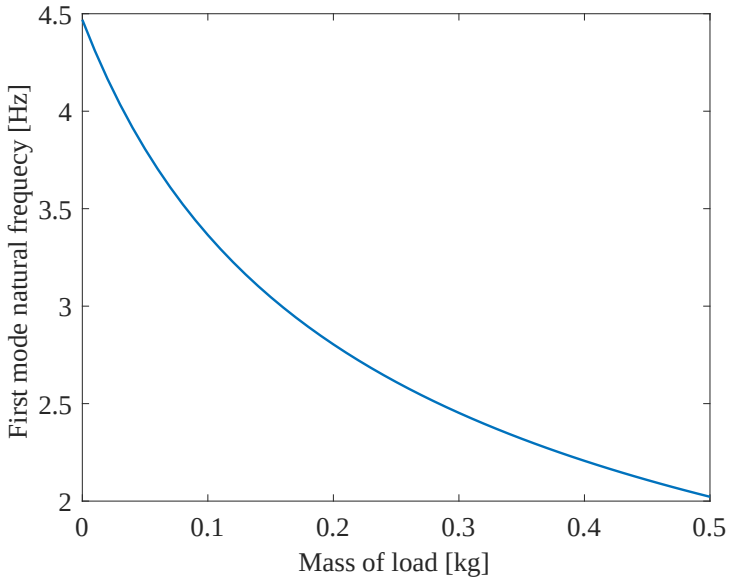

Figure 4.3: The relationship between the first mode frequency and load mass

If we can measure the natural frequency of one mode of the arm vibration in experiment, such as f_1 (Hz), according to the relationship in Eq. (4.4), β_1 is obtained, substitute it into the frequency equation (4.5), the mass of load could be estimated.

The load mass estimation flow is given as: initial vibration $\rightarrow y_1(t) \rightarrow$ DWT $\rightarrow$ reconstructed of the approximation of the first frequency band $\rightarrow$ FFT $\rightarrow f_1 \rightarrow$ equation (4.4) $\rightarrow \beta_1 \rightarrow$ equation (4.5)$\rightarrow$ load mass $\hat{m}_t$.

4.3 On-line wavelet transform

The DWT decomposes a time domain signal into an orthogonal set of wavelets, presented in time-frequency domain, which is useful for different purposes. However, most DWT applications are off-line needing the entire signal. These approaches are not suitable for the real-time vibration control. To solve the problem and apply wavelet transforms to arm vibration controls, a real-time wavelet approach is implemented in this section.

The on-line DWT usually utilizes a moving window . When the control loop starts, the on-line DWT must wait for the available signal with length equal to l_n. The lager the l_n, the more significant time delay. On the other hand, with smaller l_n, the DWT results in lower accuracy. In this dissertation, the size of the moving window l_n depends on the sampling frequency and the vibration frequency band considered in the controller. For a certain f_s, the considered frequency band decides the wavelet decomposition levels L, then the size of the moving window l_n is decided.

To deal with the boundary effects, one of the methods is artificially extend the signals at boundaries before processing. Symmetric extension is usually adopted to keep the continuity. However, the whole symmetrization will increase the computation load, probably causes time delay for the control and lower the performance. Therefore, we extend the data stream using short-symmetrical, the length of extension is denoted as l_t, $l_w = l_n + l_t$, l_w is the length of signal for on-line DWT, requiring $l_w \geq 2^L$. The moving window

and $\hat{y}$ are defined as follows.

$$W_i = \begin{cases} none, & i < l_n \\ y(i-l_n+1), \cdots, y(i), y(extension), & i \geq l_n \end{cases} \tag{4.6}$$

$$y(extension) = [y(i), \cdots, y(i-l_t+1)]$$

$$\hat{y}(i) = \begin{cases} y(i), & i < l_n \\ y_{wti}(l_n), & i \geq l_n \end{cases} \tag{4.7}$$

where $y_{wti} = DWT(W_i)$ is the output of the on-line DWT for the moving window W_i. The on-line DWT process is shown in Fig. 4.4.

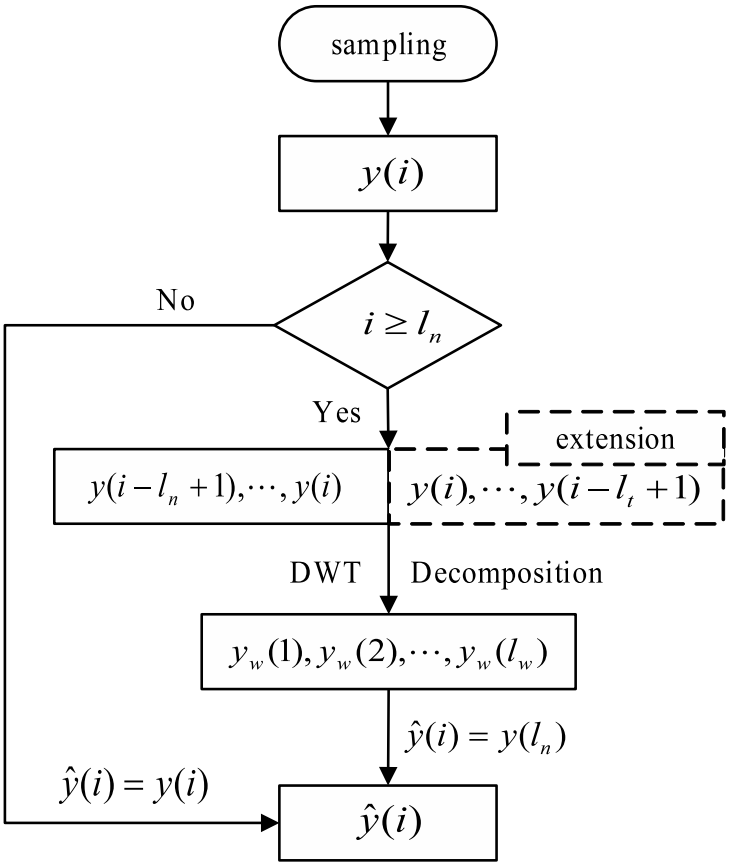

Figure 4.4: On-line DWT processing flow

4.4 Operator-based control design with DWT

For some nonlinear systems, the disturbances are complicated and unknown. It is difficult to satisfy the factorization conditions and robustness condition as shown in (2.19). In addition, if the disturbances include high frequency signal, the system output will fluctuate severely; the performances of the system will degrade. Therefore, we use an on-line DWT in the operator-based control, the control scheme is shown in Fig. 4.5. A DWT processor is added between the system output y_a and operator A to decompose the output y_a into time-frequency domain. According to the characteristics of the system dynamic, the necessary signal components are extracted and reconstructed as $\hat{y}$. If the unwanted disturbances are fully removed, namely $\hat{y} \simeq y$, the coprime condition (2.18) approximates the condition (2.15), then the desired operators A and B could be obtained more easily.

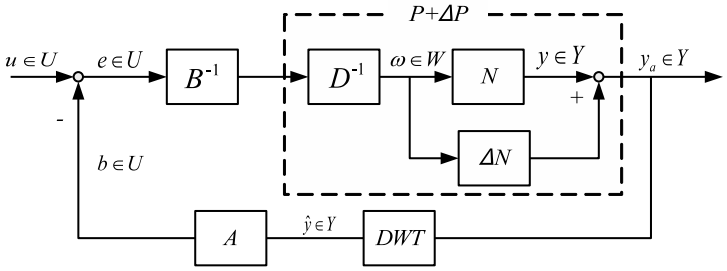

Figure 4.5: Nonlinear operator-based robust control with DWT

4.4.1 Control scheme for the Arm-Motor system

Based on the discrete wavelet transform (DWT) and the operator-based nonlinear control, we propose a control scheme as shown in Fig. 4.6. It includes

two wavelet-operator-based controllers, the Controller 1 is designed to control the linear motor motion; the Controller 2 is designed to control the behaviour of piezoelectric actuator. They work together to satisfy all of the requirements. ref_1 and y_0 are the target position and real-time position of the linear motor respectively. The control flow is shown in Fig. 4.7, where y_{a1} and y_{a2} are displacements of the arm vibration at OA and AB segments, respectively. u_0, u_1 and u_2 are the control inputs for the linear motor, Arm 1 and Arm 2, respectively. K_P, K_I, K_1 and K_2 are the tuning parameters for the designed controllers. Through the Controller 1, the linear motor is controlled to move to the destination fast while reducing the vibration of the arm. The Controller 2 further reduce the vibration of arm by controlling the piezoelectric actuator output. The system outputs are measured by the two piezoelectric sensors; the sampled signals contain noise and disturbances. Therefore, two wavelet transform processor works together with the operator-based controllers, remove the undesired uncertainties and disturbances, keep the system stable and robust.

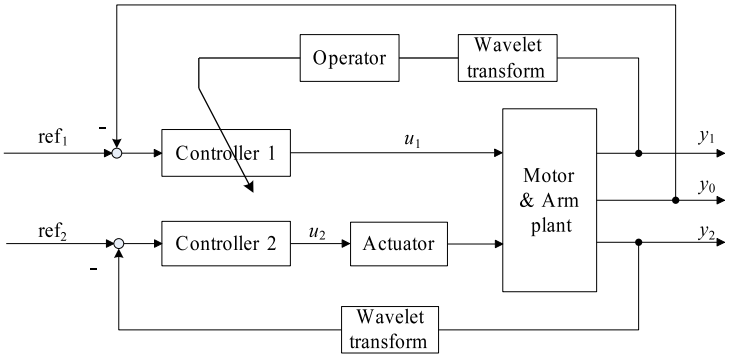

Figure 4.6: Proposed control scheme for the arm with load

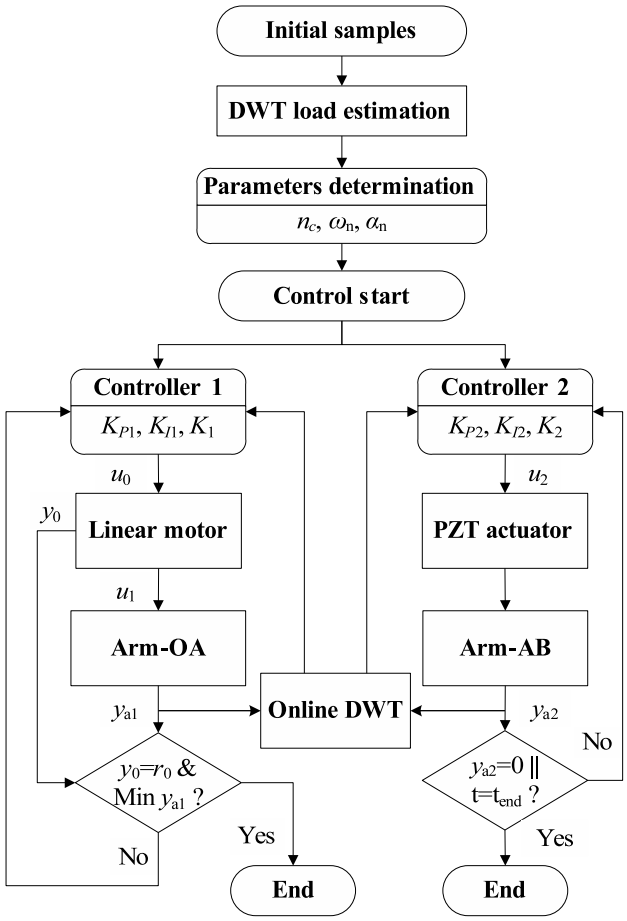

Figure 4.7: Proposed control flow chart

As shown in the dynamics of the arm vibration (4.2) and (4.3), they are superposition of infinite modes vibration. It is difficult to design the operator-based controllers with thus models. Therefore, the dominant vibration modes should be selected without loss of the system characteristic. According to the contributions of different modes in the whole vibration, we propose a

threshold and the dominant vibration modes are determined as follows.

$$\begin{aligned} r_{mode}(n_c) &:= \frac{J_2^{n_c}(l_2)}{\sum_{n=1}^{n_c} J_2^n(l_2)} \geq r_{th} \\ r_{mode}(n_c+1) &< r_{th} \end{aligned} \tag{4.8}$$

where $r_{mode}(n_c)$ stands for the contributions of the n_c mode in the first n_c modes vibration, r_{th} is the threshold. It means that in the whole displacement, the proportion of the modes higher than $n_c + 1$ is small enough, they are neglected. In the controlled plant, we only consider the first n_c modes of arm vibration.

Remark 4.1: *r_{mode} is derived from the relative vibration dynamics of Arm 2 (4.3). Considering am impulse force is applied on the arm, without control, the n mode response at the tip of the arm is denoted as $y_2^n(l_2, t)$, then*

$$r_{mode}(n_c) := \frac{|y_2^{n_c}(l_2,t)|_{max}}{|\sum_{n=1}^{n_c} y_2^n(l_2,t)|_{max}} \approx \frac{J_2^{n_c}(l_2)}{\sum_{n=1}^{n_c} J_2^n(l_2)}$$

4.4.2 Control design for the linear pulse motor

As shown in the control scheme Fig. 4.6, the linear motor control has two output y_0 and y_1 with only one input u_0. The control target is to allow the linear motor to the destination as fast as possible while reducing the arm vibration.

By using the right coprime factorization method, plant $P_1 + \Delta P_1$ is factorized as follows.

$$D_1(\delta_1)(t) = e^{-\bar{\alpha}t}\delta_1(t), \tag{4.9}$$

$$[N_1 + \Delta N_1](\delta_1)(t) = (1+\Delta_1)\sum_{n=1}^{N_d} f_1^n J_1^n e^{-\alpha_n t}\int_0^t e^{-\hat{\alpha}_n \tau}\sin\omega_{dn}(t-\tau)\delta_1(\tau)d\tau, \tag{4.10}$$

where $\bar{\alpha} = \sum_{n=1}^{N_d} \alpha_n$, $\hat{\alpha}_n = \bar{\alpha} - \alpha_n$.

It is necessary to mention that the dynamics of the arm vibration are superposition of infinite modes. It is difficult to design an operator-based controllers with all models. Therefore, the dominant vibration modes should be determined without loss of the system characteristic. It depends on the sampling interval and vibration dynamics in experiments. To allow the linear

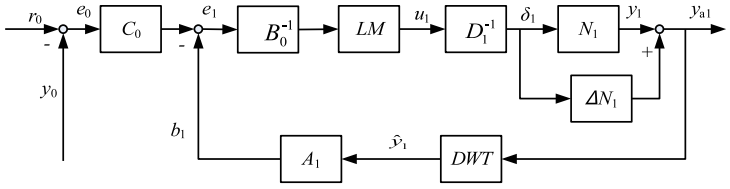

Figure 4.8: Operator-based linear motor motion control using DWT

motor to the destination r_0 in finite time, a PI tracking controller C_0 is used. To reduce the arm vibration, a wavelet-based operator is involved, working as a feedback compensator. the compensator depends on the arm vibration. The control scheme for linear motor control considering arm vibration is shown in Fig. 4.8, where LM represents for the linear motor, A_1, B_0 are the designed operators to satisfy the stable conditions. The real output y_{a1} includes disturbances and uncertainties, which will feedback an undesired fluctuation signal, it will cause the linear motor unnecessary motion resulting in performance degradation. Therefore a DWT is utilized to work with the operator A_1, to remove the undesired disturbances in the signal. The tracking controller C_0 is shown as follows.

$$C_0 := K_{I1} \int_0^t e_0(\tau) d\tau + K_{P1} e_0(t) \tag{4.11}$$

where K_{I1} and K_{P1} are design parameters, $e_0(t)$ is the error between the output $y_0(t)$ and the target value $r_0(t)$. To balance the speed of the linear motor and the arm vibration, a cost index J proposed in last chapter is used. By tuning the gain parameters K_{I1} or K_{P1} and the parameter for the operator, a desired motor motion is obtained.

Based on the operator theory, according to the factorization as in (4.9) and (4.10), we design operators A_1 and B_1 to satisfy the stable condition.

$$A_1(\hat{y}_1)(t) = b_1(t) = \frac{e^{\bar{\alpha}_1 t} - K_1}{J_{c1}\omega_{d1}}\eta_1(t), \tag{4.12}$$

$$\eta_1(t) = \ddot{\hat{y}}_1 + 2\alpha_1\dot{\hat{y}}_1 + (\alpha_1^2 + \omega_{d1}^2)\hat{y}_1, \tag{4.13}$$

$$B_1(u_1)(t) = K_1 u_1(t). \tag{4.14}$$

where $J_{c1} = C f_1^1 J_1^1$, C is a parameter decided by ω_n; K_1 is a tuning parameter for control the feedback from operator A_1. Then the force input of the motor is shown as follows.

$$u_1(t) = {K_1}^{-1}\left[C_0(e_0)(t) - b_1(t)\right] \tag{4.15}$$

Operators A_1 and B_1 works together with the DWT processor to guarantee the robust stability of the system. Operator C_0 along with the operator feedback allow the linear motor to move fast while resulting in less arm vibration.

4.4.3 Control design for vibration of Arm 2 with the piezoelectric actuator

At the same time with the motor motion control, the piezoelectric actuator actuates to further reduce the arm vibration. By using the right coprime

factorization method, plant $P_2 + \Delta P_2$ is factorized as follows.

$$D_2(\delta_2)(t) = e^{-\bar{\alpha}t}\delta_2(t), \tag{4.16}$$

$$[N_2 + \Delta N_2](\delta_2)(t) = (1+\Delta_2)\sum_{n=1}^{N_c} J_2^n e^{-\alpha_n t}\int_0^t e^{-\hat{\alpha}_n\tau}\sin\omega_{dn}(t-\tau)\delta_2(\tau)d\tau. \tag{4.17}$$

Applying a control voltage u_2, the piezoelectric actuator outputs a moment M_p represented as follows.

$$M_p(t) = D_{PI}(u_2)(t) + \Delta_{PI}(u_2)(t) \tag{4.18}$$

$$D_{PI}(u_2(t)) = Ku_2(t) = \int_0^{H_t} p(h)dhu_2(t) \tag{4.19}$$

The first term D_{PI} is an invertible operator, another term Δ_{PI} represents for residual uncertain part including the hysteresis, it needs to be compensated by the controller. For the details of the model, please refer to the reference [24].

Without loss of the system stability, D_{PI} is combined with the operator D_2, and denote as $\tilde{D}_2 = D_{PI}^{-1}D_2$. Δ_{PI} and the driving force from the motor F_{02} are equivalently compensated before the BIBO stable loop. The $\hat{y}_2$ is obtained through the wavelet transform. Then, by using the above mentioned robust right coprime factorization method, operators A_2 and B_2 for the new plant $\tilde{P}_2 = N_2\tilde{D}_2^{-1}$ are obtained as follows.

$$A_2(\hat{y}_2)(t) = \frac{e^{\bar{\alpha}_2 t} - K_2K^{-1}}{J_{c2}\omega_{d2}}\eta_2(t), \tag{4.20}$$

$$\eta_2(t) = \ddot{\hat{y}}_2 + 2\alpha_2\dot{\hat{y}}_2 + (\alpha_2^2 + \omega_{d2}^2)\hat{y}_2,$$

$$B_2(u_2)(t) = K_2K(u_2)(t). \tag{4.21}$$

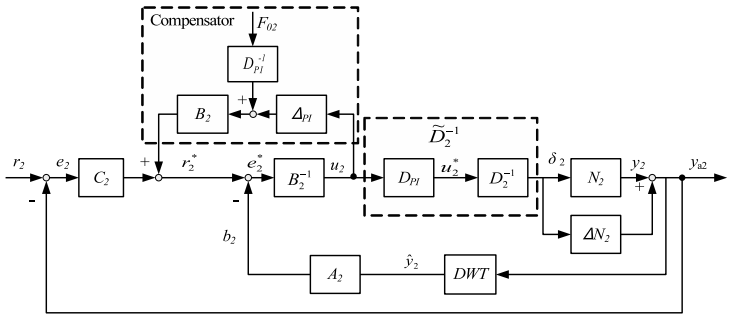

Figure 4.9: Operator-based control for Arm 2 with DWT considering hysteresis

where K_2 is a tuning parameter working for the operator B.

Fig. 4.9 is the control design for Arm 2 with a modified hysteresis compensation, which is different from it in Chapter 3. The BIBO stability of the system is guaranteed by the operators A_2, B_2 and the DWT processor. Moreover, the most uncertainties have been removed by the wavelet transform, therefore, the designed control is said to be robust. The plant output is deduced as follows.

$$y_{a2}(t) = (N_2 + \Delta N_2)\tilde{U}^{-1}[r_2^*(t) + B_2(\Delta_{PI} + D_{PI}^{-1}F_{02})] \tag{4.22}$$

As shown in Fig. 4.9, the external force F_{02} and the non-invertible part Δ_{PI} are compensated by the controller C_2 as follows.

$$C_2 := K_{I2}\int_0^t e_2(\tau)d\tau + K_{P2}e_2(t) - B_2(\Delta_{PI} + D_{PI}^{-1}F_{02})$$

where $e_2(t)$ represents for the difference between the output y_{a2} and the reference r_2; K_{I2} and K_{P2} are the PI gains. The fist two terms work for tracking the target. The last term works as a feed-forward compensator, compensating the Δ_{PI}. Therefore, the tracking compensator C_2 working

along with A_2, B_2 and the DWT processor, further reduce the arm vibration and keep the system stable and robust.

With the above two operator-based control design, the arm vibration is theoretically reduced as small as possible while the linear motor is allow to move fast. The whole system is guaranteed to be stable and robust.

4.5 Numerical simulations and discussion

To verify the effectiveness of the proposed design, simulations were conducted under Matlab. The parameters of the L-shaped arm mentioned above are listed in Table 3.1.

4.5.1 The modified contol without DWT

To validate the new model of the arm vibration and the modified hysteresis compensation, we performed the simulations based on the proposed control design as shown in Fig. 4.8 and Fig. 4.9 without DWT and compared with the control design in Chapter 3. The results are shown as follows.

Fig. 4.10 is the result under the proposed control in Fig. 4.8 without DWT using the new arm vibration model. It shows that with the new developed arm model in this chapter, the arm vibration is reduced. Fig. 4.11 is the result under the proposed control comparing with the result using the original model in last chapter, which illustrates the better effectiveness of the new model.

Fig. 4.12 and Fig. 4.13 are the results using the modified arm model in the control in Fig. 4.9 without hysteresis compensation and DWT, these results

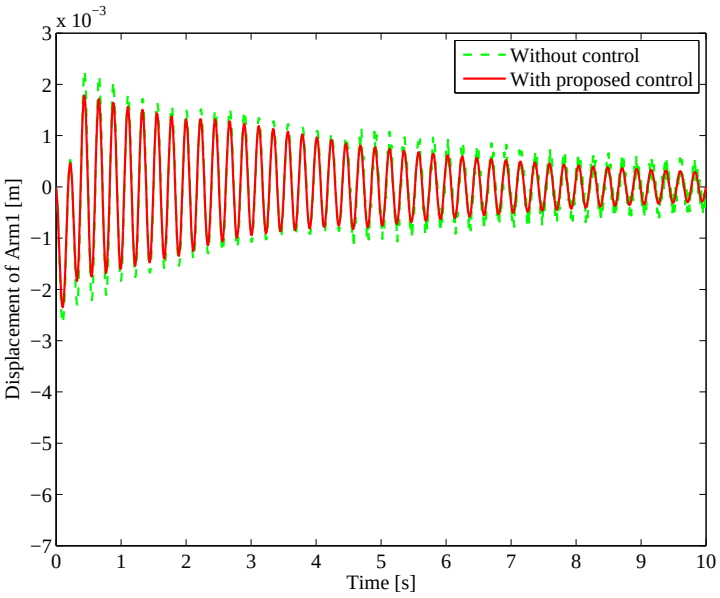

Figure 4.10: Vibration of Arm 1 with and without control

show that the new model is also effective in the control of Arm 2 vibration.

Fig. 4.14 and Fig. 4.15 are the results using the modified hysteresis compensation in the control in Fig. 4.9 without DWT, the results indicate that the modified hysteresis compensation is effective to compensate the nonlinearity of the piezoelectric actuator, with the compensation, the vibration of the arm is further reduced.

4.5.2 Operator-based control with DWT

To validate the effectiveness of the proposed on-line DWT in the operator-based control design, we conducted simulations including load estimation, vibration control of Arm 1 and Arm 2, the results are shown as follows.

Using these parameters, under free vibration, the first natural frequencies

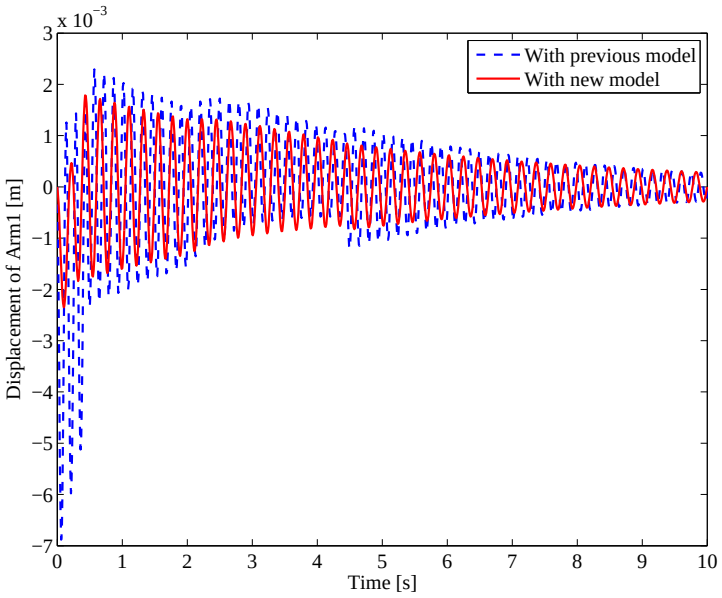

Figure 4.11: Vibration of Arm 1 with new model

Table 4.1: Load mass estimation in simulation

m_t (kg)	$\hat{m}_t$ (kg)	ω_1 (rad/s)	$\hat{\omega}_1$ (rad/s)	errors (%)
0.02	0.018	26.1781	26.3845	0.79
0.05	0.0497	23.911	23.9301	0.08
0.08	0.0808	22.133	22.0893	0.2
0.1	0.106	21.1424	208621	1.33
0.15	0.1536	19.144	19.0214	0.64
0.2	0.1936	17.6177	17.7942	1

of the arm with different loads is estimated by using DWT and FFT method, the results are listed in Table 4.1. As shown in the table, the estimation error is less than 0.2 %; the result indicates that the load estimation method proposed in thin dissertation is effective. The error depends on the sample frequency and the calculation accuracy of WDT and FFT by Matlab.

To determine the dominant modes considered in the control plant, we

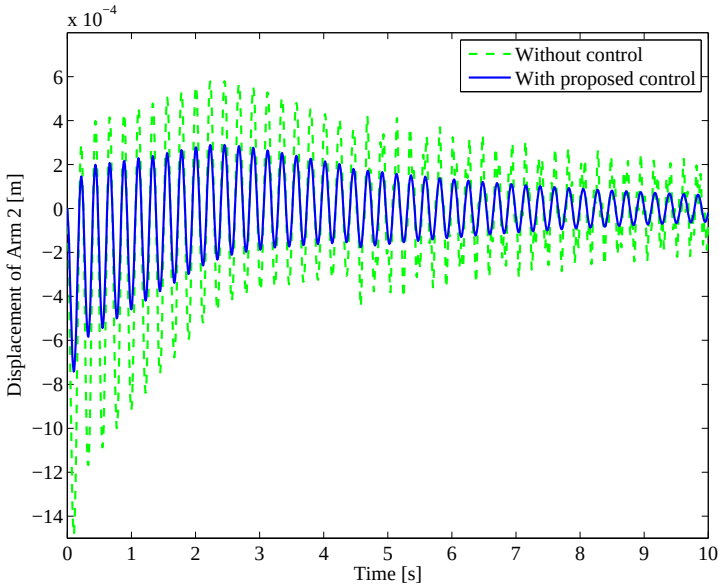

Figure 4.12: Vibration of Arm 2 with and without control

set the threshold $r_{th} = 0.01$. Substituting the vibration parameters into the modes decision equation (4.8), it was determined $n_c = 3$, namely, the first three modes of arm vibrations are considered in the the plants. For a certain load, according to the first three modes frequencies and the sample frequency, the decompose level L and the reconstruction gains were determined; other parameters in the plant and controller were calculated accordingly.

The forced vibration of the arm with load $m_t = 0.02$ kg was simulated by using the proposed method comparing with the previous operator-based method. The sampling interval in the simulation was 0.01 s, the Daubechies 4 wavelet was used in the DWT processor. The size of the moving window was decided as $l_n = 50$, the extension length $l_t = 14$, thus $l_w = 64 = 2^6$. The decompose level was set as 5. The motion of the linear pulse motor is shown

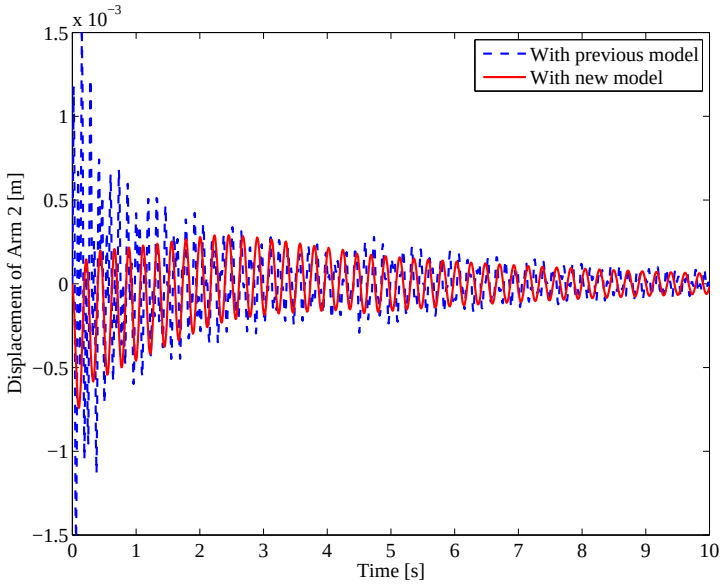

Figure 4.13: Vibration of Arm 2 with new model

in Fig. 4.16. By comparing with the vibration results, we can find that, the motor stopped at time 4.56 s.

The vibrations of the segment OA and AB are shown respectively. The displacements of Arm 1 (segment OA) is shown in Fig. 4.17 and Fig. 4.18. The vibration result comparison between the proposed control and without control is shown in Fig. 4.17. The green dashed line is the arm vibration without control, the red solid line is the vibration with wavelet-operator control. We added an Gaussian white noise between 4.5 s and 5 s to simulate the unknown disturbances, and a sine wave signal $1.5 \times 10^{-5} \sin 240t$ after 5 s to simulate the higher modes vibrations of the arm. The result shows that, with the proposed wavelet-operator-based control the undesired disturbances are removed, the vibration of the arm is reduced and stabilized. Fig. 4.18

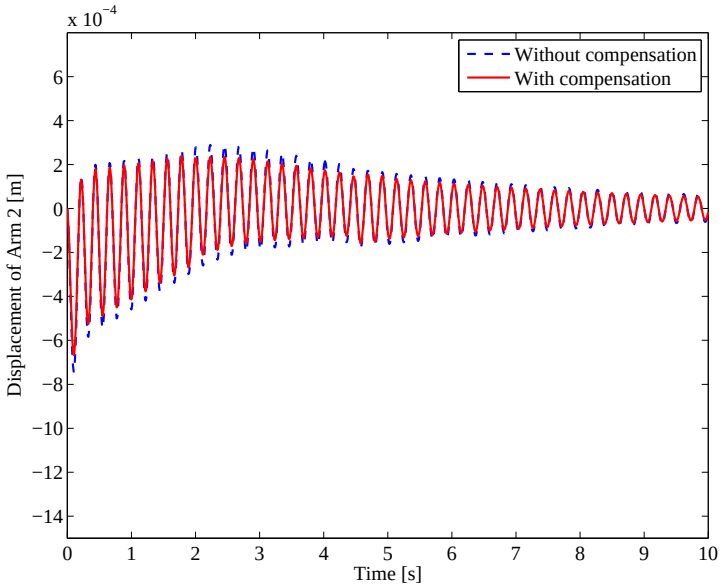

Figure 4.14: Vibration of Arm 2 with and without compensation

is the comparison between the proposed control and the previous operator-based control. The blue dashed line is the vibration of arm with the previous operator-based control without DWT. As seen from the result, with DWT processing the vibration of the arm is further reduced, and the stability of the system is more easily ensured. Considering the input constrain of the piezoelectric actuator, the voltages decided by control system were limited within ± 100 V.

For the Arm 2 (segment AB) vibration, using piezoelectric actuator, we conduct two experiments to verify the proposed controller, including the operator control without and with wavelet transform.

For comparison, the results are shown together with the result without wavelet transform in Fig. 4.19 and Fig. 4.20. The vibration of Arm 2 with

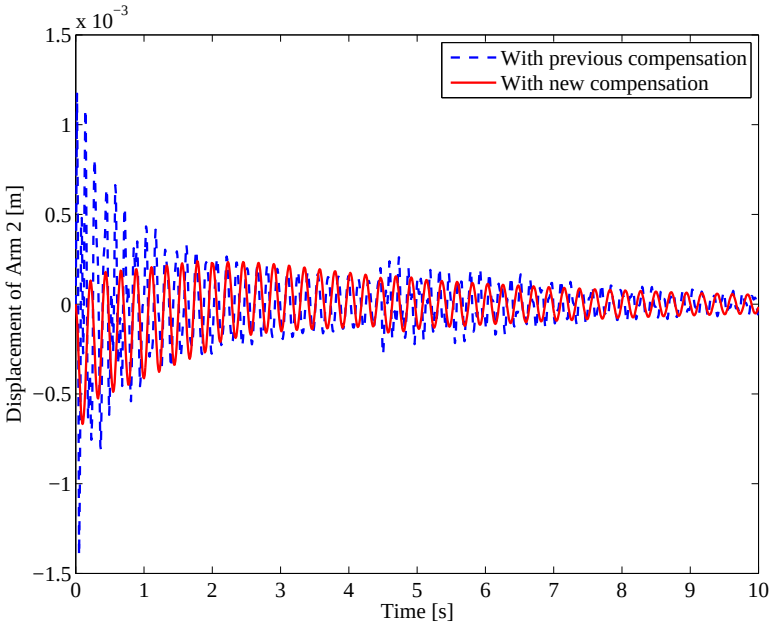

Figure 4.15: Vibration of Arm 2 with modified compensation

and without control are shown in Fig. 4.19. The green dashed line is the result without control, the red solid line is vibration with wavelet-operator control. The result shows that with the proposed control, the vibration of the arm is reduced. Comparison between the proposed control with and without hysteresis compensation is shown in Fig. 4.20. The blue dashed line is the vibration of arm without hysteresis compensation, the red solid line with compensation. The result shows that the hysteresis compensator with the proposed control can reduce the arm vibration further.

The robustness evaluation for the proposed control is shown in Fig. 4.21. The robustness indexes in process are all less than 1, which confirms that the robust stability of the proposed control are ensured. Therefore, the proposed control scheme for the L-shaped arm in this dissertation is effective. With

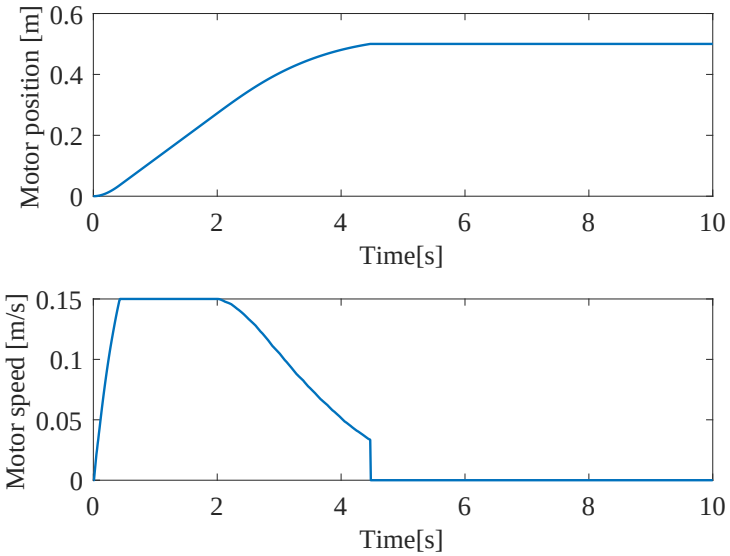

Figure 4.16: Position and speed of the linear motor

the on-line DWT, the plant outputs better results.

4.6 Conclusion

In this Chapter, the vibration control of the L-shaped arm with unknown load is studied. The linear motor is controlled to be fast while reducing the vibration of the arm. Meanwhile, the piezoelectric actuator is controlled to further reduce the vibration of the arm. The hysteresis of the piezoelectric actuator is compensated based on the Prandtl-Ishlinskii model.

By considering the whole arm as a two dimensional Euler-Bernoulli beam, the vibration of the L-shaped arm with unknown load was modelled. With the new model, the operator-based robust control was designed by using a short-symmetrical on-line wavelet transformation. After being processed by the on-line DWT, the vibration signal of the arm has less disturbances, the

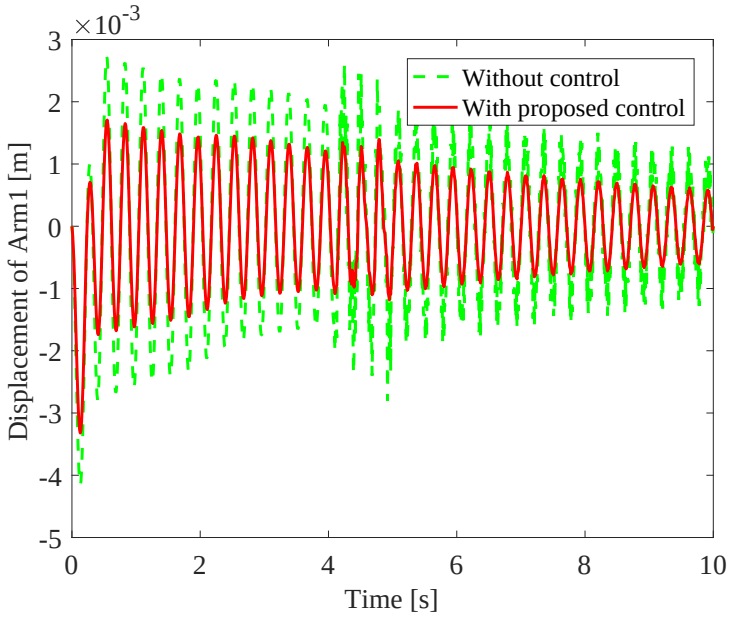

Figure 4.17: Vibration of Arm 1 with and without control

robust stability of the system are easily guaranteed. The load mass was estimated by wavelet based on the frequency equation .

Simulations were conducted to validate the new arm model, the modified hysteresis compensation and the operator-based nonlinear control with on-line DWT, the results illustrate that the proposed operator-based active control design using on-line DWT is effective and can guarantee the system robust stability. To validate the effectiveness of proposed control design, experiments will be conducted in the next chapter.

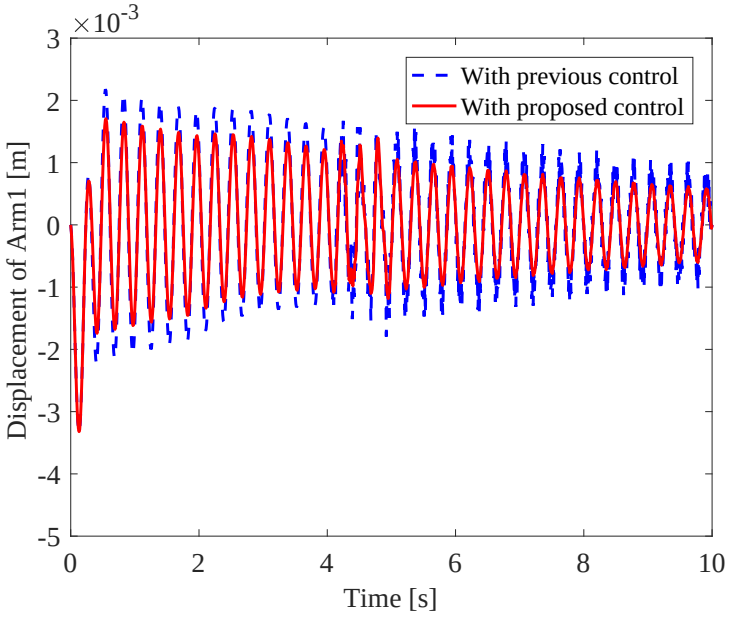

Figure 4.18: Vibration control of Arm 1 with and without DWT

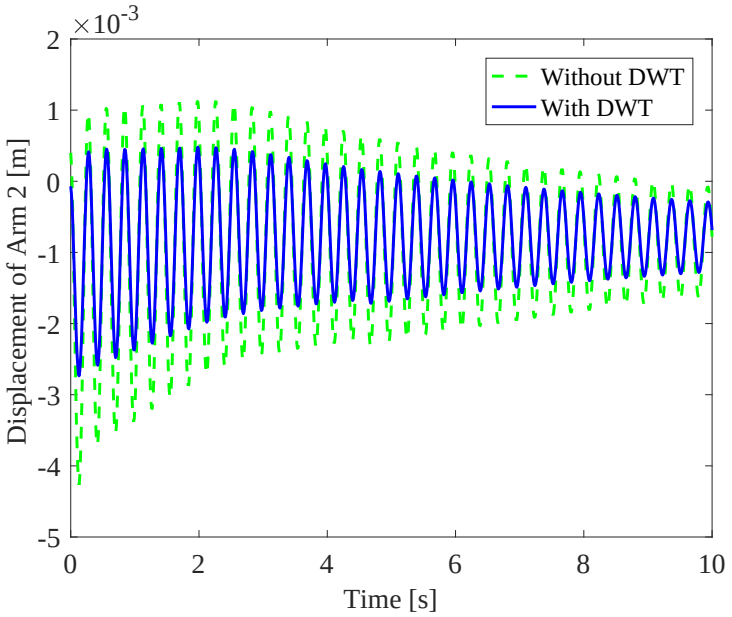

Figure 4.19: Vibration of Arm 2 with piezoelectric actuator

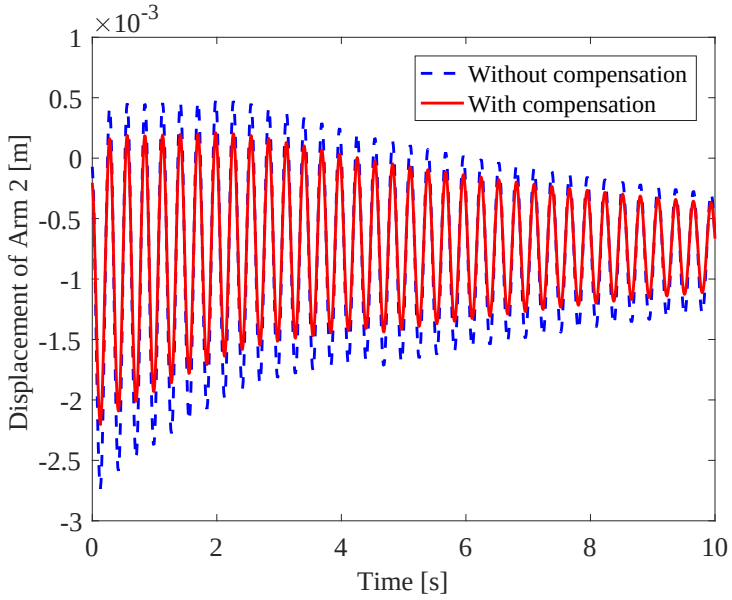

Figure 4.20: Vibration of Arm 2 with and without compensation

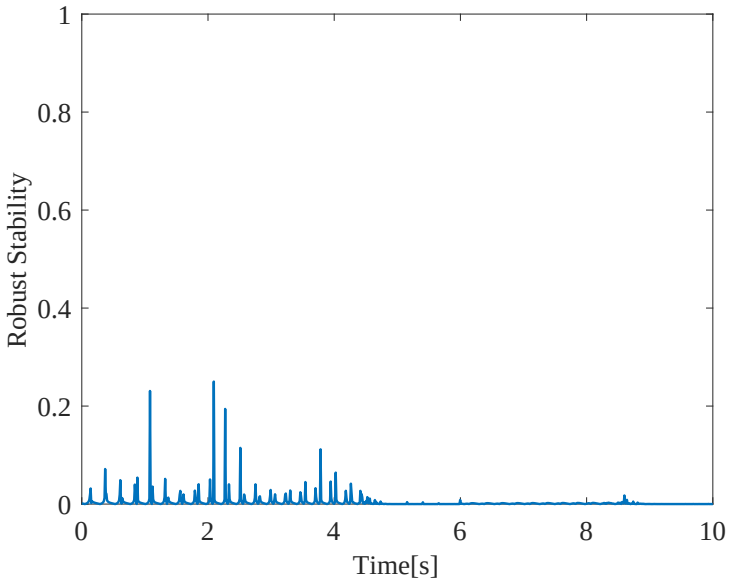

Figure 4.21: Robustness of the proposed control

Chapter 5

Experimental study on the control design

5.1 Introduction

The L-shaped arm vibration without and with load have been studied in Chapter 3 and Chapter 4 respectively. The proposed control designs have been validated by the corresponding simulation results. To further test the performances of these two control designs, we conduct the experiments correspondingly.

In **Section 5.2**, the structure of the L-shaped arm vibration experimental system is introduced, the main parameters of the devices are identified.

In **Section 5.3**, using the optimal linear motor motion control and the L-shaped arm vibration control with piezoelectric actuator proposed in Chapter 3, experiments are conducted comparing with the conditional PI control.

In **Section 5.4**, using the operator-based motor motion control and arm vibration control with on-line DWT proposed in Chapter 4, comparative experiments are conducted for the L-shaped arm with unknown load. Different

loads are estimated using the proposed estimation method.

In **Section 5.5**, the conclusion of this Chapter is drawn.

5.2 Experiment system structure

An uniform L-shaped arm vibration control experiment system is set up as shown in Fig. 5.1. The up end of the arm is clamped with a pulse linear motor; the linear motor drives the the arm to destination along the motor guide horizontally.

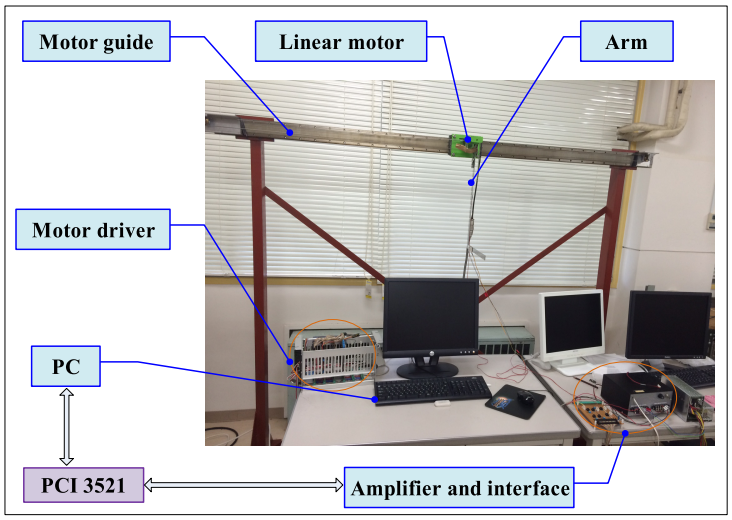

Figure 5.1: Experimental device

The linear pulse motor is HRM 0205, driven by a driver LD-300 (both made by THK CO.,LTD). The motor driver communicates with the PC by using a PCI board SMC-4P (PCI) (made by CONTEC CO.,LTD). The motor moves 0.05 mm for every pulse input. The non-zero minimum speed of the linear motor and minimum acceleration rate are decided by the PCI

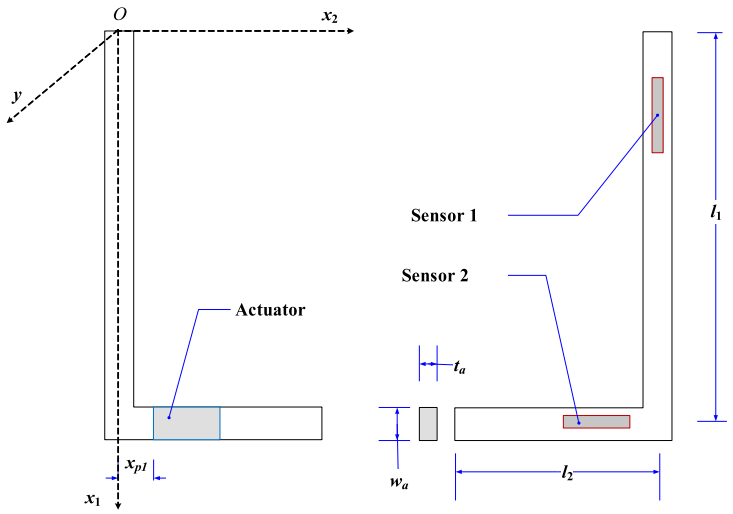

Figure 5.2: Schematic diagram of the arm

board. The maximum speed and acceleration rate are limited for safety, the parameters of the linear motor are listed in Table 3.2.

Table 5.1: Parameters of the Piezoelectric Actuator

Parameter	Definition	Value	Units
t_p	Thickness	0.5×10^{-3}	m
w_p	Width	20×10^{-3}	m
l_p	Length	0.05	m
x_{p1}	Location on Arm 2	0.04	m
d_{31}	Electric charge constant	-2.1×10^{-10}	m/V
E_p	Young's modulus	6.2×10^{10}	N/m^2

Two piezoelectric sensors are pasted on one side of the arm to measure the relative vibration displacements of the arm. One piezoelectric actuator is mounted on the other side of the arm to suppress its vibration, as shown

in Fig. 5.2. The actuator (C-6, made by FUJI Ceramics Corporation) and sensors (C-63, made by FUJI Ceramics Corporation) used in this dissertation both are PZT (Pb[Zr·Ti]O_3) ceramics type material. The parameters of the actuator are listed in Table 5.1. The proposed controllers in this dissertation are programmed in Microsoft Visual C++ under Windows XP operating system, the sensor and control input signals for piezoelectric actuator are processed by the PCI board (PCI-3521, made by Interface Corporation). A voltage amplifier (HOPS-0.3B10, made by Matsusada Precision) is used between the PCI board and the actuator to amplify the input voltages (restricted within ±100 V).

5.3 Experiments on system without load

The general aim of this study is to reduce the arm vibration while let the motor move fastly. To validate the effectiveness of the proposed design scheme, several experiments were conducted comparatively. The parameters of the linear pulse motor, the L-shaped arm and the piezoelectric actuator in experimental system are shown in Tables 3.2, 5.1 and 3.1. The sampling frequency in the experiments was 200 Hz; it was bigger than twice the third mode frequency of the arm vibration. The density function $p(h)$ of the hysteresis model (2.3) was identified by a characteristic experiment represented as the following equation, where $h \in [0, 100]$.

$$p(h) = 0.00032 \times e^{-0.00086(h-1)^2}. \tag{5.1}$$

The filters mentioned above were designed into a first-order infinite im-

pulse response (IIR) low-pass filter combined with bi-quad IIR notch filter. The low-pass filter was used to attenuate the high frequencies noise signals, the notch filter was used to attenuate certain frequency signal caused by piezoelectric sensor's measurement noise. The cut-off frequency of filters was determined by vibration experiments. The displacements of Arm 1 were measured by sensor 1.

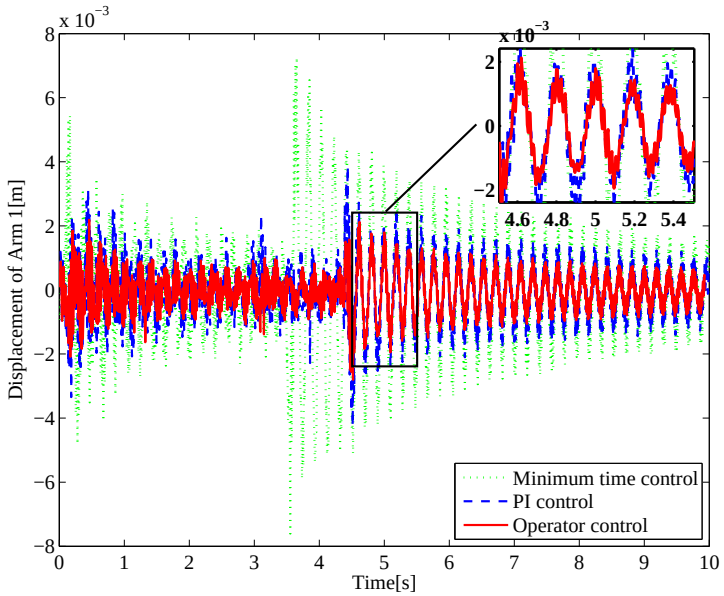

Figure 5.3: Vibration of Arm 1 with motion control (without piezoelectric actuator)

To validate the proposed motor control, we conducted three experiments for comparison, including the proposed optimal operator control (the piezoelectric actuator on Arm 2 didn't work), a conventional PI control and a minimum time control, the results are shown in Fig. 5.3. The dotted line in Fig. 5.3 represents for the vibration of Arm 1 with minimum time control. In

this situation, only considering the time consumption, the linear motor was controlled to run for a distance of 0.5 m at the maximum speed and acceleration, the minimum time consumption was 3.49 s. The results indicate that the maximum acceleration leaded to a maximum arm vibration especially at the moment the linear motor starts and stops.

In Fig. 5.3, the dashed line is the displacement with PI control, the solid line is the displacement with the proposed optimal operator feedback control. The time consumption of the linear motor were both tuned at 4.36 s for these two control methods. The result illustrates that with PI control, the arm vibration is reduced, but the travel time of the linear motor is longer than the minimum time control. The proposed optimal operator control further reduced the vibration of arm, especially after the motor stopped. It indicates that with the operated feedback signal, the motor was ensured to run at an optimal trajectory resulting in reduced arm vibration, while the plant was kept stable. The extra undesired vibration around 0.5 s and 3 s was presumably caused by the uneven contact and friction between linear motor and motor guide.

To validate the proposed control for Arm 2, we conducted two experiments including the operator control without and with hysteresis compensator. The input voltages for the piezoelectric actuator were limited within ± 100 V for safety. For comparison, the results are shown together with the result without actuator in Fig. 5.4. The output of the plant without actuator is shown in dash-dot line, the dashed line is the result by using actuator without considering the hysteresis, while the displacement of Arm 2 with

actuator with proposed hysteresis compensation. The result indicates that the piezoelectric actuator can reduce the arm vibration with the proposed control. With the proposed hysteresis compensation, the vibrations of arm are further reduced at most of time during the motor motion.

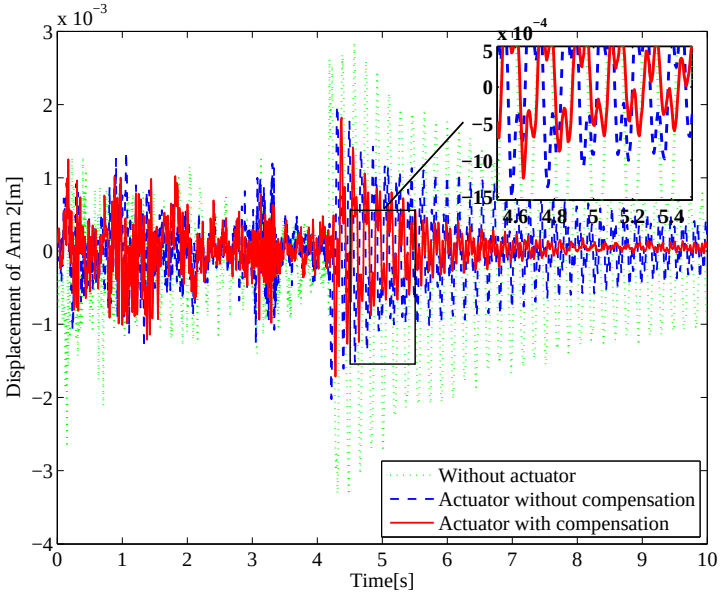

Figure 5.4: Vibration of Arm 2 with and without actuator (linear motor with operator control)

To show the effectiveness clearly, an evaluation index $\int_0^\tau y_2^2(t)dt$ derived from the cost function(3.12) is used to evaluate the vibration power of the arm, which is called cumulative vibration intensity. The vibration index of Arm 2 without actuator, with actuator no compensation and actuator with compensation are shown in Fig. 5.5 in dash-dot line, dashed line and solid line, respectively. From which, we conclude that the arm vibration can be reduced effectively with piezoelectric actuator, and with the proposed hys-

teresis compensation the arm vibration can be further reduced. The results illustrate that both the control design for actuator and the hysteresis compensator are effective.

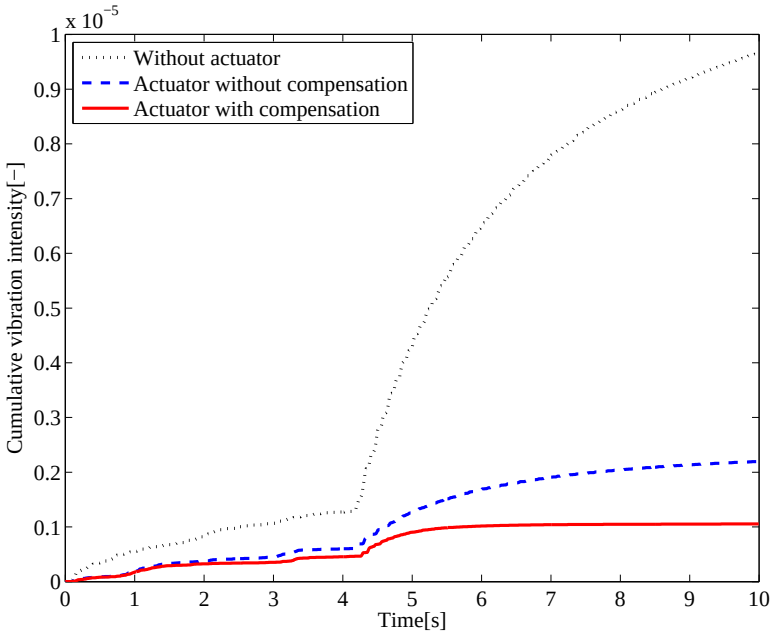

Figure 5.5: Cumulative vibration intensity of Arm 2 with and without actuator

Therefore, the proposed control scheme for the piezoelectric actuator in this dissertation is effective to suppress the vibration of arm; with the hysteresis compensator, the plant outputs better results.

The robust stability evaluations for the proposed control are shown in Fig. 5.6. The values of y-coordinate were calculated by $\|[A_2(N_2 + \Delta N_2) - A_2 N_2]M^{-1}\|_{Lip}$. It is evident that the value are much less than 1 during the experiment. According to the definition of robustness (2.19), the result indicates that the proposed control is robust stable. The robustness includes

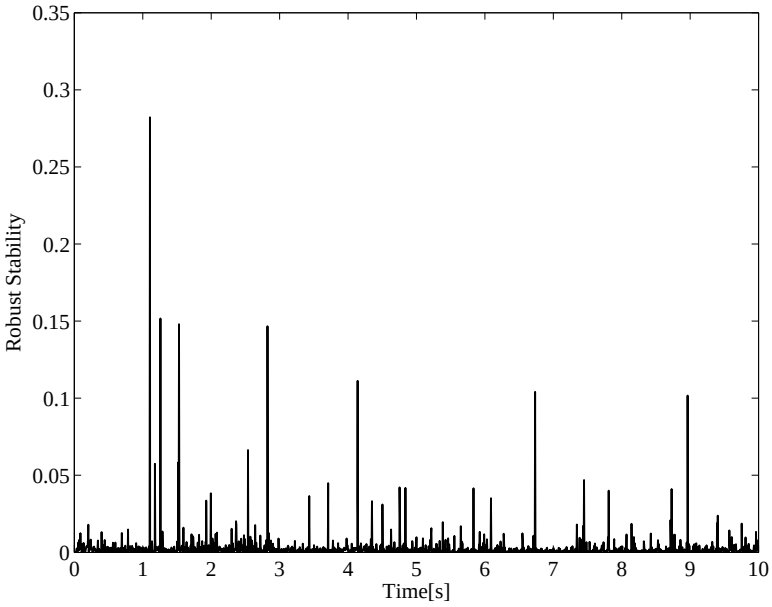

Figure 5.6: Robustness of the proposed system

all of the mentioned uncertainties.

5.4 Experiments on system with load

To test the performance of the proposed control design, we conducted several experiments comparing with the previous work. The proposed controller was performed by through Microsoft Visual C++ 2010 and run on a PC with Windows XP system. Limited by the performance of the PC in experiments, the sampling frequency was determined as 100 Hz.

According to the sampling frequency and the vibration dynamics of the arm, the dominant modes was determined as $N_d = 2$, namely, the first two modes of arm vibrations were considered in the the plants. For a certain load, according to the first three modes frequencies and the sample frequency,

Table 5.2: Load mass estimation in experiment

m_t (kg)	$\hat{m}_t$ (kg)	f_1 (Hz)	error (%)
0.021	0.0189	4.153	10.0
0.042	0.0408	3.893	2.8
0.087	0.0808	3.465	7.1
0.108	0.1072	3.307	9.0
0.152	0.1541	3.036	1.4
0.204	0.1937	2.787	5.0

the decompose level L and the reconstruction gains were determined; other parameters in the plant and controller were calculated accordingly. In the experiment, the load mass estimation flow is shown as:

Initial vibration $\rightarrow y_1(t) \rightarrow$ DWT $\rightarrow$ reconstructed of the approximation at the level with frequency band including $f_1 \rightarrow$FFT $\rightarrow f_1 \rightarrow$ equation (4.4) $\rightarrow \beta_1 \rightarrow$ equation (4.5)$\rightarrow$ load mass $\hat{m}_t$.

Using this method, we tested with five different loads, the results are listed in Table 5.2. The first column m_t is the real load mass we applied; the second column $\hat{m}_t$ is the estimated load mass; the third column f_1 is the tested vibration frequency of the first mode; the last column is the estimation error, less than 10 %. Considering the impact of disturbances in experiments, the proposed load estimation method is said to be effective.

To test the proposed nonlinear control method, we conducted experiments with load $m_t = 0.042$ kg and compared with previous operator-based method (without on-line DWT). The Daubechies 4 wavelet was used in the DWT processor. The size of the moving window was decided as $l_n = 24$, the extension length $l_t = 8$, thus $l_w = 32 = 2^5$. The decompose level was set

as 4. For different situations the linear motor was controlled to arrive the destination within 4.36 s. The motion of the linear motor is shown in Fig. 5.7.

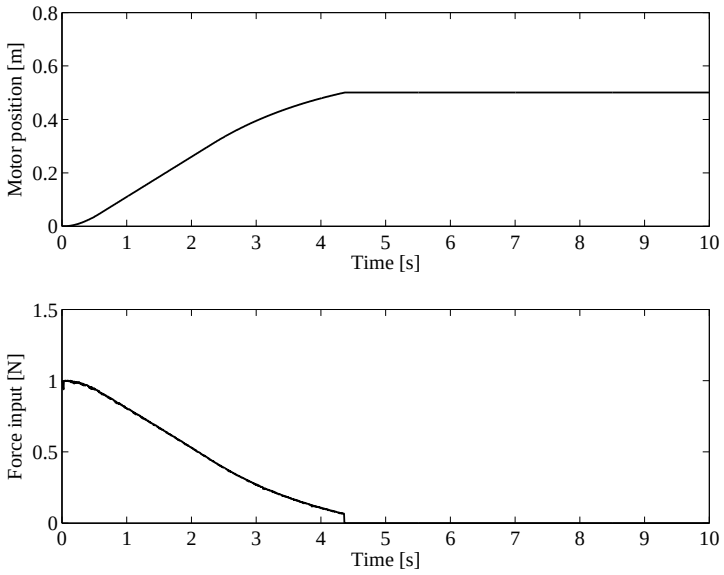

Figure 5.7: Position and force input of the linear motor

With the proposed controller, forced by the linear motor, the resulted displacements of Arm 1 (segment OA) are demonstrated in Fig. 5.8 and Fig. 5.9. Fig. 5.8 is the vibration result comparison with proposed control and without control. The arm vibration without control is shown in blue dashed line, the vibration with wavelet-operator control is shown in red solid line. As seen from the result, the vibration of the arm was reduced by using the proposed wavelet-operator control and the system was stabilized. Fig. 5.9 is the comparison between the proposed control and the previous operator-based control without DWT. The vibration of arm with the previous operator-based control is shown in blue dashed line, the proposed control in

red solid line. As seen from the result, with the DWT processor the vibration of the arm was further reduced, and the stability of the system was more easily ensured.

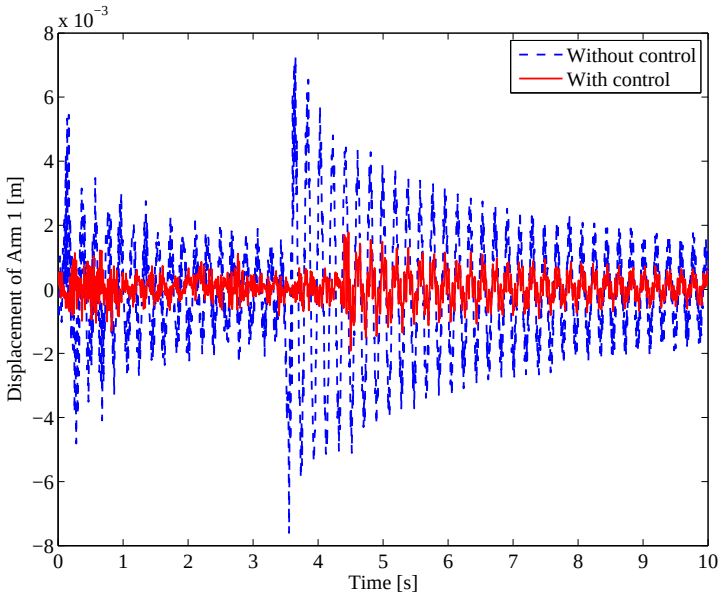

Figure 5.8: Vibration of Arm 1 with and without control

For the Arm 2 (segment AB) vibration control using piezoelectric actuator, we conducted experiments to verify the proposed controller. The vibration result with DWT is shown in red solid line in Fig. 5.10, the result without DWT is shown in blue dashed line. The result shows that the proposed control reduced the arm vibration more effectively. Fig. 5.11 shows the comparison between the proposed control with and without hysteresis compensation. The arm vibration with hysteresis compensation is shown in red solid line, the result without compensation in blue dashed line. The result shows that the hysteresis compensator with the proposed control can reduce

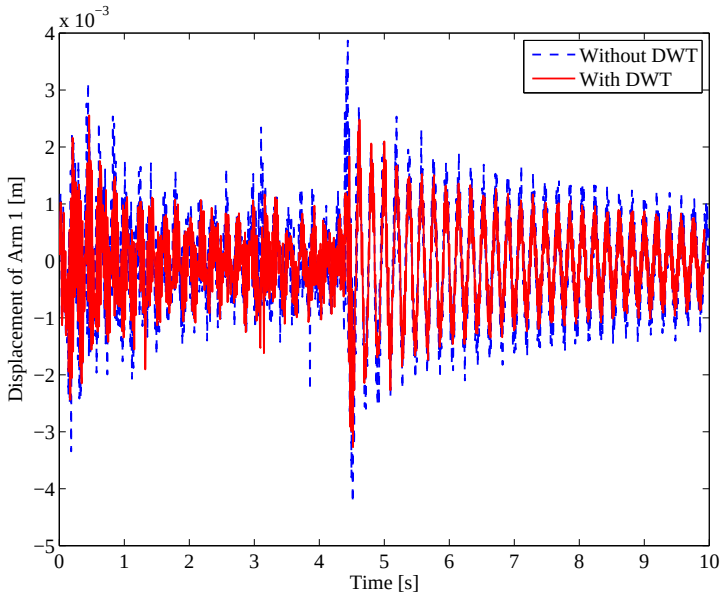

Figure 5.9: Vibration of Arm 1 with and without DWT

the arm vibration further.

To illustrate the control effect more clearly, we defined the root of mean square error (RMSE) of the results with time as

$$RMSE(nT) = \sqrt{\frac{1}{n}\sum_{i=1}^{n}(y_2(i) - r_2)^2} \tag{5.2}$$

where T is the sampling interval, n is the sampling number. The RMSE of Arm 2 displacements with time for different situations are shown in Fig. 5.12. It can be seen from the results that the vibration of Arm 2 was reduced more effectively with the proposed control than the previous control; the arm vibration was further reduced by using the hysteresis compensation. Therefore, the proposed control design in this study could reduce the L-shaped arm vibration effectively. With the on-line DWT, the control performance was

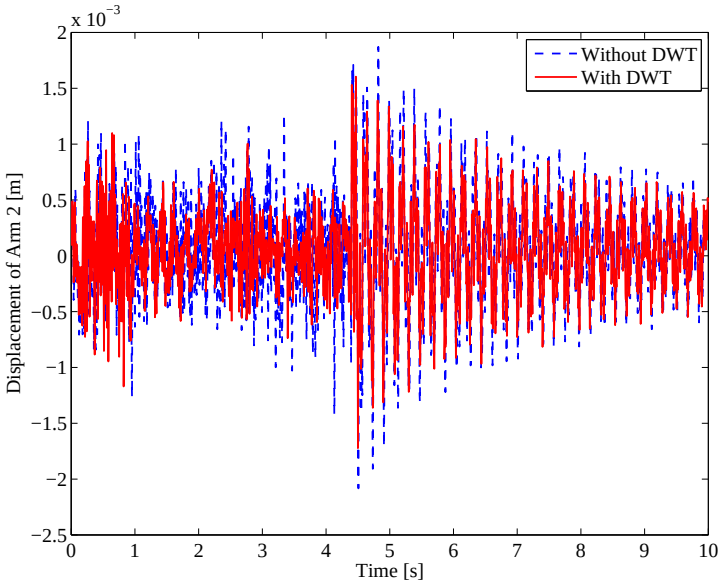

Figure 5.10: Vibration of Arm 1 with and without control

improved.

5.5 Conclusion

In this chapter, we tested the control designs proposed in Chapter 3 and Chapter 4 by experiments.

For the L-shaped arm without load, comparing with the PI control and minimum time control, the operator-based optimal motion control was performed for the linear motor. Then, using the proposed vibration control of Arm 2 with piezoelectric actuator, the experiments were performed along with the PI control. The results indicate that the proposed control design is effective and can guarantee the system robust stability.

For L-shaped arm with load, we conducted several comparative experi-

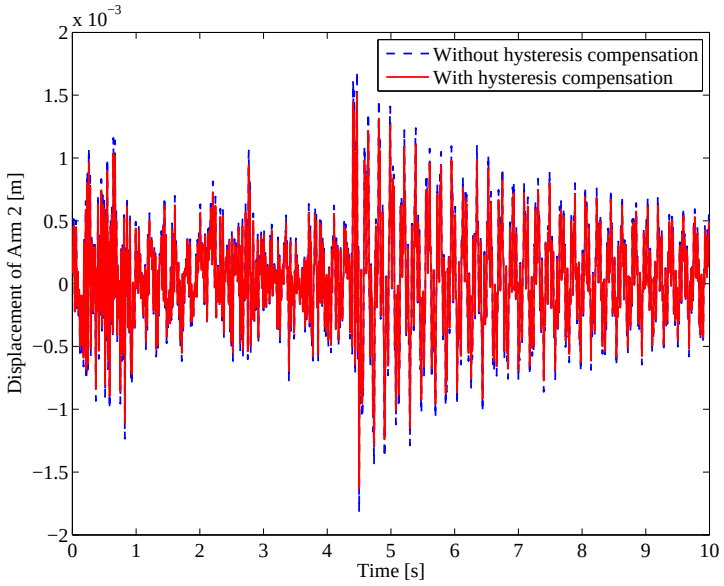

Figure 5.11: Vibration of Arm 1 with and without DWT

ments to validate the proposed control design using the operator-based approach and the on-line DWT. The results illustrated that the arm vibration was reduced effectively, the operator-based right coprime factorization could guarantee the system robust stability and with the on-line DWT, the performance of the operator-based control was improved, the load mass was easily estimated.

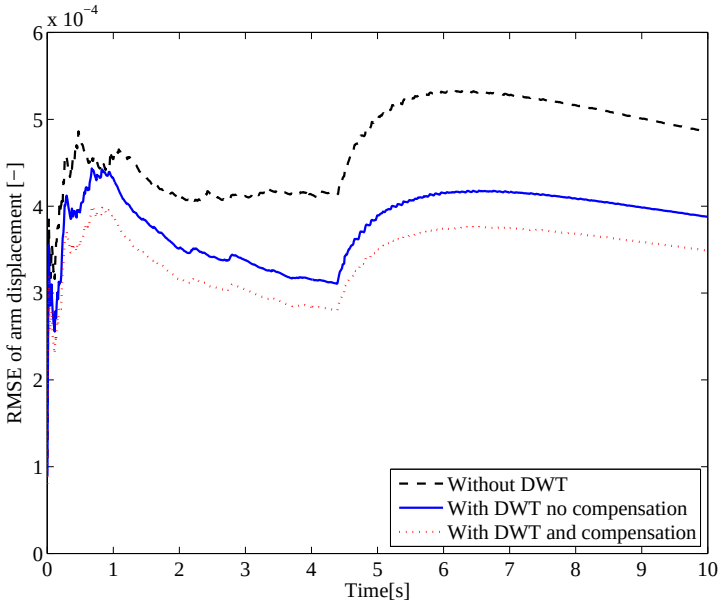

Figure 5.12: Position and force input of the linear motor

Chapter 6

Conclusions

In this dissertation, an L-shaped arm driven by a linear pulse motor is studied to find approaches to control motor motion and the forced vibration of arm at the same time. The arm without load and with load were researched respectively. Two different modelling methods of the arm were employed and two different nonlinear control designs were proposed correspondingly. Simulations and experiments for different situations and different control design were conducted to validate their effectiveness.

In **Chapter 2**, the Euler-Bernoulli theory for the flexible arm vibration is introduced, which provides the theoretical basis for modelling the L-shaped arm in this dissertation. The Prandtl-Ishlinskii model provides the method to model the hysteresis of the piezoelectric actuator. Some fundamental definitions and the theoretical basis of operator-based nonlinear control theory establish the foundation for the control design in this dissertation. The DWT is the theoretical basis for uncertainties removing and the load estimation.

In **Chapter 3**, operator-based robust nonlinear control was proposed to

control the forced vibration of arm. By considering the L-shaped arm as two connected Euler-Bernoulli beams, the dynamics on arm vibration involving linear motor and piezoelectric actuator was modelled. Two operator-based robust nonlinear control systems were proposed in this chapter, the first one was designed to make the motor not only move to destination in certain time but also reduce the vibration of arm. Another one was designed to control the input of the piezoelectric actuator, the hysteresis nonlinearity of the actuator was modelled using a Prandtl-Ishlinskii hysteresis model, and the nonlinear part is compensated in the tracking controller. Finally, to confirm the effectiveness of the proposed control design, simulations were conducted comparing with the PI control, the results illustrate that the operator-based control systems designed in this dissertation are more effective and can guarantee the system to be stable and robust.

In **Chapter 4**, the vibration control of the L-shaped arm with unknown load was studied. The linear motor is required to be fast while reducing the vibration of the arm. Meanwhile, the piezoelectric actuator was utilized to further reduce the vibration of the arm. Fist, the L-shaped arm with unknown load was modelled by considering it as a whole two dimensional Euler-Bernoulli beam. The relationship between the arm vibration and the load mass was given. Second, the operator-based robust control was designed by using a short-symmetrical on-line wavelet transformation. After being processed by the on-line DWT, the vibration signal of the arm has less disturbances, the robust stability of the system are easily guaranteed. The load mass was estimated by wavelet based on the frequency equation.

The hysteresis of the piezoelectric actuator was compensated based on the Prandtl-Ishlinskii model. Finally, simulation was conducted under Matlab, the results illustrate that the proposed operator-based active control design using on-line DWT is effective and can guarantee the system robust stability.

In **Chapter 5**, we tested the control designs proposed in Chapter 3 and Chapter 4 by though experiments. For the L-shaped arm without load, comparing with the PI control and minimum time control, the operator-based optimal motion control was performed for the linear motor. Then, using the proposed vibration control of Arm 2 with piezoelectric actuator, the experiments were performed along with the PI control. The results indicate that the proposed control design is effective and can guarantee the system to be stable and robust.

For the L-shaped arm with unknown load, we conducted several comparative experiments to validate the proposed control design using the operator-based approach and the on-line DWT. The results illustrate that the arm vibration is reduced effectively, the operator-based right coprime factorization could guarantee the system robust stability and with the on-line DWT, the performance of the operator-based control is improved, the load mass is easily estimated.

In conclusion, this dissertation provides a nonlinear forced vibration control design method for the underactuated systems with multiple outputs and less control inputs, it can guarantee the system robust stability. The proposed method in this dissertation can also be used to reduced the impact of the uncertainties and disturbances of the system. Moreover, the on-line

DWT has potential in processing the complicated system signal in time and frequency domain and estimating some unknown parameters.

However, some limitations of this study are worth noting. The models of the arm vibration and the hysteresis of the actuator were simplified to some extent; more accurate models could probably improve the control effect. The linear motor control was limited by the motor characteristic and the interface board, the real time command sent by the controller are not fully executed. The sampling intervals and computing speed were limited by the PC's capacity especially for the on-line DWT program, which requiring high computational performance. Further work will consider the impact of the uncertainties in detail especially the transient vibration of linear motor and use a more accurate system model and high-performance devices to improve the control effectiveness.

Bibliography

[1] E. M. Abdel-Rahman, A. H. Nayfeh and Z. N. Masoud, "Dynamics and control of cranes: a review," *Journal of Vibration Control*, vol. 9, pp. 863-908, 2003.

[2] L. Ramlia, Z. Mohameda, A. M. Abdullahia, H. I. Jaafar and I. M. Lazim, "Control strategies for crane systems: A comprehensive review," *Mechanical Systems and Signal Processing*, vol. 95, pp. 1-23, 2017.

[3] A. Zippo, G. Ferrari, M. Amabili, et al. "Active vibration control of a composite sandwich plate," *Composite Structures*, vol. 128, pp. 100-114, 2015.

[4] W. Yu, X. Li, F. Panuncio, "Stable neural PID anti-swing control for an overhead crane," *Intelligent Automation & Soft Computing*, vol. 20, pp. 145-158, 2014.

[5] L. D. Viet, "Crane sway reduction using Coriolis force produced by radial spring and damper," *Journal of Mechanical Science and Technology*, vol. 29, pp. 973-979, 2015.

[6] J. Vaughan, D. Kim and W. Singhose, "Control of tower cranes with double-pendulum payload dynamics," *IEEE Transactions on Control Systems Technology*, vol. 18, pp. 1345-1358, 2010.

[7] K. B. Waghulde, B. Sinha, M. M. Patil and S. Mishra, "Vibration control of cantilever smart beam by using piezoelectric actuators and sensors," *International Journal of Engineering and Technology*, vol. 2, no. 4, pp. 259-262, August 2010.

[8] X. Chen, C. Su and T. Fukuda, "Robust vibration control for flexible arms by using sliding mode method," *Asian Journal of Control*, vol.5, no. 4, pp. 594-604, December 2003.

[9] C. Y. Lin and P. Y. Chen, "Hysteresis compensation and high-performance tracking control of piezoelectric actuators," *Proc. IMechE, Part I: Journal of Systems and Control Engineering*, vol. 226, no. 8, pp. 1050-1059, July 2012.

[10] A. Banos, "Stabilization of nonlinear systems based on a generalized bezout identity," *Automatica*, vol. 32, no. 4, pp. 591-95, 1996.

[11] E. D. Sontag, "Smooth stabilization implies coprime factorization," *IEEE Transactions on Automatic Control*, vol. 34, no. 4, pp. 435-443, 1989.

[12] O. Staffans, "Admissible factorizations of Hankel operators induce well-posed linear systems," *Systems & Control Letters*, vol. 37, no. 5, pp. 301-307, 1999.

[13] M. S. Verma, "Coprime fractional representations and stability of nonlinear feedback systems," *International Journal of Control*, vol. 48, no. 3, pp. 897-918, 1988.

[14] M. S. Verma and L. R. Hunt, "Right coprime factorizations and stabilization for nonlinear systems," *IEEE Transactions on Automatic Control*, vol. 38, no. 2, pp. 222-231, 1993.

[15] G. Chen and Z. Han. "Robust right coprime factorization and robust stabilization of nonlinear feedback control systems," *IEEE Transactions on Automatic Control*, vol. 43, no. 10, pp. 1505-1510, October 1998.

[16] S. Shah, Z. Iwai, I. Mizumoto and M. Deng, "Simple adaptive control of processes with time-delay," *Journal of Process Control*, vol. 7, no. 6, pp. 439-449, December 1997.

[17] M. Deng and N. Bu, "Robust control for nonlinear systems using passivity-based robust right coprime factorization," *IEEE Transactions on Automatic Control*, vol. 57, no. 10, pp. 2599-2604, October 2012.

[18] M. Deng, A. Inoue and K. Ishikawa, "Operator-based nonlinear feedback control design using robust right coprime factorization," *IEEE Transactions on Automatic Control*, vol. 51, no. 4, pp. 645-648, April 2006.

[19] N. Bu and M. Deng, "System design for nonlinear plants using operator-based robust right coprime factorization and isomorphism," *IEEE Transactions on Automatic Control*, vol. 56, no. 4, pp. 952-957, 2011.

[20] M. Deng and N. Bu, "Isomorphism-based robust right coprime factorisation of non-linear unstable plants with perturbations," *IET Control Theory Appl.*, vol. 4, no. 11, pp. 2381-2390, 2010.

[21] M. Deng, N. Bu and A. Inoue, "Output tracking of nonlinear feedback systems with perturbation based on robust right coprime factorization," *Journal of Innovative Computing, Information & Control*, vol. 5, no. 10, pp. 3359-3366, October 2009.

[22] Bu. N and M. Deng, "Isomorphism-based robust right coprime factorization realization for nonlinear feedback systems. *Proc IMechE, Part I: J Systems and Control Engineering* 2011; 225(6): 760-769.

[23] S. Wen, and M. Deng , "Operator-based robust nonlinear control and fault detection for a Peltier actuated thermal process," *Mathematical and Computer Modelling*, vol. 57, no. 1, pp. 16-29, 2013.

[24] M. Deng, *Operator-Based Nonlinear Control Systems Design and Applications*, Wiley, New Jersey, 2014.

[25] S. G. Mallat, "A theory for multiresolution signal decomposition: the wavelet representation," *IEEE transactions on pattern analysis and machine intelligence*, vol. 11, no. 7, pp. 674-693, 1989.

[26] I. Daubechies, *Ten Lectures of Wavelets*, SIAM, 1992.

[27] S. Mallat, *A Wavelet Tour of Signal Processing-The Sparse Way*, Academic Press, 3rd ed., 2008.

[28] I. Daubechies, "Orthonormal bases of compactly supported wavelets," *Communications on Pure and Applied Mathematics*, vol. 41, no. 7, pp. 909-996, 1988.

[29] C. K. Chui. *An Introduction to Wavelets*, Academic Press, 1992.

[30] G. Strang and T. Nguyen, *Wavelets and Filter Banks*, SIAM, 1996.

[31] T. Kijewski and A. Kareem, "Wavelet transforms for system identification in civil engineering," *Computer-Aided Civil and Infrastructure Engineering*, vol. 18, pp. 339-355, 2003.

[32] R. X. Gao and R. Yan, *Wavelets: Theory and Applications for Manufacturing*, Springer Science & Business Media, 2010.

[33] P. Chaovalit, A. Gangopadhyay, G. Karabatis and Z. Chen, "Discrete wavelet transform-based time series analysis and mining," *ACM Computing Surveys (CSUR)*, vol. 43, no. 2, 2011.

[34] S. Parvez and Z. A. Gao, "A wavelet-based multiresolution PID controller," *IEEE Transactions on Industry Applications*, vol. 41, no. 2, pp. 537-543, 2005.

[35] H. Su, Q. Liu, and J. Li, "Boundary effects reduction in wavelet transform for time-frequency analysis," *WSEAS Transactions on Signal Processing*, vol. 8, no. 4, pp. 169-179, 2012.

[36] P. Qi, S. Jovanovic, J. Lezama and P. Schweitzer, "Discrete wavelet transform optimal parameters estimation for arc fault detection in low-

voltage residential power networks," *Electric Power Systems Research*, vol. 143, pp. 130-139, 2017.

[37] M. Cole, P. Keogh, C. Burrows and N. Sahinkaya, " Wavelet domain control of rotor vibration," *Proc. IMechE, Part C: J Mechanical Engineering Science*, vol. 220, no. 2, pp. 167-184, 2006.

[38] R. Xia, K. Meng, F. Qian and Z. Wang, "Online wavelet denoising via a moving window," *Acta Automatica Sinica*, vol. 33, no. 9, pp. 897-901, 2007.

[39] R. L. Neitzel, N. S. Seixas and K. K. Ren, "A review of crane safety in the construction industry," *Applied Occupational and Environmental Hygiene*, vol. 16, pp. 1106-1117, 2001.

[40] W. Singhose, L. Porter, M. Kenison and E. Kriikku, "Effects of hoisting on the input shaping control of gantry cranes," *Control Engineering Practice*, vol. 8, pp. 1159-1165, 2000.

[41] K. A. F. Moustafa, E. H. Gad, A. M. A. El-Moneer and M. I. S. Ismail, "Modelling and control of overhead cranes with flexible variable-length cable by finite element method," *Transactions of the Institute of Measurement and Control*, vol. 27, pp. 1-20, 2005.

[42] Y. Fang, W. E. Dixon, D. M. Dawson, and E. Zergeroglu, "Nonlinear coupling control laws for an underactuated overhead crane system," *IEEE/ASME Transactions on Mechatronics*, vol. 8, no. 3, pp. 418-423, 2003.

[43] N. Sun, Y. Fang, Y. Zhang, and B. Ma, "A novel kinematic coupling-based trajectory planning method for overhead cranes," *IEEE/ASME Transactions on Mechatronics*, vol. 17, no. 1, pp. 166-173, 2012.

[44] Y. Fang, B. Ma, P. Wang, and X. Zhang, "A motion planning-based adaptive control method for an underactuated crane system," *IEEE Transactions on Control Systems Technology*, vol. 20, no. 1, pp. 241-248, 2012.

[45] D. Liu, J. Yi, D. Zhao, and W. Wang, "Adaptive sliding mode fuzzy control for a two-dimensional overhead crane," *Mechatronics*, vol. 15, no. 5, pp. 505-522, 2005.

[46] C. Chang, "Adaptive fuzzy controller of the overhead cranes with nonlinear disturbance," *IEEE Transactions on Industrial Informatics*, vol. 3, no. 2, pp. 164-172, 2007.

[47] C. Chang and T. Chiang, "Overhead cranes fuzzy control design with deadzone compensation," *Neural Computing and Applications*, vol. 18, no. 7, pp. 749-757, 2009.

[48] L. Ramlia, Z. Mohameda, A. M. Abdullahia, H. I. Jaafar and I. M. Lazim, "Control strategies for crane systems: A comprehensive review," *Mechanical Systems and Signal Processing*, vol. 95, pp. 1-23, 2017

[49] A. Abe, "Anti-sway control for overhead cranes using neural networks. *International Journal of Innovative Computing, Information and Control*, vol. 7, no.7(B), pp. 4251-4262, July 2011.

[50] N. Sun, Y. Fang, Y. Zhang and B. Ma, "A novel kinematic coupling-based trajectory planning method for overhead cranes," *IEEE/ASME Transactions on Mechatronics*, vol. 17, no. 1, pp. 166-173, 2012.

[51] Z. Kang, S. Fujii, C. Zhou, and K. Ogata, "Adaptive control of a planar gantry crane by the switching of controllers," *Transactions of the Society of Instrument and Control Engineers*, vol. 35, no. 2, pp. 253-261, 1999.

[52] S. Wen, M. Deng and A. Inoue, "Operator-based robust nonlinear control for gantry crane system with soft measurement of swing angle," *International Journal of Modelling, Identification and Control*, vol. 16, no. 1, pp. 86-96, 2012.

[53] S. Bi, M. Deng and S. Wen, "Operator based output tracking control for nonlinear uncertain systems with unknown time-varying delays," *IET Control Theory & Applications*, vol. 5, no. 5, pp. 693-699, March 2011.

[54] S. Bi and M. Deng, "Operator based robust control design for nonlinear plants with perturbation," *International Journal of Control*, vol. 84, no. 4, pp. 815-821, 2011.

[55] M. Deng, S. Bi, and A. Inoue, "Robust nonlinear control and tracking design for multi-input multi-output nonlinear perturbed plants," *IET Control Theory & Applications*, vol. 3, no. 9, pp. 1237-1248, 2009.

[56] S. Bi, L. Wang, Y. Zhao, and M. Deng, "Operator-based robust control for nonlinear uncertain systems with unknown backlash-like hysteresis,"

International Journal of Control Automation and Systems, vol. 14, no. 2, pp. 469-477, April 2016.

[57] S. Zhang, R. Schmidt and X. Qin, "Active vibration control of piezoelectric bonded smart structures using PID algorithm," *Chinese Journal of Aeronautics*, vol. 28 no. 1, pp. 305-313, 2015.

[58] A. Oveisi, and T. Nestorovi, "Robust observer-based adaptive fuzzy sliding mode controller. *Mechanical Systems and Signal Processing*, vol. 76, pp. 58-71, 2016.

[59] R. Talebitooti, K. Daneshjoo and S. A. Jafari, "Optimal control of laminated plate integrated with piezoelectric sensor and actuator considering TSDT and meshfree method, " *European Journal of Mechanics - A/Solids*, vol. 55, pp. 199-211, 2016.

[60] K. Khorshidi, E. Rezaei, A. A. Ghadimi and M.Pagoli, "Active vibration control of circular plates coupled with piezoelectric layers excited by plane sound wave," *Applied Mathematical Modelling*, vol. 39, no. 3, pp. 1217-1228, 2015.

[61] M. Kuczmann, "Dynamic Preisach hysteresis model," *Journal of Advanced Research in Physics*, vol. 1, no. 1, pp.1-5, 2010

[62] Y. Bernard, E. Mendes and F. Bouillault, "Dynamic hysteresis modeling based on Preisach model," *IEEE Transactions on Magnetics*, vol. 38, no. 2, pp. 885-888, 2002.

[63] C. Natale, F. Velardi and C. Visone, "Identification and compensation of Preisach hysteresis models for magnetostrictive actuators," *Physica B: Condensed Matter*, vol. 306, no.1, pp. 161-165, 2001.

[64] G. Song, J. Zhao, X. Zhou and J. De Abreu-Garca, "Tracking control of a piezoceramic actuator with hysteresis compensation using inverse Preisach model," *IEEE/ASME Transactions on mechatronics*, vol. 10, no. 2, pp. 198-209, 2005.

[65] H. Adriaens, W. De Koning and R. Banning, "Modeling piezoelectric actuators," *IEEE/ASME transactions on mechatronics*, vol. 5, no. 4, pp. 331-341, 2000.

[66] J. J. Tzen, S. L. Jeng and W. H. Chieng, "Modeling of piezoelectric actuator for compensation and controller design," *Precision Engineering*, vol. 27, no. 1, pp. 70-86, 2003.

[67] P. Ge and M. Jouaneh, "Modeling hysteresis in piezoceramic actuators," *Precision engineering*, vol. 17, no. 3, pp. 211-221, 1995.

[68] G. Webb, A. Kurdila and D. Lagoudas, "Adaptive hysteresis model for model reference control with actuator hysteresis," *Journal of Guidance, Control, and Dynamics*, vol. 23, no. 3, pp. 459-465, 2000.

[69] I. D. Mayergoyz, *Mathematical Models of Hysteresis and Their Applications*, Academic Press, 2003.

[70] K. Kuhnen, "Modeling, identification and compensation of complex hysteretic nonlinearities: A modified Prandtl-Ishlinskii approach," *European journal of control*, vol. 9, no. 4, pp. 407-418, 2003.

[71] C. Su, Q. Wang, X. Chen, and S. Rakheja, "Adaptive variable structure control of a class of nonlinear systems with unknown Prandtl-Ishlinskii hysteresis," *IEEE Transactions on Automatic Control*, vol. 50, no. 12, pp. 2069-2074, December 2005.

[72] X. Chen, T. Hisayama and C. Su, "Adaptive control for uncertain continuous-time systems using implicit inversion of Prandtl-Ishlinskii hysteresis representation," *IEEE Transactions on Automatic Control*, vol. 55, no. 10, pp. 2357-2363, October 2010.

[73] C. Jiang, M. Deng and A. Inoue, "Robust stability of nonlinear plants with a non-symmetric Prandtl-Ishlinskii hysteresis model," *International Journal of Automation and Computing*, vol. 7, no. 2, pp. 213-218, May 2010.

[74] Y. Katsurayama, M. Deng and C. Jiang, "Operator-based experimental studies on nonlinear vibration control for an aircraft vertical tail with considering low-order modes," *Transactions of the Institute of Measurement and Control*, vol.38, no. 12, pp. 1421-1433, December 2016.

[75] N. Sun, Y. Fang, H. Chen, and B. Lu, "Amplitude-saturated nonlinear output feedback antiswing control for underactuated cranes with

double-pendulum cargo dynamics," *IEEE Transactions on Industrial Electronics*, vol. 64, no. 3, pp. 2135-2146, March 2017.

[76] N. Sun, Y. Wu, Y. Fang, H. Chen, and B. Lu, "Nonlinear continuous global stabilization control for underactuated RTAC systems: Design, analysis, and experimentation," *IEEE/ASME Transactions on Mechatronics*, vol. 22, no. 2, pp. 1104-1115, April 2017.

[77] S. S. Rao, *Mechanical Vibrations*. 5nd ed. Prentice Hall, New Jersey, 2010.

[78] S. S. Rao, *Vibration of Continuous Systems*. John Wiley & Sons, New Jersey, 2007.

[79] A. Erturk and D.J. Inman, "On mechanical modeling of cantilevered piezoelectric vibration energy harvesters," *Journal of Intelligent Material Systems and Structures*, vol. 19, no. 11, pp. 1311-1325, 2008.

[80] A. Erturk and D. J. Inman, *Piezoelectric Energy Harvesting*, John Wiley & Sons, 2011.

[81] H. J. Adriaens, W. L.Koning and R. Banning, "Modeling piezoelectric actuators," *IEEE/ASME Transactions on Mechatronics*, vol. 5, no.4, pp. 331-341, 2000.

[82] M. Al Janaideh, S. Rakheja and C. Su, "An analytical generalized Prandtl-Ishlinskii model inversion for hysteresis compensation in mi-

cropositioning control," *IEEE/ASME Transactions on Mechatronics*, vol. 16, no. 4, pp. 734-744, 2011.

[83] M. Deng, C. Jiang, A. Inoue and C. Y. Su, "Operator-based robust control for nonlinear systems with PrandtlIshlinskii hysteresis," *International Journal of Systems Science*, vol. 42, no. 4, pp. 643-652, 2011.

[84] M. Deng, C. Jiang and A. Inoue, "Operator-based robust control for nonlinear plants with uncertain non-symmetric backlash," *Asian Journal of Control*, vol. 13, no. 2, pp. 317-327, October 2010.

[85] M. Deng, A. Inoue and S. Goto, "Operator based thermal control of an aluminum plate with a Peltier device," *International Journal of Innovative Computing, Information and Control*, vol. 4, no. 12, pp. 3219-3229, 2008.

[86] M. Deng, A. Inoue and Y. Baba, "Operator-based non-linear vibration control system design of a flexible arm with piezoelectric actuator," *International Journal of Advanced Mechatronic Systems*, vol. 1, no. 1, pp. 71-76, 2008.

[87] J. Hirai, T. W. Kim, and A. Kawamura, "Position-sensorless drive of linear pulse motor for suppressing transient vibration," *IEEE Transactions on Industrial Electronics*, vol. 47, no. 2, pp. 337-345, 2000.

[88] S. Dian, Y. Arai and W. Gao, "Precision positioning control of a Sawyer motor-based two-axis planar motion stage," *International Journal of Surface Science and Engineering*, vol. 3, no. 3, pp. 253-271, 2009.

[89] J. Hirai, T. W. Kim, and A. Kawamura, "Wireless transmission of power and information and information for cableless linear motor drive," *IEEE transactions on Power Electronics*, vol. 15, no. 1, pp. 21-27, 2000.

[90] T. Miyasaka, K. Yamazaki, J. Tsuchiya, T. Shimizu, G. Kimura and M. Shioya, "Improved operating characteristics of linear pulse motor using resonant current," in *Proc. of the International Conference on Industrial Electronics, Control, and Instrumentation*, pp. 896-901, 1993.

[91] M. Sanada, S. Morimoto, and Y. Takeda, "Vibration suppression for linear pulse motor," in *Proc. of Conference on Industry Applications Society Annual Meeting*, vol. 1, pp. 517-522, 1994.

[92] D. Economou, C. Mavroidis and I. Antoniadis, "Experiments on robust vibration suppression in mechatronic systems using IIR digital filters," in *Proc. of 2001 IEEE/ASME International Conference Advanced Intelligent Mechatronics*, vol. 2, pp. 731-737, 2001.

[93] D. Economou, C. Mavroidis and I. Antoniadis, "Robust vibration suppression in flexible systems using infinite impulse response digital filters," *Journal of guidance, control, and dynamics*, vol. 27, no. 1, pp. 107-117, 2004.

[94] D. B. Rao and S. Y. Kung, "Adaptive notch filtering for the retrieval of sinusoids in noise," *IEEE Transactions on Acoustics, Speech, and Signal Processing*, vol. 32, no. 4, pp. 791-802, 1984.

[95] A. Wang, and J. O. Smith, "On fast FIR filters implemented as tail-canceling IIR filters," *IEEE Transactions on Signal Processing*, vol. 45, no. 6, pp. 1415-1427, 1997.

[96] J. Proakis and D. Manolakis, *Digital Signal Processing, Principles: Algorithms and Applications*, Prentice Hall, 3rd Edition, 1996.

[97] A. Montazeri, and J. Poshtan, "A new adaptive recursive RLS-based fast-array IIR filter for active noise and vibration control systems," *Signal Processing*, vol. 91, no. 1, pp. 98-113, 2011.

[98] M. Weeks, *Digital Signal Processing Using MATLAB and Wavelets*, Jones & Bartlett Learning, 2010.

Appendix A

Model analysis of the L-shaped arm with load

A.1 Free vibration of the arm

For the thin uniform arm as shown in Fig. 2.1 in Chapter 2, without considering the damping factor, its free transverse vibration is expressed as follows.

$$E_a I \frac{\partial^4 w}{\partial x^4} + \rho S \frac{\partial^2 w}{\partial t^2} = 0 \tag{A.1}$$

where E_a, I, ρ, S are the Young's modulus, moment of inertia, density, and cross-sectional area of the arm, respectively. Using the method of separation of variables, the solution can be expressed as

$$w(x,t) = \Phi(x)T(t) \tag{A.2}$$

Substituting Eq. (A.2) into Eq. (A.1) and rearranging it yields

$$\frac{E_a I}{\rho S \Phi(x)} \frac{d^4\Phi(x)}{dx^4} = -\frac{1}{T(t)} \frac{d^2 T(t)}{dt^2} = \omega^2 \tag{A.3}$$

it can be rewritten as two equations:

$$\frac{d^4\Phi(x)}{dx^4} - \beta^4\Phi(x) = 0 \tag{A.4}$$

$$\frac{d^2T(t)}{dt^2} + \omega^2 T(t) = 0 \tag{A.5}$$

where

$$\beta^4 = \frac{\rho S\omega^2}{E_a I} \tag{A.6}$$

The solution of Eq. (A.5) is given by

$$T(t) = X\cos\omega t + Y\sin\omega t \tag{A.7}$$

where X and Y are constants can be obtained from the initial conditions. The solution of Eq. (A.4) is expressed as

$$\Phi(x) = C_1\cos\beta x + C_2\sin\beta x + C_3\cosh\beta x + C_4\sinh\beta x \tag{A.8}$$

where C_1, C_2, C_3, and C_4 are constants; the function $\Phi(x)$ is known as the normal mode of the arm. The natural frequencies of the arm can be determined from Eq. (A.6) as

$$\omega = 2\pi f = \beta^2\sqrt{\frac{E_a I}{\rho S}} \tag{A.9}$$

The unknown constants C_1, to C_4 and the value of β can be determined from the known boundary conditions of the arm.

For any arm, there is an infinite number of normal modes with one natural frequency corresponding to each normal mode. If the nth natural frequency is denoted as ω_n and the corresponding normal mode as $\Phi^n(x)$, the total

free vibration response of the beam can be found by superposing the normal modes as

$$w(x,t) = \sum_{n=1}^{\infty} \Phi_n(x)(X_n \cos \omega_n t + Y_n \sin \omega_n t) \tag{A.10}$$

where the constants X_n and Y_n can be determined from the initial conditions of the beam.

A.2 Free vibration of the L-shaped arm

The following analytical modal analysis is given for the transverse vibrations of the L-shaped arm with a tip mass rigidly attached at the free end as shown in Fig. A.1.

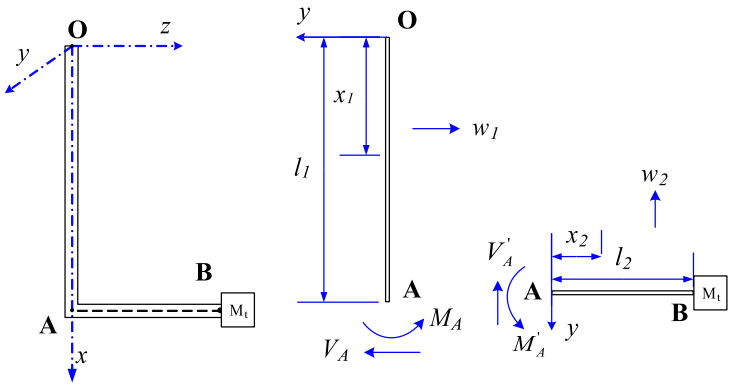

Figure A.1: Transverse vibration of the L-shaped arm

Denoting w as the transverse displacement in y direction along the neutral axis of the L-shaped arm. The forced transverse arm vibration without damping is expressed as

$$E_a I \frac{\partial^4 w}{\partial x^4} + \rho S \frac{\partial^2 w}{\partial t^2} = q(x,t) \tag{A.11}$$

where $q(x,t)$ is the external distributed forces on the arm, including the linear motor driving force and the piezoelectric actuator moment.

For easy analyse the arm vibration, we denote the displacement of segments OA and AB as $w(x_1,t)$ and $w(x_1,t)$, respectively, $0 \leq x_1 \leq l_1$, $0 \leq x_2 \leq l_2$. They are determined using the same method mentioned in last section as follows.

$$w(x_1,t) = \Phi_1(x_1)(X\cos\omega t + Y\sin\omega t) \tag{A.12}$$

$$w(x_2,t) = \Phi_2(x_2)(X\cos\omega t + Y\sin\omega t) \tag{A.13}$$

where

$$\Phi_1(x_1) = C_1^1\cos\beta x_1 + C_2^1\sin\beta x_1 + C_3^1\cosh\beta x_1 + C_4^1\sinh\beta x_1 \tag{A.14}$$

$$\Phi_2(x_2) = C_1^2\cos\beta x_2 + C_2^2\sin\beta x_2 + C_3^2\cosh\beta x_2 + C_4^2\sinh\beta x_2 \tag{A.15}$$

For OA segment, the boundary conditions can be stated as

$$\Phi_1(0) = 0, \qquad M_A = E_aI\left.\frac{d^2\Phi_1}{dx_1^2}\right|_{x_1=l_1}$$

$$\left.\frac{d\Phi_1}{dx_1}\right|_{x_1=0} = 0, \qquad V_A = E_aI\left.\frac{d^3\Phi_1}{dx_1^3}\right|_{x_1=l_1}$$

For AB segment, the boundary conditions can be stated as

$$\left.\frac{d\Phi_2}{dx_2}\right|_{x_2=0} = 0, \qquad M_A^{'} = E_aI\left.\frac{d^2\Phi_2}{dx_2^2}\right|_{x_2=0}$$

$$E_aI\left.\frac{d^2\Phi_1}{dx_1^2}\right|_{x_2=l_2} = 0, \qquad V_A^{'} = E_aI\left.\frac{d^3\Phi_2}{dx_2^3}\right|_{x_2=0}$$

$$E_aI\frac{\partial^3 w(l_2,t)}{\partial x_2^3} = m_t\frac{\partial^2 w(l_2,t)}{\partial t^3}, \qquad \Phi_2(0) = \Phi_1(l_1)$$

$$M_A^{'} = M_A, \qquad V_A^{'} = V_A$$

Using all the boundary conditions yields

$$C_1^1(\cos\beta l_1 - \cosh\beta l_1) + C_2^1(\sin\beta l_1 - \sinh\beta l_1) - C_1^2 - C_3^2 = 0 \tag{A.16}$$

$$C_1^1(\cos\beta l_1 + \cosh\beta l_1) + C_2^1(\sin\beta l_1 + \sinh\beta l_1) - C_1^2 + C_3^2 = 0 \tag{A.17}$$

$$C_1^1(\sin\beta l_1 - \sinh\beta l_1) - C_2^1(\cos\beta l_1 + \cosh\beta l_1) + C_2^2 = 0 \tag{A.18}$$

$$C_1^2\cos\beta l_2 + C_2^2(\sin\beta l_2 + \sinh\beta l_2) - C_3^2\cosh\beta l_2 = 0 \tag{A.19}$$

$$\begin{aligned} &C_1^2(\sin\beta l_2 + \lambda\cos\beta l_2) - C_2^2[\cos\beta l_2 + \cosh\beta l_2 - \lambda(\sin\beta l_2 - \sinh\beta l_2)] \\ &+ C_3^2(\sinh\beta l_2 + \cosh\beta l_2) = 0 \end{aligned} \tag{A.20}$$

where $\lambda = \omega^2 m_t/(E_a I\beta^3)$. Setting the determinant of the coefficient matrix Eqs. (A.16) to (A.20) yields the frequency equation of the arm vibration as

$$\begin{aligned} &\sin\beta l^-\sinh\beta l^+ - \sinh\beta l^-\sin\beta l^+ - 2\cos\beta l_2\cosh\beta l_2 - 2\cos\beta l_1\cosh\beta l_1 \\ &- 2\cos\beta l^+\cosh\beta l^+ - 2 - \frac{m_t\beta}{\rho S}(2\cos\beta l^+\sinh\beta l^+ - 2\cosh\beta l^+\sin\beta l^+ \\ &+ 2\cos\beta l_2\sinh\beta l_2 - \cosh\beta l_2\sin\beta l_2 + \cos\beta l^-\sinh\beta l^+ - \cosh\beta l^-\sin\beta l^+ \\ &- \sin\beta l^-\cosh\beta l^+ - \sinh\beta l^-\cos\beta l^+) = 0 \end{aligned} \tag{A.21}$$

where $l^+ = l_1 + l_2$, $l^- = l_1 - l_2$, m_t is the mass of load.

For the given system parameters l_1, l_2, m_t, ρ and S, one can solve for the roots of Eq. (A.21) obtaining β; it has infinite positive eigenvalues for the infinite natural modes of vibration. Hence the nth mode shape of the arm at segments OA and AB can be expressed as

$$\Phi_1^n(x_1) = C_1^n\big[\cos\beta_n x_1 - \cosh\beta_n x_1 + \sigma_1^n(\sin\beta_n x_1 - \sinh\beta_n x_1)\big] \tag{A.22}$$

$$\Phi_2^n(x_2) = C_2^n(\sigma_2^n\cos\beta_n x_2 + \sigma_3^n\cosh\beta_n x_2 + \sin\beta_n x_2 - \sinh\beta_n x_2) \tag{A.23}$$

where C_1^n and C_2^n are the unknown constants for the nth mode vibration, could be obtained from the orthogonality conditions and the boundary conditions. σ_1^n, σ_2^n, σ_3^n are coefficients depending on the vibration mode, which are listed as follows.

$$\sigma_1^n = \frac{\sin\beta_n l_1 \sin\beta_n l_2 + \sin\beta_n l_1 \sinh\beta_n l_2 - \sin\beta_n l_2 \sinh\beta_n l_1 - \sigma_{u1}}{\cos\beta_n l_1 \sin\beta_n l_2 + \cos\beta_n l_1 \sinh\beta_n l_2 + \cosh\beta_n l_1 \sin\beta_n l_2 + \sigma_{b1}}$$

$$\sigma_2^n = \frac{\cos\beta_n l_2 \cosh\beta_n l_2 - \sin\beta_n l_2 \sinh\beta_n l_2 - 2\frac{m_t\beta_n}{\rho S}\cosh\beta_n l_2 \sin\beta_n l_2 + 1}{\cos\beta_n l_2 \sinh\beta_n l_2 + \cosh\beta_n l_2 \sin\beta_n l_2 + 2\frac{m_t\beta_n}{\rho S}\cos\beta_n l_2 \cosh\beta_n l_2}$$

$$\sigma_3^n = \frac{\cos\beta_n l_2 \cosh\beta_n l_2 + \sin\beta_n l_2 \sinh\beta_n l_2 + 2\frac{m_t\beta_n}{\rho S}\cos\beta_n l_2 \sinh\beta_n l_2 + 1}{\cos\beta_n l_2 \sinh\beta_n l_2 + \cosh\beta_n l_2 \sin\beta_n l_2 + 2\frac{m_t\beta_n}{\rho S}\cos\beta_n l_2 \cosh\beta_n l_2}$$

$$\sigma_{u1} = \sinh\beta_n l_1 \sinh\beta_n l_2 + 2\cos\beta_n l_1 \cos\beta_n l_2 + 2\cosh\beta_n l_1 \cosh\beta_n l_2$$

$$\sigma_{b1} = \cosh\beta_n l_1 \sinh\beta_n l_2 + 2\cos\beta_n l_2 \sinh\beta_n l_1 + 2\cosh\beta_n l_2 \sinh\beta_n l_1$$

The undamped natural frequency of free vibration for the nth mode is obtained from Eq. (A.9) as

$$\omega_n = 2\pi f_n = \beta_n^2 \sqrt{\frac{E_a I}{\rho S}} \tag{A.24}$$

Therefore, the free vibration of the L-shaped arm can be as a linear combination of all the natural modes motion of the arm.

$$w(x_1, t) = \sum_{n=1}^{\infty} \Phi_1^n(x_1)(X_n \cos\omega_n t + Y_n \sin\omega_n t) \tag{A.25}$$

$$w(x_2, t) = \sum_{n=1}^{\infty} \Phi_2^n(x_2)(X_n \cos\omega_n t + Y_n \sin\omega_n t) \tag{A.26}$$

where the $\Phi_1^n(x_1)$ and $\Phi_2^n(x_2)$ are the ith natural modes and $X_n \cos\omega_n t + Y_n \sin\omega_n t$ is a time-dependent function to be determined.

A.3 Forced vibration due to initial conditions

Considering the strain-rate damping, the forced vibration of the L-shaped arm is represented as

$$E_a I \frac{\partial^4 w}{\partial x^4} + c_s I \frac{\partial^5 y(x,t)}{\partial x^4 \partial t} + \rho S \frac{\partial^2 w}{\partial t^2} = q(x,t) \tag{A.27}$$

In view of orthogonality of the eigenfunctions, using Eq. (A.24) and Duhamel integral, the solution of Eq. (A.27) for zero initial conditions is given as

$$w(x_1,t) = \sum_{n=1}^{\infty} \frac{\Phi_1^n(x_1)}{\omega_{dn}} \int_0^t Q_1^n(\tau) e^{-\zeta_n \omega_n (t-\tau)} \sin \omega_{dn}(t-\tau) d\tau \tag{A.28}$$

$$w(x_2,t) = \sum_{n=1}^{\infty} \frac{\Phi_2^n(x_2)}{\omega_{dn}} \int_0^t Q_2^n(\tau) e^{-\zeta_n \omega_n (t-\tau)} \sin \omega_{dn}(t-\tau) d\tau \tag{A.29}$$

where $Q_1^n(t)$ and $Q_1^n(t)$ are the generalized forces corresponding to the nth mode given by

$$Q_1^n(t) = \int_0^l \Phi_1^n(x_1) q_1(x,t) dx \tag{A.30}$$

$$Q_2^n(t) = \int_0^l \Phi_2^n(x_2) q_2(x,t) dx \tag{A.31}$$

Appendix B

Publications

Journal papers

1. **Y. Wu** and M. Deng, Operator-based robust nonlinear optimal vibration control for an L-shaped arm driven by linear pulse motor, *International Journal of Control, Automation and Systems*, vol. 15, no. 5, pp. 2026-2033, October 2017.

2. **Y. Wu** and M. Deng, Experimental study on robust nonlinear forced vibration control for an L-shaped arm with reduced control inputs, *IEEE/ASME Transactions on Mechatronics*, vol. 22, no. 5, pp. 2186-2195, October 2017.

3. **Y. Wu** and M. Deng, Operator-based robust nonlinear vibration control for an L-shaped arm with unknown load by using on-line wavelet transform, *IET Control Theory & Applications*, ID: CTA-2017-0337 (Conditionally accepted).

Proceedings papers

1. **Y. Wu** and M. Deng, Operator-based vibration control for an L-type arm of crane systems using piezoelectric actuator, *Proc. of the 12th IEEE International Conference on Networking, Sensing and Control*, pp. 197-210, 2015 (Best Student Paper Award).

2. **Y. Wu**, M. Deng and L. Jin, Experimental study on nonlinear vibration control of an L-shape arm, *Proc. of the 2015 International Conference on Advanced Mechatronic Systems*, pp. 589-593, 2015.

3. **Y. Wu**, M. Deng and L. Jin, A modified design on operator-based nonlinear vibration control for an L-shape arm with load, *Proc. of the 2017 International Conference on Advanced Mechatronic Systems*, pp. 42-45, 2017.

Other papers

1. **Y. Wu** and M. Deng, Vibration analysis of linear-motor-driven L-shaped arm, *The papers of Technical Meeting on Control, IEE Japan*, CT-12-019, pp.11-14, 2015.

2. M. Umemori, **Y. Wu** and M. Deng, Operator-based robust nonlinear optimal vibration control for an L-shaped arm, *The papers of Technical Meeting on Control, IEE Japan*, CT-17-10, pp. 27-32, 2017 (in Japanese).